ENHANCED INDUCED STRAIN ACTUATOR PERFORMANCE THROUGH DISCRETE ATTACHMENT TO STRUCTURAL ELEMENTS

by

Zaffir Ahmed Chaudhry

Dissertation submitted to the Faculty of the

Virginia Polytechnic Institute and State University

in partial fulfillment of the requirements for the degree of

Doctor of Philosophy

in

Mechanical Engineering

APPROVED:

Dr. Craig A. Rogers, Chairman

Dr. Charles E. Knight

Dr. Eric. R. Johnson

Dr. Liviu Librescu

Dr. Chen Liang

July, 1992
Blacksburg, Virginia

ENHANCED INDUCED STRAIN ACTUATOR PERFORMANCE THROUGH DISCRETE ATTACHMENT TO STRUCTURAL ELEMENTS

by

Zaffir Ahmed Chaudhry

Committee Chairman: Dr. Craig A. Rogers

Mechanical Engineering

(ABSTRACT)

In intelligent structures, structural deformation is generally controlled by either embedding or surface bonding the induced strain actuator to the structure. With bonded or embedded actuators used for inducing flexure, the developed in-plane force contributes indirectly through a locally-generated moment. Control authority in this configuration is thus limited by actuator offset distance. The focus of this research was to investigate a new concept in which the actuator, as opposed to being bonded, is attached to the structure at discrete points. This configuration is fundamentally different from the bonded/embedded configuration in that the actuator and the structure between the two discrete points can deform independently; and the in-plane force of the actuator, which contributes only indirectly in the case of bonded actuator, can directly influence out-of-plane displacements of the structure. Additionally, the actuator offset distance can be optimized with respect to actuator force/strain saturation for increased authority.

Two implementations of this concept as applied to beam structures were investigated. In the first, the actuator (e.g., shape memory alloy actuator wire) does not possess any

flexural stiffness; and therefore, remains straight between the two attachment points. In the second implementation, the actuator (PZT's and electrostrictive) possesses flexural stiffness, and bends with the structure. The formulation and experimental results for both implementations are presented. Enhanced authority is demonstrated by comparing the static response of the discretely attached actuator beam systems with their bonded counterpart systems.

ACKNOWLEDGEMENTS

I would like to express my sincere appreciation and gratitude to all my committee members for all the help, advice, and valuable suggestions and comments they offered me throughout my study. I am very grateful to Dr. Craig Rogers, my major professor, for allowing me the time to explore new ideas, and for his confidence in me at all stages of my research. I would also like to thank Dr. Eric Johnson for getting me interested in nonlinear structural mechanics, and for his continued advice.

I also wish to thank all the staff and students in the Center for Intelligent Material Systems and Structures for their gracious support at all times. I would especially like to thank Chet Namboodri for many fruitful discussions on intelligent materials systems, and Steve Booth for all the help with the experimental work. My special thanks to Ms Beth Howell for her meticulous proof-reading of my papers.

My special thanks to my wife, without whose support this endeavor would not have been possible. Also my special gratitude to my parents for their continued support and prayers.

I would also like to gratefully acknowledge the support of the Office of Naval Research and the National Science Foundation.

Table of Contents

Chapter 1

Chapter 2

Chapter 3

Chapter 4

Chapter 5

List of Figures

List of Tables

Chapter 1

Introduction to Intelligent Structures

Intelligent material systems have been identified as one of the most important emerging materials technology areas for space and aerospace and are regarded by some as the first really new idea relating to structural materials since the introduction of structural composites in the 1960's (Davidson, 1990). They are expected to revolutionize what structures and material systems are capable of doing. The intention of this chapter is to give a short overview of concepts for intelligent structures and to make the reader aware of the prospects of this new, interdisciplinary approach.

1.1 Definition of an Intelligent Structure:

There is no universally accepted definition of the term intelligent structure (also described as smart, sense-able, multifunctional or adaptive); however, they can be thought of as structures with incorporated additional functions beside the function of load carrying. These additional functions may be sensing (internal and external), communication, data processing or shape changing. To achieve this multifunctionality, additional elements must be incorporated into the structure, thus increasing their operational efficiency. They are often modeled on biological systems with:

- Sensor acting as a nervous system
- Actuator acting like muscles
- Real time processors acting as a brain to control the system

Biological systems through their sensory systems, muscles (actuators), and the brain (control system) continuously evolve and adapt to changing needs and environments. The inspiration and motivation for this new field is also to create a higher form of material systems and structures by providing the "life" functions of sensing, actuation, control and intelligence to materials and structures. In addition to the capability of adaption, natural systems operate in a mode to reduce energy consumption. In the same vain the goal of intelligent material systems proposed by Rogers (1992) is to "replace mass and energy with intelligence". Thus by studying the different methods by which nature creates adaptive functions, we can develop synthetic methods to mimic those of nature.

The three major components of the intelligent structure; the sensors, the actuators, and the control system are now discussed.

1.2 Sensor Systems

Integrated sensors can either have internal or external applications (Dittrich, 1990). Internal sensors are used to monitor the structure itself, by measuring temperature, strain

or vibration, or by detecting damages due to overloading or impact. External sensors are focussed to the outside of the structure, mainly for detecting electromagnetic energy. The most common sensor elements are described below.

1.2.1 Fiber Optic Sensors

It is possible to embed fiber optic sensors into composite structures during manufacturing to allow internal interrogation of material. They are most versatile and look the most promising. They are compatible with the fabrication process and are capable of withstanding strains of the same magnitude as the composite itself. They offer the prospect of continuously monitoring the composite structure at all stages of its life through fabrication, test qualification and service. Optical fiber sensors can be designed to detect a whole range of physical parameters including temperature, strain, pressure, electric fields and magnetic fields. Distributed and quasi-distributed measurements have been demonstrated using optical radar techniques by monitoring reflected signals (Davidson, 1990). In a recent report by Culshaw and Michie (1992) it has been shown that properly treated optical fibers can be embedded in a composite panel as thin as 1mm without any degradation in the mechanical performance of the composite panel.

1.2.2 Piezoelectric Sensors

Piezoelectric ceramics and polymers are also very good sensors which are widely used. Piezoelectric sensors are built of materials that generate an electrical response to an applied force or pressure. Because of the brittle nature of piezoelectric ceramics the piezoelectric sensors are generally made of one of the family of polymers, polyvinyldene fluoride, also known as PVDF of PVF_2. Because it is a polymer it can be formed into very thin sheets and adhered to almost any surface (Rogers, 1990).

1.2.3 Piezoelectric Rubber

Most applications which require a piezoelectric transducer, for example, underwater hydrophones or pressure sensors, use a ceramic material called PZT (lead zirconium titanate). When subjected to a mechanical strain, this produces a voltage of the order of 3μV/Pa - a usefully high value that requires nothing more sophisticated than a charge amplifier to buffer the extremely high source impedance of this capacitive transducer to an analogue signal-conditioning circuit. PZT has many advantages; it is chemically inert, it has a reasonably high sensitivity, and it can be used over a wide range of pressures without serious non-linearity. The biggest drawback of the material is its mechanical fragility; like all ceramics (Rogers, 1990). This problem has now been overcome to a large extent. Neurgaonkar et al. (1992) have recently reported the development of highly densified PZT and PLZT piezoelectric ceramics which not only exhibit higher electromechanical coupling but also have much better physical properties.

1.2.4 PZT Paint

A new sensor recently introduced at the Center for Intelligent Material Systems and Structures is the PZT paint. The paint is fabricated by grinding piezoceramics to micron sized particles and mixing them with a typical lacquer or enamel. It is intended to simplify processing and attachment of a sensor to a structure. The paint can be applied with a spray or a brush and cures at room temperature in less than one hour. It may be activated by applying a dc field across its electrodes. When stressed, the paint exhibits the direct piezoelectric effect.

1.3 Actuator Systems

Actuator systems can be divided into two broad categories. In the first categories are the actuators that are widely applied to the surface or are embedded. In the second category are actuators used in truss like structures where they replace some of the truss elements of the structure (Wada, Fanson, and Crawley, 1990). The actuators in the first category are almost invariably induced strain actuators like piezoelectric actuators, whereas in the second category the active truss members can be conventional displacement actuators (screwjacks), where the length of the member is controlled, or force actuators (voice coil), where the load in the member is controlled. This second category of actuators are widely used in active trusses. Deployable space structures will make use of such active trusses

not only for deployment but also for making fine resolution adjustments of the structural surfaces (Natori et al., 1988).

Induced strain actuators develop strains in response to an applied nonmechanical stimulus like electric field, temperature or magnetic field. This developed strain can be used to apply controlled forces to the structure. The most commonly used induced strain actuators are discussed in the following section.

1.3.1 Shape Memory Alloys

Shape memory alloys based on NiTi were first investigated by the Naval Ordnance Laboratory and are hence referred to as Nitinol. The shape-memory effect (SME) can be described very basically as follows: an object in the low-temperature martensitic condition, when plastically deformed and the external stress removed, will regain its original (memory) shape when heated. The process or phenomenon, is the result of a martensitic transformation taking place during heating (Jackson et al., 1972; Schetky, 1979). The shape recovery performance of Nitinol is phenomenal. Plastic strains of typically six-to eight percent may be completely recovered by heating the material so as to transform it to its austenite phase. Restraining the material from regaining its memory shape can create stresses of 100,000 psi. It is these force and displacement capabilities that are exploited for electromechanical actuators (Liang and Rogers, 1990).

Nitinol actuators embedded in composite structures can be used to modify the static and dynamic structural response by actively changing the stiffness of the structure, or by alternately activating agonist and antgonist pairs of actuators embedded in a material off the neutral axis (Rogers and Robertshaw, 1988).

1.3.2 Electrorheological Fluids

Electrorheological fluids, which have the ability to alter their flow characteristics by the presence of an electrical field, are changing the way electromechanical devices are being conceived. The response of a an ER fluid, which takes only milliseconds, is in the form of a progressive gelling that is proportional to field strength. With no field present, the fluid flows as freely as water or hydraulic oil. If the electrified ER fluid gel is sheared with sufficient force, it flows. But when the applied shear force is below a critical value, the gel reacts as a solid with a measurable stiffness. The phenomenon suggests a number of unusual engineering applications such as nonslip fluid clutches, valves with no moving parts, and tunable dampers and vibration isolators (Rogers, 1990). ER fluids have certain drawbacks which limit their extensive use at the present time. They are; insufficient stability of properties, a relatively narrow temperature range of activity, and a rather low mechanical response (Korobko, 1992).

1.3.3 Piezoelectric Actuators

Currently the most researched and used induced strain actuators are piezoceramic. The dimensions of a piezoelectric material change on application of an electric field and such materials can be bonded externally or embedded internally into composite structures to act as actuators. Piezoelectrics are available in ceramic or polymer form. Piezoceramics are simple, compact, light weight structures which can be incorporated easily into structures. Although piezoelectric actuators have a limited stroke (200-400 μstrain) they are especially popular because of their high band-width (greater than 20 Khz.) and their ability to produce extensional as well as compressive strain. In addition to structural control applications they have found widespread use in a diverse range of innovative applications including surface acoustic wave (SAW) filters, micropositioning controllers, ultrasonic motors, and frequency analyzers (Uchino, 1986).

Piezoelectric actuators also have the potential to act as actuators, since a load applied to the piezoelectric results in an electric charge. Hence if the voltages generated are sufficiently high to be monitored and if the loads generated can be made large enough to cause displacements, in say a large flexible space structure, it is conceivable that the piezoelectric may act as both actuator and sensor (Davidson, 1990).

1.3.4 Electrostrictive Actuators

Electrostrictive actuators are also made of ferromagnetic material but unlike piezoelectric

materials electrostriction is a second order effect. The strain induced is proportional to the square of the electric field. They are stroke limited to about 1000 μstrain and require high voltages. Electrostrictive actuators exhibit less hysterises compared to piezoelectrics. They also exhibit no aging or creep since no poling is necessary for electrostriction strains (Uchino, 1986).

1.4 Control Systems

For structures containing both sensors and actuators, signals from the sensors will need to be received and interpreted by a controller which will trigger the actuators to alter the structural response. A number of real time controllers for this task are being considered (Ahrens, 1989). Neural networks based control systems which are inspired by biological systems are receiving a great deal of attention and offer certain features which are not available in conventional control systems. The special feature which distinguishes this control system from other controllers is its ability to learn, and modify the control scheme with time. A neural network is a massively parallel, interconnected network of basic computing elements, that individually function rather slowly and imperfectly, but collectively learn to perform complex tasks, as for instance in pattern recognition, which even the largest serial computer cannot match. A network typically consists of an array of input processors that are subjected to a stimulus which is processed and an output signal is generated. This output signal then becomes an input to other processors in the

network. This feed-through mechanism terminates in a set of output nodes where the network response to the input stimulus is available. Both the structure of the network and the connectivity of its processors have a significant influence on its overall behavior (Hajela and Berke, 1990).

Although neural network based controllers do not exist in suitable forms to act as the "brain" in a fully intelligent structure, it is an area where rapid advances are expected and looks to be the most promising way forward (Grossman and Thursby, 1989).

1.5 Application Areas for Intelligent Structures

At the present stage most of the research work relating to intelligent material systems is at a research stage with the aim of demonstrating the feasibility for use in real time structures. In a report published by the Japan Science and Technology Agency (released November 30, 1989) on the concept of intelligent materials, the following material systems, among others, were listed as Intelligent Materials Currently Imaginable:

- Material which restrain the advance of cracks by producing compression stress around them through volume change from stress-induced transformation at the tip of the crack, when the cracks are produced in strong parts due to repeated stress. [Recognition/Discrimination, Redundancy]

· Materials which recognize the load speed of stress and generate a large force against the shock stress by discriminating whether it is shock or static stress. [Recognition/Discrimination, Redundance]

· Materials which give a warning and suppress the advance of generated deformation, damage, etc., or repair themselves to their original form in the course of time (automobile bodies, aircraft, etc.). [Self-Diagnosis, Prediction/Notification, Self-Repair]

· Materials which are usable over an extremely wide range of temperatures up to ultra-high temperature with the suitable change in composition by transformation on chemical reaction according to the environment (heat-resistant materials for the space shuttle, etc.) [Self- Adaptation/Surrounding-Adjustment]

Most recently some of the potential payoffs of intelligent structures in DoD applications were highlighted by Crowson (1992). Table 1.1 lists these applications and potential payoffs.

1.5.1 Current Areas of Research

From the point of view of present research, the application areas can be divided into four

broad categories:

- Non-Destructive Evaluation
- Damage Control
- Vibration and Acoustic Control
- Motion and Shape Control

1.5.1.1 Non-Destructive Evaluation

In the area of non-destructive tesing fiber optic sensors are being actively researched for the health monitoring of structures. Integrated optical fibers can reliably detect cracks and, under certain conditions, delaminations in composite structures, thereby making a quick pre/post-flight or continuous damage check possible. Optical fibers for damage detection have been intensively investigated by DORNIER for aircraft applications, with promising results (Dittrich, 1990).

More recently a Health Monitoring System (HMS) designed to increase the safety of aging aircraft has been reported by Hickman, Gerardi, and Feng, (1990). By monitoring the vibration signature of a structure, HMS determines structural abnormalities using a network of sensor arrays and distributed processors. Pattern recognition techniques and artificial intelligence are utilized to classify the sensor signals and determine the type of

Table 1.1 Smart Materials and Structures Applications in DoD Systems

Application	Systems	Payoffs	Mission Benefit
Adaptive Control Surfaces	Aircraft (wings & Control Surfaces)	2x Increase in Lift-to-Drag Ratio	30% Greater Payload 50% Longer Range 30% Increase in Maneuverability
Active Acoustic Coatings for Signature Suppression	Submarines (Coatings)	60 dB Noise Suppression 100x Reduction in Settling Time	Active Stealth 2x Listening Range
Vibration Suppression and Twist Control	Helicopters (Blades)	Active Blade Trimming and Balancing 3% Gross Wt. Reduction	15% Increased Readiness Increased Speed- 160-200 Knots Increased Agility
Active Structural Tuning and Damping	Precision Space Structures	1μm Adjustment over 25m	Pointing Accuracy

defect. The memory of the system is formed through the learning process. A prototype system installed on the NASA Lewis DHC-6 (twin Otter) has been successfully tested in a series of experiments that demonstrate the feasibility to detect structural damage as well as leading edge ice accretion.

1.5.1.2 Damage Control

The active damage control concept has only recently been introduced by Rogers, Liang, and Li (1991) and a proof of concept model using hybrid shape memory alloy composite has been tested. When a crack propagates and is near an embedded SMA fiber, activation of the SMA changes the stress distribution at the crack tip, resulting in a reduction of the stress intensity factor. A 24% reduction in the stress intensity factor was observed in the experiment. Rogers, Liang, and Li (1991) have also investigated the use of PZT actuators for controlling fatigue of bonded joints. In an experiment where a graphite epoxy beam was bonded to a steel beam, with active control using PZT actuators the fatigue life of the joint was increased by an order of magnitude.

1.5.1.3 Vibration and Acoustic Control

Perhaps the most research work has been reported in the area of vibration and acoustic control. Bailey and Hubbard (1985) used piezoelectric actuators as active dampers for

beams. A substantial reduction in vibration decay time was reported. Fanson et al. (1989), have also used piezoelectric actuators for damping the vibration in beams. These investigations pointed out that with such actuators a number of vibration modes can be simultaneously controlled with reduced spillover of energy into higher modes. Dimitriadis, Fuller, and Rogers (1991) investigated the behavior of a pair of two-dimensional piezoelectric patches surface-bonded to an elastic plate and used as distributed vibration actuators. It was demonstrated that modes can be selectively excited and that the geometry of the actuator shape markedly effects the modal distribution of plate. The location of the piezoactuator was similarly shown to effect dramatically the vibration response of plate. Piezoactuators were shown to be very effective for active noise control of structurally radiated/transmitted noise.

Shape memory alloy hybrid composites have also been used for vibration and acoustic control (Rogers, 1990; Anders, Rogers, and Fuller, 1991). Experimental work with nitinol hybrid composite beams with 5%, 10%, and 15% nitinol volume fraction and clamped-clamped boundary conditions showed increases in the natural frequency by factors of 1.7, 2.5, and 3.0 respectively.

1.5.1.4 Motion and Shape Control

Very little experimental work has been reported in the area of motion and shape control.

Crawley and Lazarus (1989) have used piezoelectric actuators for shape control of composite and metal plates both by surface bonding and embedding the actuators in the plate. Spangler and Hall (1990) studied the feasibility of using piezoelectric actuators for actively changing the flap angle of a helicopter rotor blade. In actual wind tunnel tests of a scale model of a helicopter blade, the actual deflections achieved and effectiveness in terms of effective angle of attack were significant at flight conditions representative in a scaled sense, of the highest velocity likely to be encountered on a typical helicopter blade.

Lazarus, Crawley, and Bohlman (1990), while considering a box type wing structure have shown the potential benefits of using adaptive airfoils for aeroelastic control. In their trade studies they show that greater control authority along with a lower weight penalty is achievable using adaptive aeroelastic structures for a variety of wing designs. Song, Librescu, and Rogers (1991) while considering an adaptive swept-forward wing, modeled as a thin walled beam, have shown similar benefits of adaptive airfoils. Haftka and Adelman (1985) have proposed the use of materials with large coefficient of thermal expansion for controlling the deformations in large space structures.

Another application area in shape control is in the control of an optical surface (Chirappa and Claysmith, 1981). An optical control system with induced strain actuators is constructed by mounting induced strain actuators below the optical mirror surface. By

actiavating the induced strain actuators the desired mirror curvatures can be achieved and the focal length or the pointing direction of the mirror can be quickly and accurately changed.

The application areas of intelligent structures are by no means restricted to aerospace applications, recently the use of this concept in civil engineering type structures has been demonstrated. In an experement fibers containing timed release anti-corrosion chemicals were wrapped around the rebars in reinforced concrete, the coating on the fibers dissolves whenever their is a reduction in alklinity and releases anticorrosion chemicals (Dry, 1992).

The present state of interest of researchers from varying disciplines, in this new emerging field is aptly described by this statement from an article in Science (1992) "*Researchers of every stripe are joining in a quest to create intelligent structures that can warn of impending failure - in bridges, say - or adapt to a changing environment*".

1.6 References

Ahrens, C. P. and Claus, R. O., 1989, "Real Time Controller for Applications in Smart Structures," SPIE, Vol. 1170, pp. 384-392.

Anders, W. S., Rogers, C. A., and Fuller, C. R., "Vibration and Low Frequency Acoustic analysis of Piecewise-Activated Adaptive Composite Panels," Journal of Composite Materials, Vol. 26, No. 1, pp. 103-120.

Bailey, T. and Hubbard, J. E., 1985, "Distributed Piezoelectric-Polymer Active Vibration Control of a Cantilever Beam," J. of Guidance and Control, Vol. 8, No. 5.

Chirappa, D. J. and Claysmith, C. R., 1981, "Deformable Mirror Surface Control Techniques," J. of Guidance and Control, Vol. 4, No. 1.

Crawley, E. F. and Lazarus, K. B., 1989, "Induced Strain Actuation of Isotropic and Anisotropic Plates," AIAA Paper No. 89-1326, Proceedings, 30 th SDM Conference, Mobile, AL.

Crowson, A., 1992, "Smart Materials and Structures: An Army Perspective," Proceedings, Conference on Recent Advances in Adaptive and Sensory Materials and Their Applications, Blacksburg, Va, 27-29 April 1992, pp. 811-821.

Culshaw, B. and Michie, C., 1992, "Fiber Optic Strain and Temperature Measurement in Composite Materials - A Review of the OSTIC Program," Proceedings, Conference on Recent Advances in Adaptive and Sensory Materials and Their Applications, Blacksburg, Va, 27-29 April 1992, pp. 791-808.

Davidson, R., 1990, "The Current Status and Future Prospects of Smart Composites," Space Applications of Advanced Structural Materials, Proceedings of an International Symposium by the European Space Agency, The Netherlands, 21-23 March, pp. 429-436.

Dimitriadis, E. K., Fuller, C. R., and Rogers, C. A., 1991, "Piezoelectric actuators for Distributed Vibration Excitation of Thin Plates," J. of Vibration and Acoustics, Vol. 113, January, pp. 100-107.

Dittrich, K. W., 1990, "Multifunctional Structures for Aerospace Applications," Space Applications of Advanced Structural Materials, Proceedings of an International Symposium by the European Space Agency, The Netherlands, 21-23 March, pp. 437-441.

Dry, C., 1992, "Passive Smart Structures for Sensing and Actuation," Proceedings, Conference on Recent Advances in Adaptive and Sensory Materials and Their Applications, Blacksburg, Va, 27-29 April 1992, pp. 207-223.

Fanson, J. L., Blackwood, G. H., and Chu, C. C., 1989, "Active-Member Control of Precision Structures," Proceedings, 30 th SDM Conference, Mobile, AL.

Grossman, B. G. and Thursby, M. H., 1989, "Smart Structures Incorporating Artificial Neural Networks, Fiber Optic Sensors and Solid State Actuators," SPIE, Vol 1170, pp. 316-325.

Haftka, R. T. and Adelman, H. M., 1985, "An Analytical investigation of Shape Control of Large space Structures by Applied Temperatures," AIAA Journal, Vol. 23, No. 3.

Hajela, P. and Berke, L., 1990, "Neurobiological Computational models in Structural analysis and Design," AIAA Paper No. 90-1133, Proceedings, 31 st SDM Conference, Long Beach, Ca, 2-4 April, 1990, pp. 345-355.

Hickman, G. A., Gerardi, J. J., and Feng, Y., "Application of Smart Structures to Aircraft health Monitoring," Proceedings, 1 st Joint U.S./Japan Conference on Adaptive Structures, Nov. 13-15, 1990, Maui, Hawaii, pp. 966-984.

Ivam, A., 1992, "Animating the Material World," Science, Vol. 255, January, 1992.

Jackson, C. M., Wagner, H. J., and Wasilewski, R. J., 1972, "55-Nitinol The Alloy with a Memory: Its Physical Metallurgy, Properties, and applications," NASA-SP-5110.

Korobko, E. V., 1992, "The Main Properties of ERF's and Their Applications," Proceedings, Conference on Recent Advances in Adaptive and Sensory Materials and Their Applications, Blacksburg, Va, 27-29 April 1992, pp. 3-56.

Lazarus, K. B., Crawley, E. F., and Bohlman, J. D., 1990, "Static Aeroelastic Control using Strain Actuated Adaptive Structures," Proceedings, 1 st Joint U.S./Japan Conference on Adaptive Structures, Nov. 13-15, 1990, Maui, Hawaii.

Liang, C. and Rogers, C. A., 1990, "One-Dimensional Thermomechanical Constitutive Relations of Shape Memory materials," J. of Intelligent Material Systems and Structures, Vol. 1, No. 2, pp. 164-170.

Measures, R. M., 1988, "Fiber Optic Sensors - The Key to Smart Structures," SPIE, Vol. 1120, Fiber Optics.

Neurgaonkar, R. R., Oliver, J. R., and Nelson, J. G., 1992, "Ferroelectric Properties of highly Densified PZT and PLZT Piezoelectric Ceramics," Proceedings, Conference on Recent Advances in Adaptive and Sensory Materials and Their Applications, Blacksburg, Va, 27-29 April 1992, pp. 175-182.

Natori, M., Shibayama, Y., and Sekine, K., 1989, "Active Accuracy Adjustment of Reflectors Through the Change of Element Boundary," Proceedings, 30 th SDM Conference, Mobile, AL.

Rogers, C. A., 1992, "Recent Findings in Active Structural Control," ASCE Ninth

Engineering Mechanics Conference, Texas A&M University, College Station, Texas, May 25-27, 1992.

Rogers, C. A., 1990, "Active Vibration and Structural Acoustic Control of Shape Memory Alloy Hybrid Composites: Experimental Results," International Congress on Recent Developments in Air-and Structure-Borne sound and Vibration, Auburn University, 6-8 March, 1990, pp. 695-708.

Rogers, C. A., 1990, "Intelligent Material Systems and Structures," Proceedings, U.S.-Japan Workshop on Smart/Intelligent Materials and Systems, Honolulu, Hawaii, 19-23 March.

Rogers, C. A., Liang, C., and Li, S., 1991, "Active Damage Control of Hybrid Material Systems Using Induced Strain actuators," Proceedings, 32 nd SDM conference, Baltimore, Md, 8-10 April.

Rogers, C. A. and Robertshaw, H. H., 1988, "Shape Memory Alloy Reinforced Composites," Engineering Science Reprints 25, ESP25.88027, Society of Engineering Sciences.

Schetky, L, 1979, "Shape Memory Alloys," Scientific American, Vol. 241, p. 74.

Song, O., Librescu, L., and Rogers, C. A., 1991, "Static Aeroelasticity Behavior of Adaptive Aircraft Wing Structures Modelled as Composite Thin-Walled Beams," Proceedings, International Forum on Aeroelasticity and Structural Dynamics, Aachen, Germany, 3-6 June 1991; pp. 46-55.

Spangler, R. L. and Hall, S. R., 1990, "Piezoelectric Actuators for Helicopter Rotor Control," AIAA Paper No. 90-1076, Proceedings, 31 st SDM Conference, Long Beach, Ca, 2-4 April, 1990.

Uchino, K, 1986, "Electrostrictive Actuators: Materials and Applications," American Ceramic Society Bulletin, 65(4): pp. 647-652.

Wada, B. K., Fanson, J. L., and Crawley, E. F., 1990, "Adaptive Structures," J. of Intelligent Material Systems and Structures, Vol. 1, No. 2.

Chapter 2

The Mechanism of Control with Induced Strain Actuators

The mechanism by which an induced strain actuator exerts control over a structure and the best way to enhance this control are the subject of this chapter. At the very outset, it is important to note that induced strain actuators are not the only means of achieving structural control. Conventional actuators like proof-mass dampers and gas-jets have long been used for active structural control (Zimmerman et al., 1984; Skidmore and Hallauer, 1985; Schaffer and Holzach, 1985; Hallauer and Lamberson, 1989). However, induced strain actuators have something special to offer. They need not be separate elements attached after construction; they can be integrated into the structure and thus do not change the overall structural properties like eigen-frequencies and mode shapes. Furthermore, in contrast to conventional point force actuators, induced strain actuators do not require a back reaction.

To facilitate further discussion of actuation mechanisms, induced strain actuators must be formally defined: *Any actuator that develops strains in response to a stimulus, in principle, can be thought of as an induced strain actuator.* The strains which the actuator develops may be due to effects such as material phase change, electromechanical coupling,thermomechanical coupling or magnetomechanical coupling. In the absence of

all mechanical constraints, the strain which develops in an actuator is termed as free induced strain, Λ. The total strain in the actuator can thus be written as:

$$\varepsilon = \varepsilon_m + \varepsilon_{th} + \Lambda \ ,$$

Total strain = mechanical strain + thermal strain + free induced strain

Free induced strain is the mechanism by which induced strain actuators exert control on the structure to which they are attached. Actuator free strain provides structural stress, strain, and/or displacement utilized for control. With the above expression it is possible to model the induced strain actuator structure interaction irrespective of the details of how Λ relates to a certain stimulus.

2.1 Mechanisms of structural control

The two elementary components of an active structure are the induced strain actuator, and the structure to which it is attached. These components integrated together form a system. Generally, the actuators are assembled symmetrically about the plate or beam structure as shown in Fig. 2.1. When the actuators are activated in phase they exert a pure compressive or extensional force on the substrate structure. When activated out-of-phase where one actuator contracts and the other expands, a force couple is produced and induces flexure in the substrate structure. This configuration is the most common mode

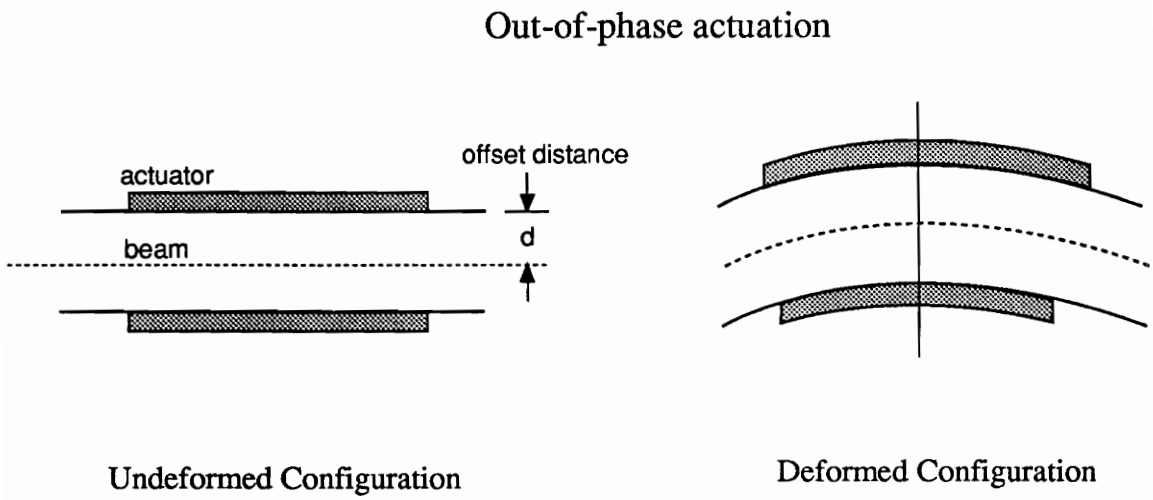

Figure 2.1 Symmetric actuator/substrate geometry. Bending action.

in which actuators are used to influence structural response. In a case where the actuator is bonded on one side of the structure only, the structure becomes unsymmetric and the bending and extensional response are coupled.

The actuator and the structure can be assembled in either of three ways:

i) by surface bonding the actuator to the structure

ii) by embedding the actuator within the structure

iii) by attaching the actuator to the structure at discrete points.

The first two configurations although physically different are mechanically identical, since the induced strain actuator is continuously connected with the structure. The third configuration is fundamentally different from the first two configurations, and as yet has much in common with the first two. The differences are first highlighted, and the commonalities will be presented later.

2.2 Differences between bonded and discretely attached actuators

The first principle which must be recognized is that an actuator embedded in a structure along its neutral axis, when activated in contraction, will not buckle or bend the structure. This principle holds for any level of compressive force that the actuator may apply to the

structure. If the actuator is embedded or surface bonded at an offset from the neutral axis of the structure, the structure will bend, but again not buckle. Thus, from the point of view of buckling action, an embedded or a surface bonded actuators are no different. When a structure with embedded actuators deforms, the actuators also deform along with the structure, and therefore the distance between the line of action of the force exerted by the actuator on the structure and the structure remains unchanged, and hence no buckling. This principle is treated in detail in Chapter 3.

The purpose of embedded actuators is by no means to buckle the structure in which they are embedded. But the fact that they cannot buckle the structure brings out a more subtle limitation of such actuators - that the in-plane force of the actuators does not directly contribute to modifying the structural response. The most force that the actuator exerts on a structure is in-plane, and as pointed out, the in-plane force does not directly contribute to the out-of-plane displacements. In the case of actuators offset from the neutral axis, the in-plane force contributes only indirectly, i.e., in the development of a moment on the structure. The moment is the product of the actuator force and actuator offset distance.

When an actuator is attached to the structure at discrete points, the scenario is different. In such a configuration, the structure and the actuator can deform independently; thus the in-plane force of the actuator, which does not contribute directly in case of bonded

actuators, can cause out-of-plane displacements of the structure. Now, since the in-plane force of the actuator is coupled to the out-of-plane displacements, structural buckling is a possibility. Practically, with the limited stroke of the currently available induced strain actuators, true buckling is not possible. Available actuators would stroke saturate much before large displacements occur in the structure.

It is important to recognize that by simply attaching the actuators at discrete locations (as opposed to bonding) the in-plane force does not immediately begin to contribute to the out-of-plane displacements, especially for flat structures. For the in-plane force to influence out-of-plane motion in a flat structure, an initial minimum out-of-plane displacement must occur first. However, for thin plate like structures, where the initial offset distance is of the order of the plate thickness, even a small out-of-plane displacement can make a substantial difference between bonded and discretely attached actuator performance.

2.3 Possible Configurations of Discretely Attached Actuators

The problem of a structure with discretely attached actuators can be formulated in two ways, depending upon whether the actuator being used has significant or negligible flexural stiffness. This division is not necessary, but it simplifies the analysis, as will be shown. The two configurations, along with their peculiarities, are introduced in the

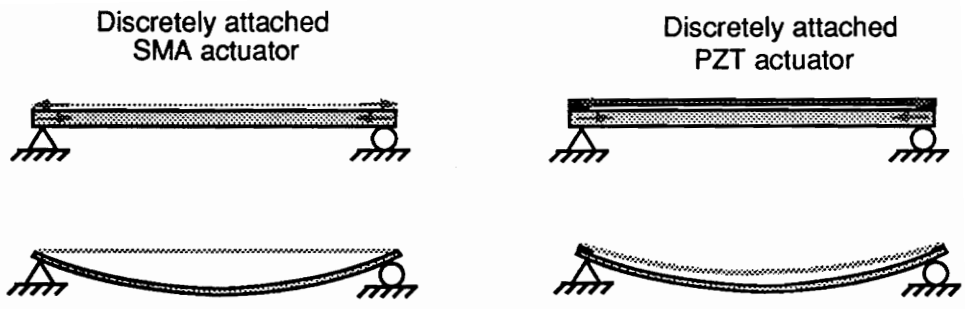

Figure 2.2 Possible configurations of discretely attached actuators.

following sections.

2.3.1 Actuators with negligible flexural stiffness

When an actuator, such as a shape memory alloy available in the form of a wire, is attached to the structure at two discrete points; it exerts point forces on the structure, with the direction of the force along a straight line joining the two points of attachment (See Fig. 2.2). Because the actuator has negligible flexural stiffness, it essentially behaves like a pre-tensioned cable between the two points. In such an event the structural response can be computed without any regard to the flexural stiffness of the actuator. In principle, for a given actuator force or energy input this configuration is the most effective, but because of the band-width limitation of the shape memory alloy actuators it can only be used for low frequency control applications. Furthermore, such an actuator can only produce a compressive force at least in the simple configuration outlined earlier. In spite of these limitations, for quasistatic applications this configuration provides a tremendous improvement in structural control possible with bonded or embedded actuators. The formulation and the experimental results for this configuration are presented in Chapter 4.

2.3.2 Actuators with flexural stiffness

In the case of actuators like piezoceramics, which are available in the form of plates and have significant flexural stiffness, the actuator no longer remains straight between the two attachment points but bends along with the structure (See Fig. 2.2). In this case the structural response is coupled to the actuator's flexural stiffness, and the formulation must reflect this coupling. It is, of course, possible to recover the solution for the first configuration (where the actuator has negligible flexural stiffness) from this formulation by setting the flexural stiffness ratio between actuator and structure very low. Since this configuration has very close physical resemblance to the bonded actuator configuration it is appropriate to point out another difference between the bonded and this configuration. The difference lies in the ability, in this case, to increase the actuator offset distance (the offset distance in the present context represents the distance through which the actuator is lifted off of the surface of the structure plus the surface distance from the neutral axis at the two points of attachment) without any increase in the flexural stiffness of the actuator-structure composite system. By offsetting the actuator as above, the flexural stiffness of the composite structure as seen by an external transverse load is increased, but from the point of view of the actuator itself inducing flexure into the structure, there is no change in the flexural stiffness. Recognition of the above fact is a key point in understanding the mechanics of active structure. It will be shown in Chapter 5 that the offset distance is a key parameter which if used properly can substantially enhance control compared to the bonded actuator configuration. The other parameters which influence control in this configuration and their optimization is discussed in Chapter 5.

2.4 Relationship between discretely attached and bonded actuator configurations

An actuator discretely attached to a structure and an actuator bonded on the surface of the structure are physically similar. In fact if the actuator lies on the surface of the structure connected at two points only it would physically appear exactly the same as a bonded actuator. The formulation for the discretely attached and the bonded actuator configurations must also reflect this resemblance. This was the motivation for the work presented in Chapter 6. A brief discussion of the similarities in the two configurations is now presented.

When a bonded actuator is activated, it induces strain in the substrate structure through a build-up of shear stress in the bonding layer. As seen in Fig. 2.3, the shear stress at the edge of the actuator rises very sharply and then again drops down to zero within a distance of 2 to 3 actuator thicknesses away from the free edge (Liang and Rogers, 1989; Lin and Rogers 1991). Away from the edge, there is a uniform state of stress in the actuator and the structure (tensile in the actuator and compressive in the beam - in the case the actuator is activated to contract). Thus, the transfer of force from the actuator to the structure takes place in a very small region close to the free end. This is the reason why the action of the actuator on the structure is often modelled with concentrated moments applied at the two ends of the structure.

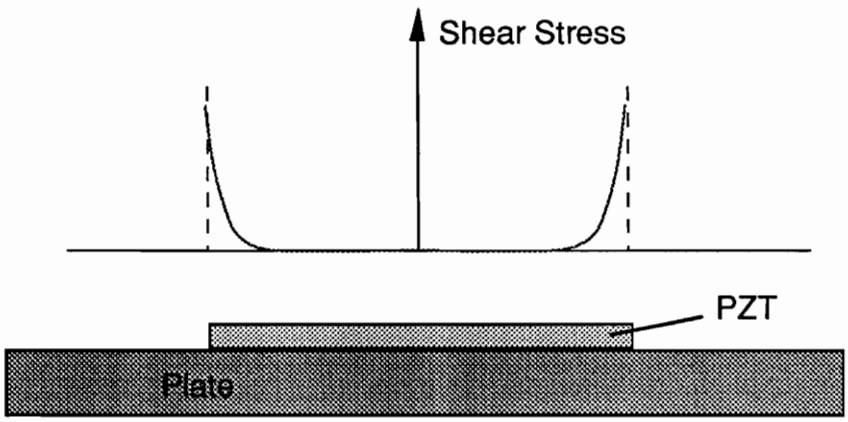

Figure 2.3 Shear stress distribution at actuator-substrate interface.

For a discretely attached actuator, the transfer of forces between the actuator and the structure also takes place at the two ends where the actuator is attached to the structure. Thus, the two configurations are alike, except for the fact that in one configuration both the actuator and the structure deform together and in the other they deform independently.

Structural response can be considered a combination of a linear part, which is purely due to the end moments, and a non-linear part which is due to the influence of the in-plane force on the out-of-plane displacements. With discretely attached actuators if the response is divided in this manner then the linear portion is equivalent to the response of the bonded actuator. Technically, the bonded actuator configuration is a degenerate of the discretely attached configuration. Formally, this means that it should be possible to derive the structural response of the bonded actuator by treating the actuator and the structure as separate bodies linked together at the two end points of the actuator. It is indeed possible to do so (as shown in Chapter 6), with one additional constraint that the strains at the interface between the actuator and the substrate be continuous. Continuity of strains at the interface conditionally conforms to the fact that the actuator and the structure are deforming together, not independently. In Chapter 6, the approach described above is used for deriving the structural response equations of a bonded actuator. These equations are shown to be the same as obtained from a more rigorous consistent plate model formulation (Crawley and Lazarus, 1989).

2.5 Research Objective

Since the introduction of the concept of intelligent structures, the only configuration of attaching actuators to the structure which has been considered is the bonded or embedded configuration. This configuration is perhaps the easiest, and it lends itself very well to the general concept of a fully integrated intelligent structure, but it does not utilize the full capabilities of available induced strain actuators. With material scientists seemingly pushing the electromechanical coupling of actuators to its limits, it is necessary to explore actuator architectures that maximize control. In this research, an alternate actuator/structure arrangement is studied, and it is shown to enhance structural control.

In order to show the feasibility of the concept a simple beam-actuator structure is considered. The necessary response equations are developed, and the experimental verification is presented. First, in Chapter 3 the difference between an internal and an external actuator force is highlighted, then the structural response to an SMA type actuator is considered in Chapter 4, followed by the structural response to PZT type actuators in Chapter 5. In Chapter 6 the response of a bonded actuator is derived from considerations similar to that of discretely attached actuator configuration.

2.6 References

Crawley, E. F. and Lazarus, K. B., 1989, "Induced Strain Actuation of Isotropic and Anisotropic Plates," AIAA Journal, Vol. 29, No. 6.

Hallauer, W. and Lamberson, S., 1989, "Experimental Active Vibration damping of a Plane Truss Using Hybrid Actuation," AIAA paper No. 89-1169, *Proceedings*, 30th SDM conference, Mobile Alabama.

Liang, C. and Rogers, C. A., 1989, "Behavior of Shape Memory Alloy Actuators Embedded in Composites," *Proceedings*, 1989 International Composites Conference, Beijing, China, 1-4 August.

Lin, M and Rogers, C. A., 1991, "Analysis of Stress Distribution in a Shape Memory Alloy Composite Beam," AIAA Paper No. 91-1164, *Proceedings* 32nd SDM Conference, Baltimore, MD, 8-10 April.

Schaefer, B. and Holzach, H., 1985, "Experimental research on Flexible Beam Modal Control," J. of Guidance Control and Dynamics, 8:597-604.

Skidmore, G. R. and Hallauer, W., 1985, "Experimental-Theoretical Study of Active Damping with Dual Sensors and Actuators," AIAA Paper No. 85-1921-CP, *Proceedings* AIAA Guidance, and Control Conference, Snowmass, CO.

Zimmerman, D. C., Inman, D. J. and Horner, G. C., 1984, "Dynamic Characterization and Microprocessor Control of the NASA/UVA Proof Mass Actuator, AIAA Paper No. 84-1077, *Proceedings* 25 th SDM Conference.

Chapter 3

Response of Composite Beams to an Internal Actuator Force

3.1 Nomenclature

P	Compressive force
Q	Conservative axial force, (See Fig. 3.4)
F	True follower force, (See Fig. 3.4)
l	Length of column
E	Young's modulus
I	Moment of inertia of column cross-section
d	Actuator offset distance
x	coordinate, (See Fig. 3.1)
$w(x)$	Transverse displacement of beam
u^0	Middle surface axial displacement
w^0	Middle surface transverse displacement
ε_x^0	Extensional strain of middle surface
κ_x^0	Curvature of middle surface
N_x	Inplane stress resultant

M_x Internal moment resultant

δu^0 Virtual middle surface axial displacement

δw^0 Virtual middle surface displacement

A_{11} In-plane stiffness

D_{11} Flexural stiffness

$( )_x$ Derivative with respect to coordinate x

3.2 Introduction

Shape memory alloy hybrid composite materials have demonstrated numerous control capabilities. One such capability is the controlled bending of structures. In this chapter the response of a cantilevered beam to an internal actuator is examined. The modelling of the compressive force exerted by the induced strain of the actuator on the beam is discussed. The results obtained from treating the force as an external follower force are presented. The response to an internal force such as exerted by an internal shape memory alloy actuator is quite different from that produced by loads due to sources external to the beam. Contrary to normal expectations such an internal force although compressive does not produce any buckling tendencies or any other instabilities in the beam. This principle which is already in use in the design of civil engineering structures is discussed in detail. If the actuators are embedded off of the neutral axis, then due to the eccentricity the beam bends, but again without any buckling tendency. The experimental results obtained for this configuration are also presented.

3.2.1 Active Control Concepts

Shape memory alloys, and nitinol in particular, have many unique properties and characteristics (Jackson et. al., 1972). One of the two most important characteristics from a structural control standpoint is the large change in the Young's modulus when the material undergoes a martensitic transformation. The other is the characteristic shape recovery effect, which manifests itself in a remarkable restoring force and/or recovery of a tremendous amount of inelastic strain. From these two basic material characteristics, it is possible to classify the structural control schemes which rely on embedded SMA fiber actuators or reinforcement as active properties tuning (APT) and active strain energy tuning (ASET) (Jia, and Rogers, 1989).

For active properties tuning, SMA fiber actuators are embedded in an advanced composite material like graphite epoxy. The embedded fibers are actuated by resistive heating, .i.e., passing an electrical current through the fibers. Once the temperature of the fibers exceeds the transition temperature, the Young's modulus of the SMA fibers may be increased in a controlled manner from 4 Mpsi to 12 Mpsi (Jackson et.al., 1972). Not only is the stiffness of the structure increased in this manner, but also the yield strength is increased.

Active strain energy tuning uses the same mechanisms as described above for active property tuning but adds another important control parameter, the restoring stress

associated with embedded inelastically elongated SMA fiber actuators 'trying' to regain their original shape by contracting.

Using either active properties tuning or active strain energy tuning can result in significant control of the structural response of a composite structure. The difference between the two concepts is that APT changes the structural response by varying the stiffness of the structure alone while ASET depends primarily on the recovery force of the plastically elongated fibers to change the structural response. Using active strain energy tuning in almost all cases results in more versatility of control than possible in APT, and can give a wide range of deflection control (Liang, Jia, and Rogers, 1989).

The ability of ASET in active vibration and structural acoustic control of SMA hybrid composites has already been demonstrated theoretically (Liang, Jia, and Rogers, 1989) and experimentally (Rogers, 1990). A constitutive model of shape memory materials, which is essential for the analysis and control of SMA hybrid composites has also been developed (Liang, and Rogers, 1990). In this paper we look at further applications of SMA strain induced actuators, and in particular examine their use for active bending control.

It must also be mentioned that SMA are not the only means for active structural control, induced strain actuators such as piezoceramic patches can also be used for active

structural control. A laminate plate theory for such actuators has been presented by Wang and Rogers (1990). However, SMA's because of the the large forces they can generate hold the most promise for applications such as active bending control.

3.2.2 SMA hybrid composite configurations

There are two possible ways of embedding shape memory alloy actuators in a composite (Rogers, Liang, and Jia, 1989). One is that inelastically elongated shape memory alloy fibers are embedded in a composite material and are constrained from contracting to their normal length during the curing process, then upon curing the inelastically deformed fibers are an integral part of the composite material and the structure. The other configuration involves the creation of 'sleeves' within the composite laminate, in which the plastically elongated shape memory alloy can be inserted and then clamped at both ends. When these fibers are heated, by passing a current through them, they try to contract to their normal undeformed length, and generate an internal force on the structure. In the first configuration the force of the actuators is a distributed force applied to the structure along the length of the fiber, whereas in the second configuration, the force of the actuator is a concentrated force applied to the structure at the end of the sleeve. It is this latter configuration which is examined in this paper.

3.3 Beam Response

3.3.1 Modelling of the actuator force

In this chapter we consider a cantilevered beam with actuators in sleeves. With this arrangement the force exerted by the actuator is a concentrated point force applied at the tip of the beam. Since the actuator is within the beam it is constrained to follow the contour of the beam, and therefore the force exerted by it is a tangential force i.e. the force which preserves its direction tangential to the deformed axis of the beam. With a sleeve arrangement, in addition to the tangential point force at the end of the beam there is a contact force also exerted by the fiber on the beam, the effect of this force will be discussed later.

In actuality the force of the actuator is an internal force, which as will be discussed later does not produce any buckling. However, in the earlier part of this investigation the force was treated as an external follower force and the results of this analysis are interesting and unusual and are therefore briefly presented here.

3.3.2 Response of the beam to an external follower force

The problem of a cantilevered beam subjected to a compressive follower force has been treated earlier, and is known as the Beck's problem (Beck, 1952). The response of a cantilevered beam to an eccentric compressive follower force, however, has not been

investigated previously. This problem is similar to Beck's column except that in this case the force is eccentric and it is possible to get a solution using the equilibrium method. This permits us to study the response of a structure to a nonconservative force, throughout the force range up to the critical load. The critical buckling load obtained using the kinetic method for this case is, however, the same as the Beck's problem.

Consider the uniform cantilevered linear elastic column under the action of a an eccentric follower force P, shown in Fig. 3.1. The force of the actuators is modelled as a concentrated follower force applied eccentrically at the free end. The length of the column is l, and the flexural rigidity EI. The follower force is offset from the neutral axis by the distance d. The offset causes a concentrated end moment Pd at the free end. This tip moment results in a nonhomogeneous boundary condition, making it possible to get a solution using the equilibrium method.

The governing equation of motion for the displacement $w(x)$ of the column is given by

$$EIw_{,xxxx} + Pw_{,xx} = 0 \tag{1}$$

The boundary conditions at the fixed end are

$$w(0) = 0, \qquad w_{,x}(0) = 0$$

and for the free end the boundary conditions are

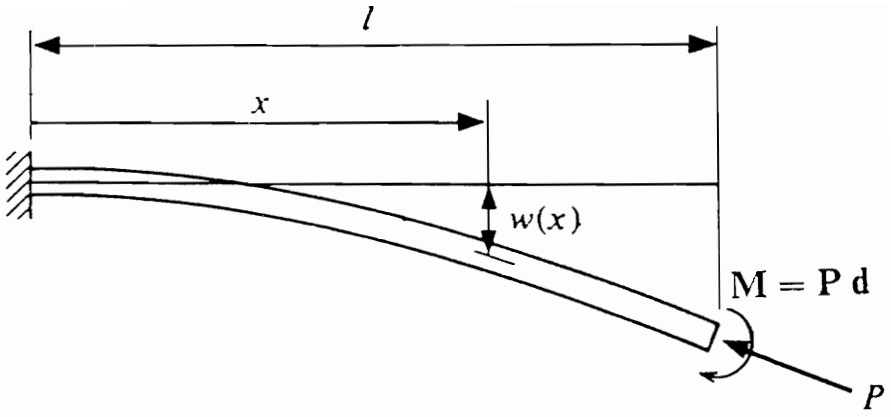

Figure 3.1 Geometry of the problem.

$$EI\,w_{,xx}(l) = Pd \qquad w_{,xxx} = 0$$

The solution of the governing equation subject to the above stated boundary conditions is

$$w(x) = -d\{\sin kl\,(\sin kx - kx) + \cos kl\,(\cos kx - 1)\} \tag{2}$$

where

$$k = \sqrt{\frac{P}{EI}}$$

The deflection of the free end simplifies to

$$w(l) = -d\{1 - kl\sin kl - \cos kl\} \tag{3}$$

Figure 3.2 is a plot of the force P vs. $w(l)$. The response of the beam is quite unusual and interesting. Initially the tip moment dominates the response and the beam bends down, but then as the vertical component of the follower force increases the beam bends upwards till it reaches the critical load. There is no static instability up to the critical load. Similar response has been reported by Plaut (1976) for an inverted double pendulum with imperfections.

The shape of the deflected beam at various load levels is shown in Fig. 3.3, where it is noticed that the sign of the bending moment caused by the eccentric tangential load does not disagree with the sense of curvature.

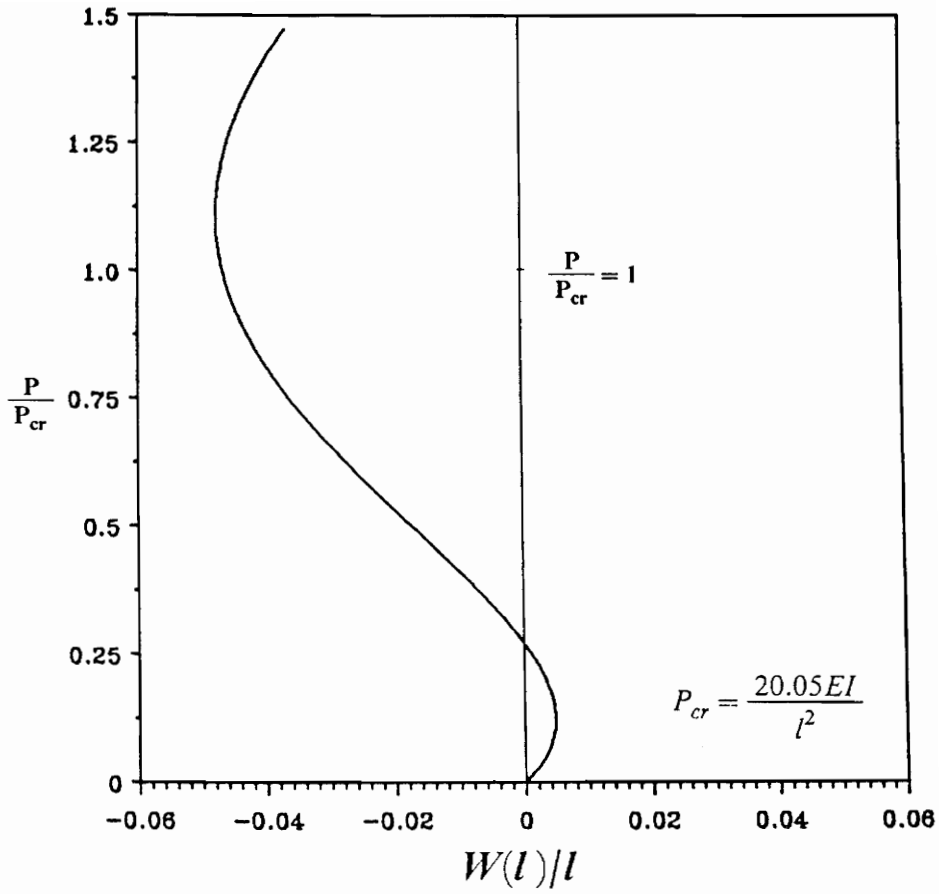

Figure 3.2 Column load-deflection curve. (offset distance=0.1 in.)

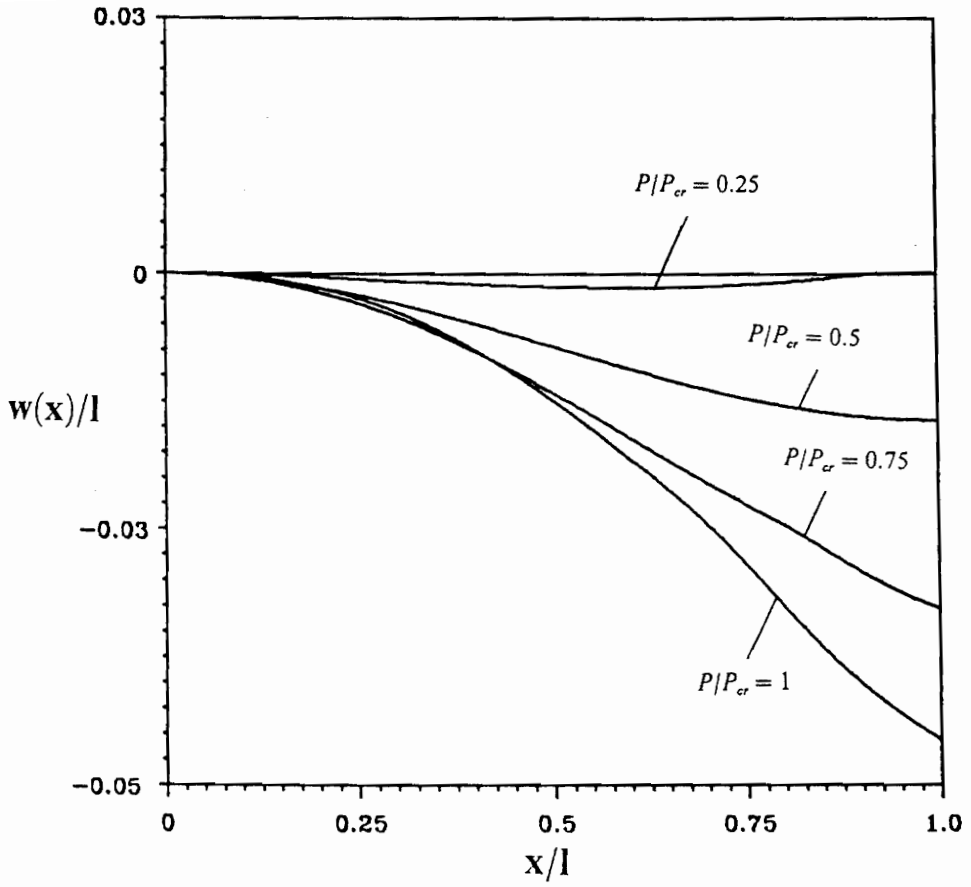

Figure 3.3 Shape of deflected beam at various load levels.

A large rotations analysis based on the full Green Lagrange strain

$$\varepsilon_x^0 = u_{,x}^0 + \frac{1}{2}\left\{(u_{,x}^0)^2 + (w_{,x}^0)^2\right\} \tag{6}$$

and the following more exact expression for curvature (Novozhilov, 1953):

$$\kappa_x^0 = \frac{w_{,xx}^0}{\sqrt{1-(\frac{dw^0}{dx})^2}} \tag{7}$$

gives the following Euler equations and boundary conditions derived using the principle of virtual work

$$\frac{d}{dx}N_x(1+u_{,x}^0) = 0 \tag{8}$$

$$\frac{d}{dx}(N_x w_{,x}^0) + \frac{d}{dx^2}\left[\frac{M_x}{\sqrt{1-(w_{,x}^0)^2}}\right] + \frac{d}{dx}\left[\frac{M_x}{\{1-(w_{,x})^2\}^{2/3}} w_{,xx}^0 w_{,x}^0\right] = 0 \tag{9}$$

Boundary Conditions

$$N_x(1+u_{,x}^0)\delta u^0=0 \tag{10}$$

$$\left[N_x w_{,x}^0+\frac{d}{dx}\left[\frac{M_x}{\sqrt{1-(w_{,x}^0)^2}}\right]+\frac{M_x}{\{1-(w_{,x}^0)^{3/2}\}}w_{,xx}^0 w_{,x}^0\right]\delta w^0=0 \tag{11}$$

$$\frac{M_x}{\sqrt{1-(w_{,x}^0)^2}}\delta w_{,x}^0=0 \tag{12}$$

where N_x and M_x are the internal axial force and moment resultants. w^0 and u^0 are the middle surface displacements in the transverse and axial directions respectively.

Using Hookes law, for a symmetric layup

$$N_x=A_{11}\varepsilon_x^0 \tag{13}$$

$$M_x=D_{11}\kappa_x^0 \tag{14}$$

the set of nonlinear equations was solved using the IMSL subroutine BVPFD. The more rigorous large rotations analysis also gives exactly the same response.

For a beam subjected to a conservative axial compressive force buckling takes place at the Euler buckling load, whereas if the force is a true follower force there is no static instability as noted above. This transition in the response of the beam from a condition of static instability to no static instability can be analyzed in another way also. This is

done by starting with a beam with a pure conservative axial force and then adding to it a follower force, gradually increasing the percentage of the follower force. The model and the results of the large rotations analysis for this configuration are shown in Fig. 3.4. The slope at the tip of the beam is neglected in computing the axial component of the follower force F, and, therefore, the total axial force P is simply the algebraic sum of Q and F. When the follower force is less than or equal to 47% of the total axial force the divergence phenomenon is observed. For the follower force percentage higher than 47% and upto 51% the numerical solution could not be obtained beyond the points indicated in Fig. 4 indicating some instability in this range. For follower force percentage greater than 51% of the total force no static instability is observed and the pattern of the the response begins to resemble that of a true follower force. At 50% the follower force and the axial conservative force are both equal and this corresponds to the case of the tangency factor η=0.5 reported by Kordas (1963). This analysis confirms the earlier results where for η<0.5 the instability is in the form of divergence and for η>0.5 there is flutter.

3.3.3 No buckling due to an internal actuator force

Now we discuss the phenomenon alluded to earlier where it was pointed out that the effect of this internal force is quite different from that produced by loads due to sources external to the member. The fundamental principle that axial loads and bending moments

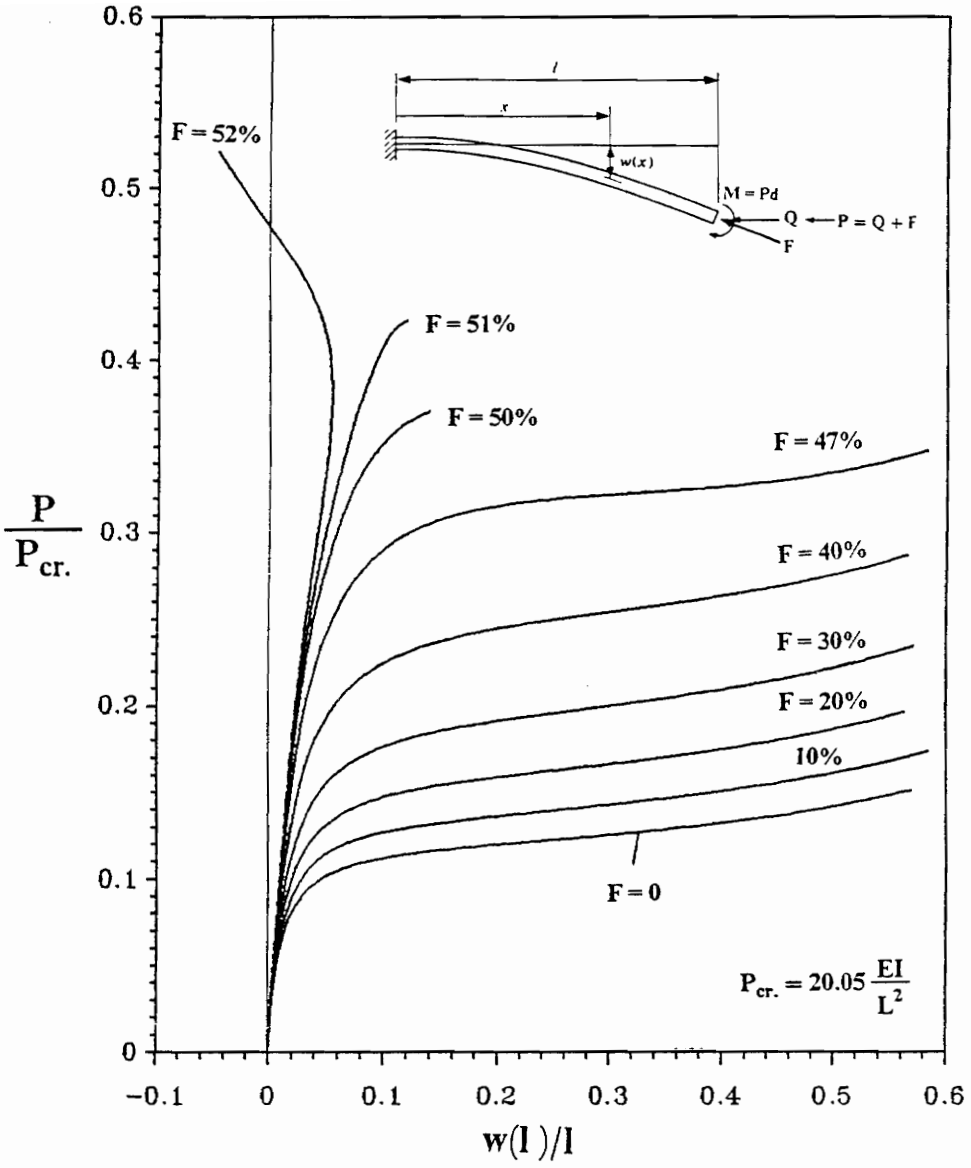

Figure 3.4 Beam response to a partial follower force.

due to internal forces do not produce any buckling tendencies is used in the design of prestressed concrete compression members. The fundamental concept is, however, repeated (Lin, 1955). Consider a column under the action of an internal actuator force. If we separate the actuator from the outer column and treat them as two free bodies as shown in Fig. 3.5. Then considering the outer member alone, it is a column under direct compression, and any slight bending of the column will result in an eccentricity on a section such as A-A, and hence in a tendency to buckle. But, considering the actuator as a free body, there will exist an equal eccentricity with an equal and opposite force, producing a tendency to straighten itself. The tendency to straighten is exactly equal and opposite to the tendency to buckle, and hence the resulting effect is zero.

A simple experiment was also performed to verify this principle for the application at hand. A square plastic tube with an internal hole was used. The beam was clamped at one end and free at the other as shown in Fig. 3.6. A flexible wire was attached at the free end of the beam and then made to pass through the hole in the beam. The wire coming out from the fixed end of the beam was attached to a load hanger where weights could be added to simulate the force of the actuators. Since the diameter of the wire was slightly smaller than the hole inside the tube there was some clearance between the wire and the inner surface of the tube. Because of the clearance the deflection of the outer column will not at first bring the actuator wire to deflect together with it, hence the eccentricity of the compressive force on the outer column is changed, thus resulting in

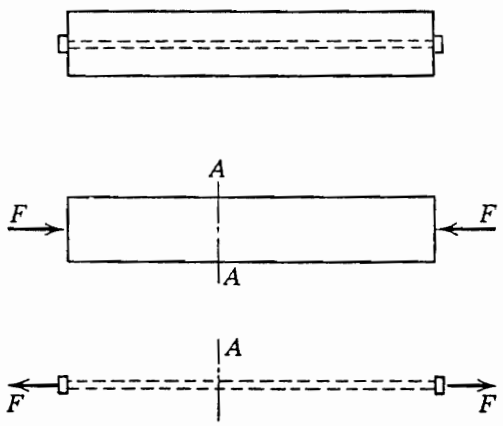

Figure 3.5 Balancing action of outer member and actuator.

column action.

Before the wire makes contact with the inner surface of the tube the problem is essentially the same as a *Tilt Buckling* problem as shown in Fig. 3.7 (Simitses, 1976). In this case although the force does not remain fixed in direction, but it passes through a fixed point. This is a case of load-behavior (during the buckling process) problems where the system may still be considered as conservative. Note that the follower-force problem does not fall in this category.

The boundary conditions for this configuration are:

$$w(0)=0 \quad w_{,x}(0)=0 \quad w_{,xx}(l)=0$$

and

$$-\left[EI\,w_{,xxx}(l)+P\,w_{,x}(l)\right]=-P\frac{w(l)}{l} \tag{15}$$

Use of these boundary conditions leads to the following characteristic equation

$$\tan kl=0 \tag{16}$$

which gives

$$(kl)_{cr}=\pi \qquad P_{cr}=\frac{\pi^2 EI}{l^2} \tag{17}$$

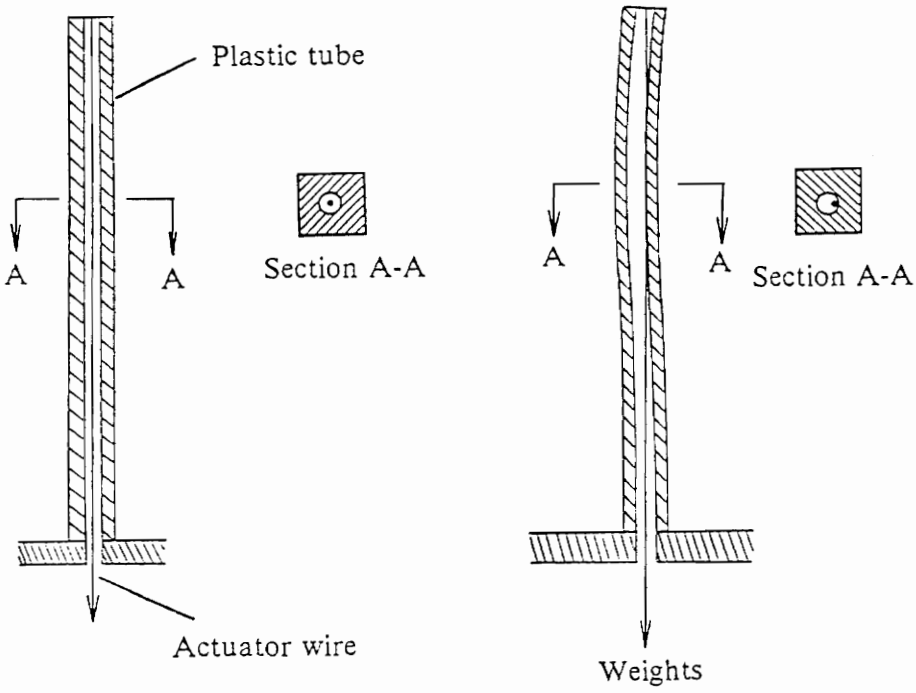

Figure 3.6 Plastic tube (a) under no load (b) tilt buckled

For the plastic tube the flexural stiffness was measured to be 41.32 lb.in^2 which for a length of 14 in. gives a critical buckling load of 2.06 lb. In the experiment because of the minimal clearance it was difficult to establish the exact force at which the tube buckled and made contact with the wire, however it was found to be between 2 and 2.5 lb., which agrees quite well with the calculated critical buckling load of 2.06 lb.

The column action is limited to the differential deflection of the column and the actuator. Once the tube made contact with the wire, there was no further column action, neither any instability such as flutter. The weight was increased much beyond the Beck's column buckling load of 4.23 lb. and no instability whatsoever was observed. The load was increased to a point (20 lb.) where the plastic tube failed at the point where the wire was attached to it at the top.

With reference to Fig. 3.6, it is also pointed out that if the actuator lies exactly at the center line of the plastic tube and there is minimal clearance between the wire and the tube, bending of the tube does not produce a change in the length of the center line. Therefore, the height of the weights does not change as the tube is bent. Hence the potential energy of the weights remains unchanged and there is no energy source to cause bending or buckling of the tube.

This concept is now being used in the design of offshore platform conductors (Stahl and

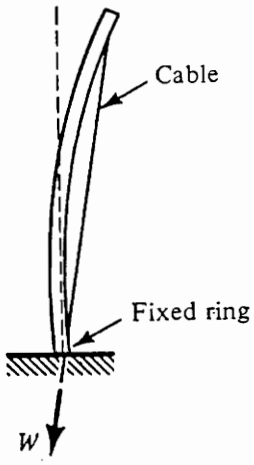

Figure 3.7 Tilt buckling configuration.

Baur, 1983). In this case the weight of the casing string hanging inside of the conductor is like an internal force similar to that of an actuator.

3.4 Experimental Results

In the case the actuators are offset from the neutral axis,the compression in the outer member is still equal and opposite to the tension in the actuators. Any deflection of the structure will still displace both of them together, and there will be no column action. The eccentric actuators, however, will produce deflection of the member due to the applied tip moment. To investigate the amount of bending control possible a fiberglass beam with sleeves was used. The sleeves were created by embedding teflon fibers (offset from the neutral axis) in the fiber glass. Upon curing the composite specimen the teflon fibers are pulled out leaving a fine sleeve throughout the length of the beam. The beam width was 1 inch and a thickness of 0.17 inches, the sleeves were offset from the middle surface by .06 inches. The flexural stiffness of the beam was measured to be 175 $lbf.in^2$. The diameter of the sleeves was .035 in. Two .03 inch prestrained nitinol wires were then inserted through the sleeves to act as the actuators. The beam was erected vertically and clamped at the bottom end as shown in Fig. 3.8. Ordinary weights were hung from the wires at the bottom to simulate their actuation. The load versus beam tip deflection is shown in Fig. 3.9 where the load has been normalized by the Beck's column critical buckling load. The solid line represents the beam tip deflection due to a pure end moment

equal to the the applied load times the eccentricity. The response of the beam is observed to be linear but the deflection is slightly more than that due to a simple end moment. Once again no instability was noted for loads up to 1.5 times the Beck's column critical buckling load. A study is underway to understand this difference between the experimental and theoretical results.

To check if the same order of deflections could be achieved by actuating the two nitinol wires the weights hung from the nitinol wires were removed and the nitinol wires were clamped at the bottom of the beam. An electrical current was applied to the wires. This causes a restoring force (due to the shape recovery effect) to be applied at the tip of the beam, and the beam bends. The beam tip deflections obtained earlier by hanging the weights were conveniently achieved, infact, for the maximum deflection ($\delta/l \geq 0.06$) the recovery stress in the nitinol wires would be only of the order of 15 Ksi. and the two nitinol wires constitute a volume fraction of less than one percent.

As far as column action is concerned, it is immaterial whether there is any frictional loss along the length of the actuator, because the tension in the actuator is always balanced by the compression in the outer member, whatever frictional losses may occur. Hence, whether there is frictional loss or not, there is no column action due to the actuator force (Lin, 1955).

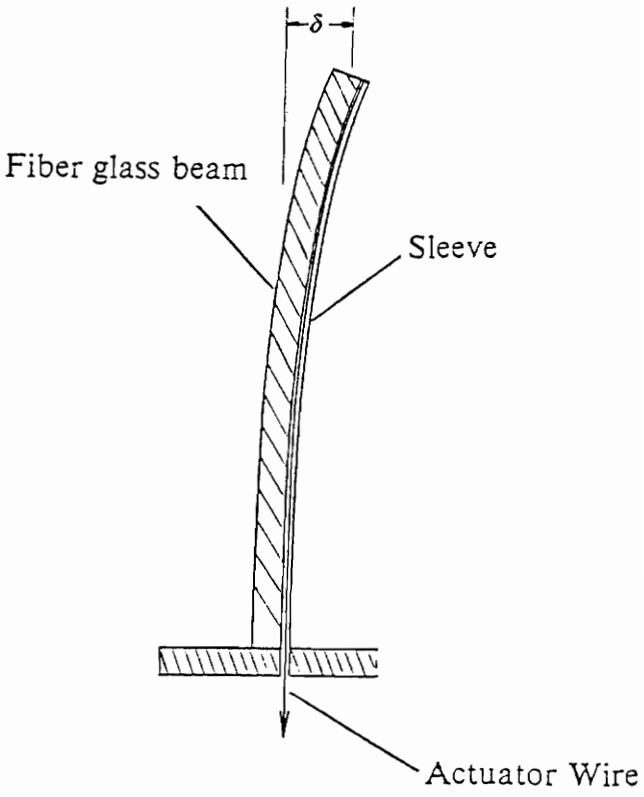

Figure 3.8 Eccentrically loaded fiber glass beam.

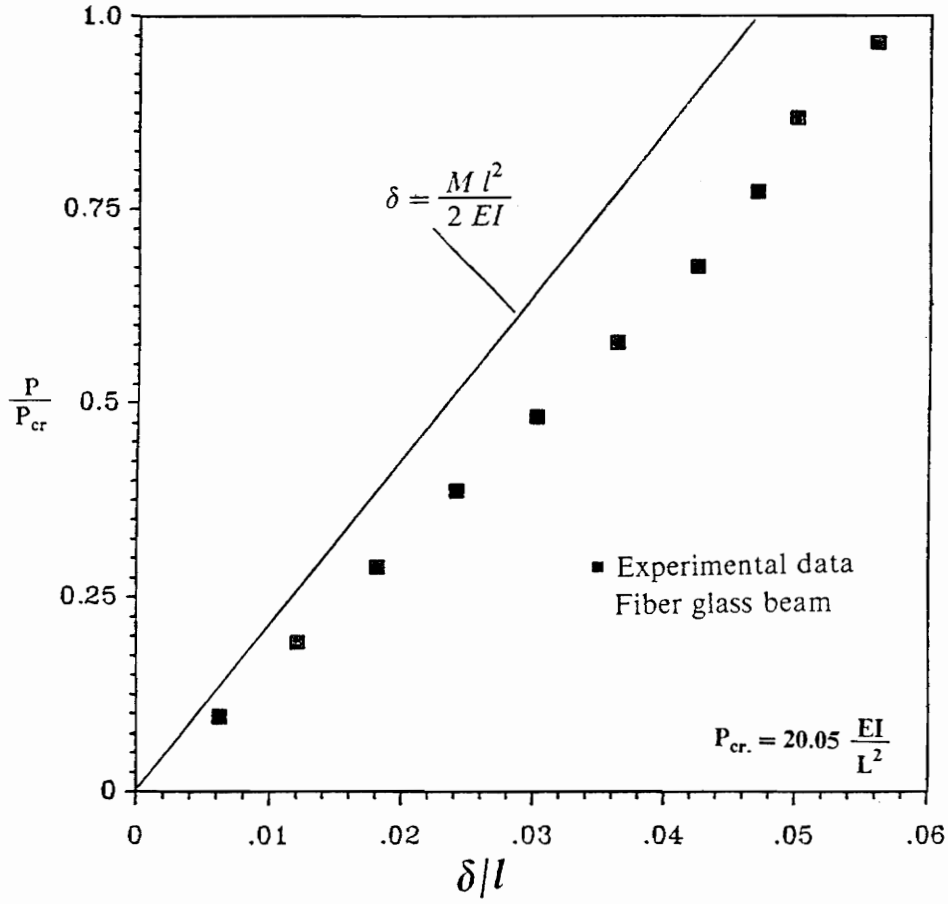

Figure 3.9 Fiber glass beam. Load versus beam tip deflection.

3.5 Conclusion

With increasing interest in shape memory alloy hybrid composites, there is a need to understand the response of structures to forces such as exerted by internal induced strain actuators. In this chapter some basic concepts relating to structural response to embedded actuators are examined. A fundamental principle that no buckling takes place due to an internal actuator, whether firmly bonded to the composite or in a sleeve, is presented. Some new results of structural response to an eccentric follower force are also presented. By simply creating a non homogeneous boundary condition the equilibrium method is used to get the response to a follower force. This response is most unusual, and gives a feel for structural response to nonconservative forces.

The experiment on bending control confirms the possibility of using shape memory alloy actuators for active bending control of structures.

3.6 References

Jackson, C. M., H. J. Wagner, and R. J. Wasilewski, 1972, "55- Nitinol- The Alloy with a Memory: Its Physical metallurgy, Properties, and Applications," NASA-SP-5110,91 p.

Jia. J and C. A. Rogers, 1989. "Formulation of a Mechanical Model for Fiber Reinforced Composites with embedded SMA Actuators," Proceedings of 8th Biennial Conference on Failure Prevention and Reliability, Montreal, Canada, 18-20 September, pp. 203-210.

Liang, C., J. Jia, and C. A. Rogers, 1989, "Behavior of Shape Memory Alloy Reinforced

Composite Plates, Part 2: Results," Proceedings of the 30th Structures, Structural Dynamics and Materials Conference, AIAA-89-1311.

Rogers, C. A., 1990, "Active Vibration and Structural Acoustic Control of Shape Memory Alloy Hybrid Composites: Experimental Results," Proceedings of the International Congress on Recent Developments in Air and Structural Borne Sound and Vibration, Auburn University, 6-8 March 1990, pp. 695-708

Liang, C., and C. A. Rogers, 1990, "A One-Dimensional Thermomechanical Constitutive Relation of Shape Memory Materials," Proceedings of the 31st Structures, Structural Dynamics and Materials Conference, AIAA-90-1027.

Novozhilov, V. V., 1953, **Foundations of the Nonlinear Theory of Elasticity**, Graylock Press, Rochester, N.Y.

Wang, B. T. and C. A. Rogers, 1990. "Laminate Plate Theory for Spatially Distributed Induced Strain Actuators," Proceedings of the Fifth Japan-U.S. Conference on Composite Materials, Tama City, Japan, 24-27 June 1990.

Rogers, C. A., C. Liang and J. Jia, 1989 "Behavior of Shape Memory Alloy Reinforced Composite Plates - Part 1: Model Formulations and Control Concepts," Proceedings of the 30th Structures, Structural Dynamics and Materials Conference, AIAA-89-1389

Beck, M. 1952, "Die Knicklast des einseitig eingespannten, tangential gedruckten Stabes,". ZAMP, Vol.3, pp.225-228.

Plaut, R. H. 1976, "Branching analysis at coincident buckling loads of nonconservative elastic systems," Technical Report VPI-E-76-15, College of Engineering, Virginia Polytechnic Institute and State University, Blacksburg, Virginia, Aug. 1976.

Z. Kordas and M. Zyczkowski 1963, "On the loss of stability of a rod under a super-tangential force," Archiwun Mechaniki Stosowanej 15 ,p.7.

Lin, T. Y. 1955, **Design of Prestressed Concrete Structures**, John Wiley & Sons, New York.

Simitses, G. J. 1976, **An introduction to the Elastic Stability of Structures**, Prentice-Hall, Inc.

Stahl, B., Baur, M. P. 1983, " Design Methodology for Offshore Platform Conductors," Journal of Petroleum Technology, November, 1983.

Chapter 4

Bending and Shape Control of Beams Using SMA Actuators

4.1 Nomenclature

P	Compressive force
V	Applied shear force, (See Fig. 1)
q	Uniformly distributed transverse force, (See Fig. 1)
l	Length of column
E	Young's modulus
I	Moment of inertia of column cross-section
d	Actuator offset distance
x	coordinate, (See Fig. 1)
$w(x)$	Transverse displacement of beam
$u(x)$	axial displacement of beam
ε_a	Actuator strain
δ	Beam tip deflection
a	x location of point on beam through which actuator passes

$( )_x$ Derivative with respect to coordinate x

4.2 Introduction

In this chapter two new configurations for enhanced bending control of beams with induced strain actuators are presented. In the first configuration the actuator is external to the beam and passes through selective points on the beam. Since the actuator is outside the beam, differential movement between the actuator and the beam is possible; this results in enhanced bending due to the buckling action of the actuator force. Before actual buckling, there is a fairly large useful range of enhanced bending. In this range the beam displacements are much greater than can be obtained by embedded or surface bonded actuators. The theoretical formulation for this configuration and its experimental verification is presented.

In the second configuration, the actuator is so placed that the actuator offset distance and hence the induced tip moment is increased with only a minimal increase in the flexural stiffness of the beam. In this configuration the actuator is placed differently from the conventional embedded actuators; however, the beam response is exactly the same as an internal offset actuator. The experimental verification of this configuration is also presented.

The ability of Shape Memory alloy (SMA), i.e., nitinol actuators to induce large displacements for both the proposed configurations has been experimentally verified and these results are presented.

4.2.1 Limitations of Embedded Actuators for Shape Control

In recent years research in the area of adaptive structures has largely focused on active vibration and acoustic control. To date, investigations into the application of adaptive structures for shape control have been fairly limited and, in almost all these investigations, the induced strain actuator considered has been the piezoceramic actuator. Crawley and de Luis (1987), and Crawley and Lazarus (1989) demonstrated shape control of beams and plates with bonded and embedded piezoelectric actuators. Kokorowski (1979), and Chirappa and Claysmith (1981) have shown the feasibility of using piezoelectric actuators for optical system mirror or reflector shape control.

One of the candidates for active shape control is the adaptive hydro- or aerodynamic lifting surface. The variable camber wing, often referred to as the mission adaptive wing, offers many advantages over the fixed geometry wing (Sobieczky, Fung, and Seebass,1978; Chacksfield, 1980; Gilbert, 1981; Redeker, Wichmann and Oelker, 1986). Today, with sophisticated design tools, materials, and induced strain actuators, it may in fact be possible to make an adaptive hydro- or aerodynamic airfoil. Lazarus, Crawley, and

Bohlman (1990) have shown the potential benefits of using adaptive airfoils for aeroelastic control. In their trade studies they have shown that strain actuated adaptive wings can be used rather than conventional lifting surfaces to increase performance while reducing weight. They have also shown how shape memory alloy actuators due to their large actuation strain capability and high elastic modulus outperformed the piezoceramic adaptive structure for static control. Song, Librescu, and Rogers (1991) have considered a thin walled box type adaptive wing and have demonstrated the enormous benefits in static aeroelastic control of a swept forward wing. Ehlers and Weisshaar (1990) have shown how the static aeroelastic control can be enhanced using an adaptive laminated piezoelectric composite wing.

In all these investigations the actuators have either been embedded or bonded to the surface of the host material, and the basic mechanism by which these actuators deform the structure is either by producing in-plane forces or by producing moments. In most applications it is the moment which is used for shape control. This moment is a linear function of distance between the bonded actuator and the neutral axis of the structure. In order to maximize this moment, this distance must be maximized, but increasing this distance increases the flexural stiffness of the structure as a square of this distance. In most investigations into static aeroelastic control with adaptive structures, the wing section is idealized as a box beam made up of a hollow core and face sheets with bonded distributed strain actuators. The hollow core between the face sheets is assumed to be

composed of a perfect weightless honeycomb. Even if the hollow core is assumed to be of zero flexural stiffness the face sheets and the actuators, because of the mere fact that they are so far away from the neutral axis, generate tremendous flexural stiffness. Therefore, for stiff wing-like structures, camber and twist control with a reasonable actuator to skin ratio would be fairly limited.

To overcome this inherent limitation of bonded or embedded strain actuators the idea of external SMA actuators attached to the structure at selective discrete points is presented. Nitinol actuators are specially suited for the bending control configuration proposed in this chapter. They are readily available in the form of wires of different sizes. As an actuator, nitinol is light weight and it has large force and displacement capabilities as well as low power consumption (Jackson et al., 1972). For example; a .01 in. diameter 10 in. long nitinol wire can lift 4.7 lb. a distance of 0.8 in. with approximately 1.4 W. This is considerably less power than would be required by a solenoid of equal lifting capacity (Schetky, 1984). Also, accurate models of shape memory alloy actuators which were not previously available for such applications are now available (Liang and Rogers, 1991). The inherent problem of hysterises in SMA actuators can also be fortunately overcome by a procedure called training.

There is only one reported case of external SMA actuators (other than robotic actuators) for adaptive control. Baz and Tampe (1989) used external Nitinol actuators for active

buckling control of beams. In their investigation, they have basically used Nitinol actuators to reduce the amount of compressive force being applied to the beam. This can at best be termed as indirect buckling control because Nitinol is used to reduce the force being applied to the beam instead of the beam reacting in some manner (like stiffening) to avoid buckling.

Ikegami et al. (1990) recently used Nitinol actuators mounted externally on a cantilever beam for active vibration control. Since the actuators were connected to the beam at very closely spaced points they essentially behave like surface bonded actuators and do not fall into the category of external actuator arrangement proposed in this chapter.

External actuators have much more control authority because with them differential movement between the actuator and the beam is possible. This differential movement results in an additional moment as the beam deflects. This additional moment can ultimately lead to the buckling of the beam, but before that occurs, there is an extremely large useful range where the beam deflections are still controlled and are much greater than those obtained due to a pure tip moment. The actuator strain in this configuration is well within the limits of SMA actuators. Several variants of this configuration are also considered and discussed in this chapter.

4.3 The Tilt Buckling Configuration

The first configuration that is considerd is a case in which one end of the actuator is attached to the free end of the cantilevered beam and the other is fixed at the clamped end of the beam. Smitses (1976) calls this configuration as buckling due to tilting of forces, and it is referred to as the tilt buckling configuration in this paper. In this case the force of the actuator does not remain fixed in direction, but passes through a fixed point, in this case the clamped end of the beam. Although here the direction of the actuator force is changing, it is a conservative mechanical force.

Since this configuration is elementary the beam column equations for this case are developed in the most general form allowing for all possible loads.

Consider the elastic column with length l and bending stiffness EI shown in Figure 4.1. The actuator is considered eccentrically located such that in addition to the axial and transverse forces it exerts on the beam, it also exerts a tip moment equal to Pd. The beam is also subjected to a vertical shear force V at the right end and a uniformly distributed transverse force q. The governing differential equation and the boundary conditions for the beam column are

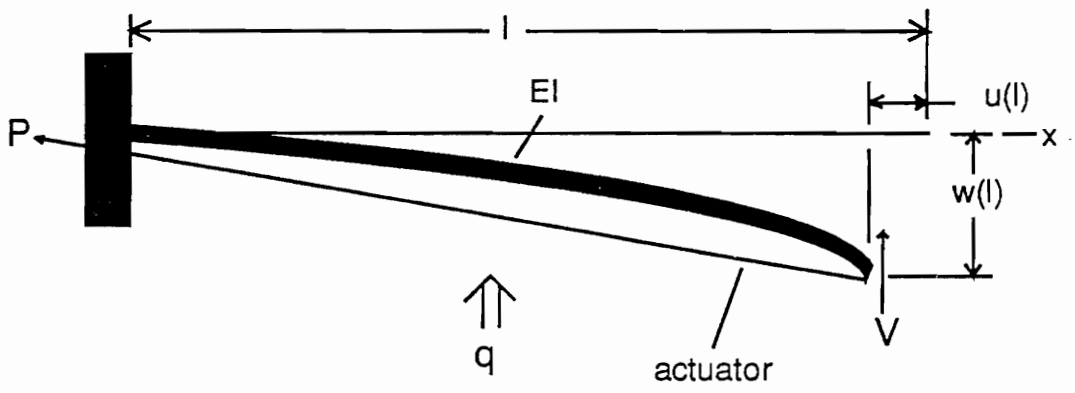

Figure 4.1 Geometry of tilt buckling configuration.

$$EIw_{,xxxx} + Pw_{,xx} = q \tag{1}$$

Boundary Conditions

at $x=0$

$$w, \quad w_{,x} = 0 \tag{2a}$$

at $x=l$

$$-EIw_{,xx} = -Pd \tag{2b}$$

$$-EIw_{,xxx} - Pw_{,x} = -V - P\frac{w}{l} \tag{2c}$$

The solution of Equation (1) with the boundary conditions is

$$w(x) = A(\sin kx - kx) + B(\cos kx - 1) + \frac{qx^2}{2P} \tag{3}$$

Where

$$A = \frac{1}{\sin kl}\left\{\frac{ql^2}{2P} - \frac{Vl}{P} - \left[\frac{q}{Pk^2} + \frac{Vl}{P} - d - \frac{ql^2}{2P}\right](\cos kl - 1)\right\} \tag{4a}$$

$$B = \frac{q}{Pk^2} + \frac{Vl}{P} - d - \frac{ql^2}{2P} \tag{4b}$$

and

$$k = \sqrt{\frac{P}{EI}}$$

By setting q, V, and d =0 we get the characteristic equation for the critical buckling load

$$\tan kl = 0 \tag{5}$$

which yields the critical buckling load

$$P_{cr} = \frac{\pi^2 EI}{l^2} \tag{6}$$

Next we examine the beam response to the eccentric actuator force, i.e., q and V = 0 but $d \neq 0$. This configuration is the basic configuration for beam bending control, and is examined in greater detail. The general solution for the transverse displacement w simplifies as follows for this case.

$$w(x) = d\left\{\frac{\cos kl - 1}{\sin kl}(\sin kx - kx) - \cos kx + 1\right\} \tag{7}$$

and the beam tip displacement simplifies as

$$w(l) = d\frac{kl(1 - \cos kl)}{\sin kl} \tag{8}$$

The response of the beam obtained from the above equation is shown in Figure 4.2 for a nominal value of the offset distance d. For comparison the beam response to a pure tip

moment Pd is also plotted in Figure 4.2. This would be the response of the beam if the actuator was embedded within the beam offset from the neutral axis through the same distance d. Also shown in Figure 4.2 is the response obtained using the exact large rotations formulation. The formulation and equations for the large rotations solution are discussed in detail by Chaudhry and Rogers (1991).

The first thing to notice from the results shown in Figure 4.2 is that for this configuration both the moderate and the large rotations formulation give the same response up to a δ/l of 0.3. Therefore, the moderate rotations formulation (Equation (7)) can be safely used to compute the beam response up to that point. The other important and most useful feature of this configuration is the enhanced bending compared to the simple tip moment response. This enhanced bending, which is possible, because of the differential movement between the beam and the actuator, is the essential advantage of using external actuators. Before the occurrence of catastrophic buckling (i.e., the sudden increase in the beam tip displacements, there is a fairly large useful range of enhanced bending, where the displacements are controlled and much greater than the those obtained due to a simple tip moment.

The actuator strain which can be computed from the deformed geometry (see Figure 1)

$$\varepsilon_a = \frac{[w(l)^2+(l-u(l))^2]^{1/2}}{l} - 1 \qquad (9)$$

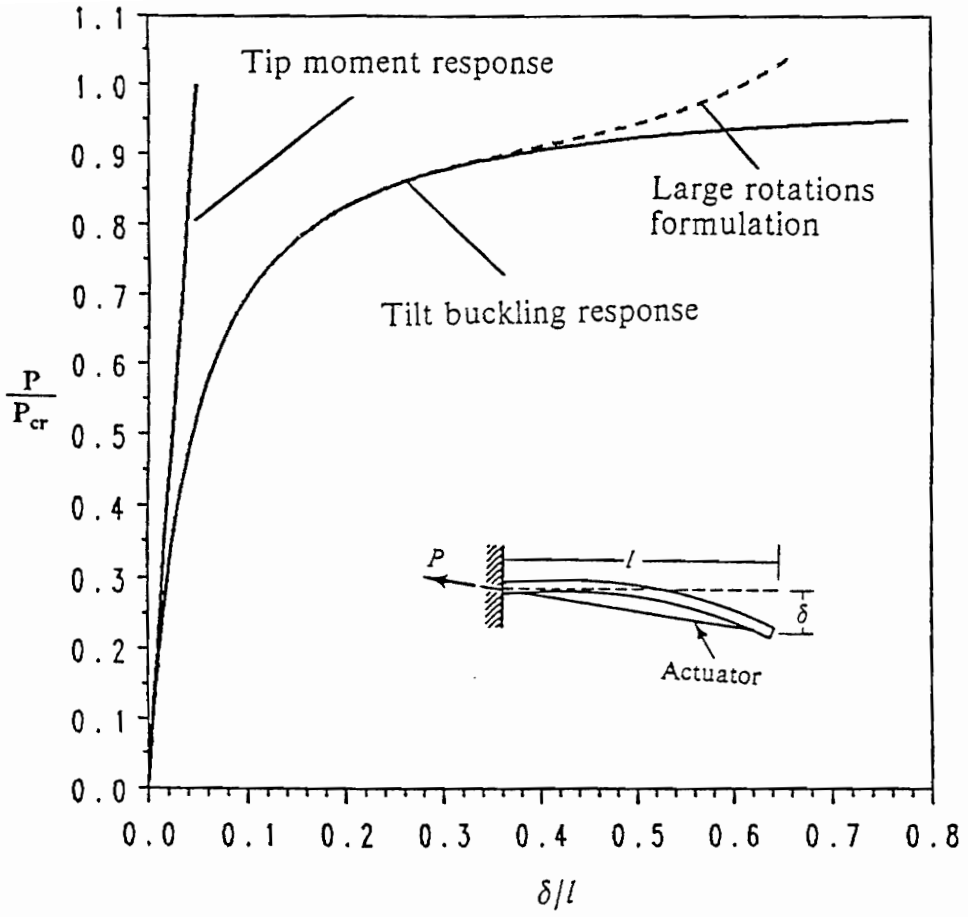

Figure 4.2 Tilt buckling response. Comparison of internal and external actuator configurations.

is well within the limits of SMA actuators.

Next, the bending control of the beam in the presence of an opposing transverse load q is examined. It is necessary to study the effect of the transverse load on the response because in some applications the beam or plate may be required to bend against a transverse load. Figure 3 shows the beam response (for a given d) for various values of $\overline{q}$(the nondimensional uniformly distributed transverse load $\overline{q}=ql^3/EI$). This figure indicates the possibility of using feedback control to achieve a desired tip deflection in the presence of an opposing transverse load. The response with an opposing tip shear load V is also similar, where again by using some sort of feedback control, a desired value of the tip deflection can be achieved.

4.4 A Variant of Tilt Buckling Configuration

4.4.1 Analysis

In the second configuration of external actuators, the actuator passes through a point on the beam, as shown in Figure 4.4. Since our interest is in bending control, we once again consider the actuator to be eccentrically located at an offset distance d. To obtain the beam response the beam is divided into two portions. The governing equations for this beam column problem are given in the two portions separately.

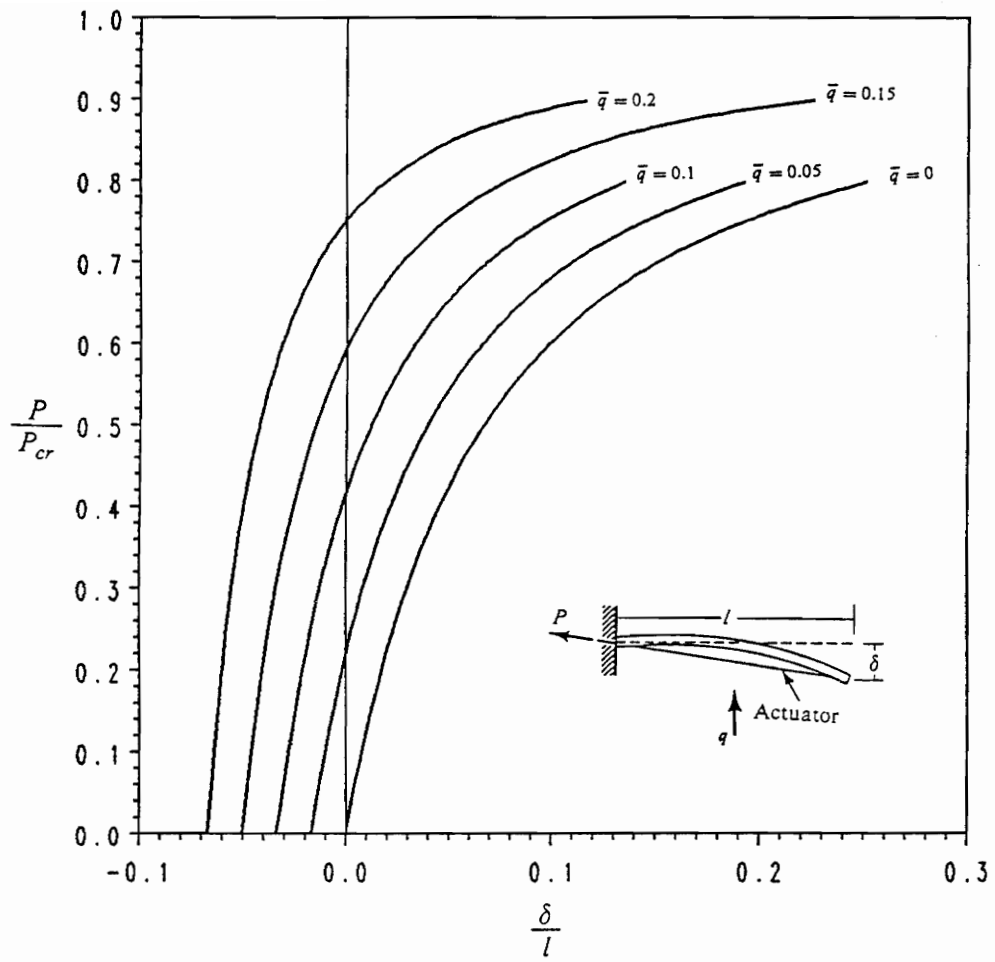

Figure 4.3 Tilt buckling response of a beam in the presence of an opposing transverse force.

$$EIw_{1,xxxx} + Pw_{1,xx} = 0 \quad 0 \le x_1 \le a \tag{10}$$

$$EIw_{2,xxxx} + Pw_{2,xx} = 0 \quad 0 \le x_2 \le l-a \tag{11}$$

where the subscripts 1 and 2 indicate the two portions of the beam. The general solution for w_1 and w_2 is given as

$$w_1 = A_1 \sin kx_1 + B_1 \cos kx_1 + C_1 x_1 + D_1 \tag{12}$$

$$w_2 = A_2 \sin kx_2 + B_2 \cos kx_2 + C_2 x_2 + D_2 \tag{13}$$

The eight constants A_i, B_i, C_i, and D_i ($i=1,2$), are solved from the following eight boundary conditions

at $x_1=0$

$$w_1 = 0, \; w_{1,x} = 0 \tag{14a}$$

at $x_1=a$

$$w_1 = w_2, \; w_{1,x} = w_{2,x}, \; w_{1,xx} = w_{2,xx} \tag{14b}$$

and

$$-EIw_{1,xxx} - Pw_{1,x} = \frac{P}{(l-a)}\{w_2(l-a) - w_2(0)\} - \frac{P}{a}w_2 - EIw_{2,xxx} - Pw_{2,x} \tag{14c}$$

at $x_2=(l-a)$

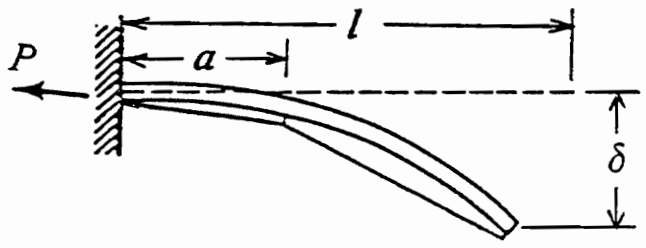

Figure 4.4 A variant of tilt buckling configuration - geometry.

$$-EI w_{2,xx} = -Pd \tag{14d}$$

and

$$-EI w_{2,xxx} - P w_{2,x} = \frac{P}{(l-a)}\{w_2(l-a) - w_2(0)\} \tag{14e}$$

First we set $d=0$ and examine the eigenvalue problem. This yields the following characteristic equation

$$\sin ka \sin k(l-a) = 0 \tag{15}$$

Solving the characteristic equation gives the critical buckling load for various values of a/l. Figure 4.5 shows the variation in the critical buckling load as a function of a/l. For $a/l=0$ the problem is that of tilt buckling, and as the point through which the actuator passes is moved to the right away from the fixed end towards the center of the beam the critical buckling load increases, and at $a/l=0.5$ (i.e., at the center of the beam) the critical buckling load is exactly four times the tilt buckling load. As the point is moved further right away from the center the buckling load decreases and at $a/l=1$ it is again equal to the tilt buckling load. By forcing the actuator to pass through one point on the beam, the critical buckling load is increased four times. It is obvious that as the number of points through which the actuator passes is increased to infinity the buckling load will also tend to infinity. An actuator passing through an infinite number of points is, in fact, like an internal actuator in contact with the beam at all points. This result also confirms the principle that a structure cannot buckle due to an internal actuator force (Chaudhry and

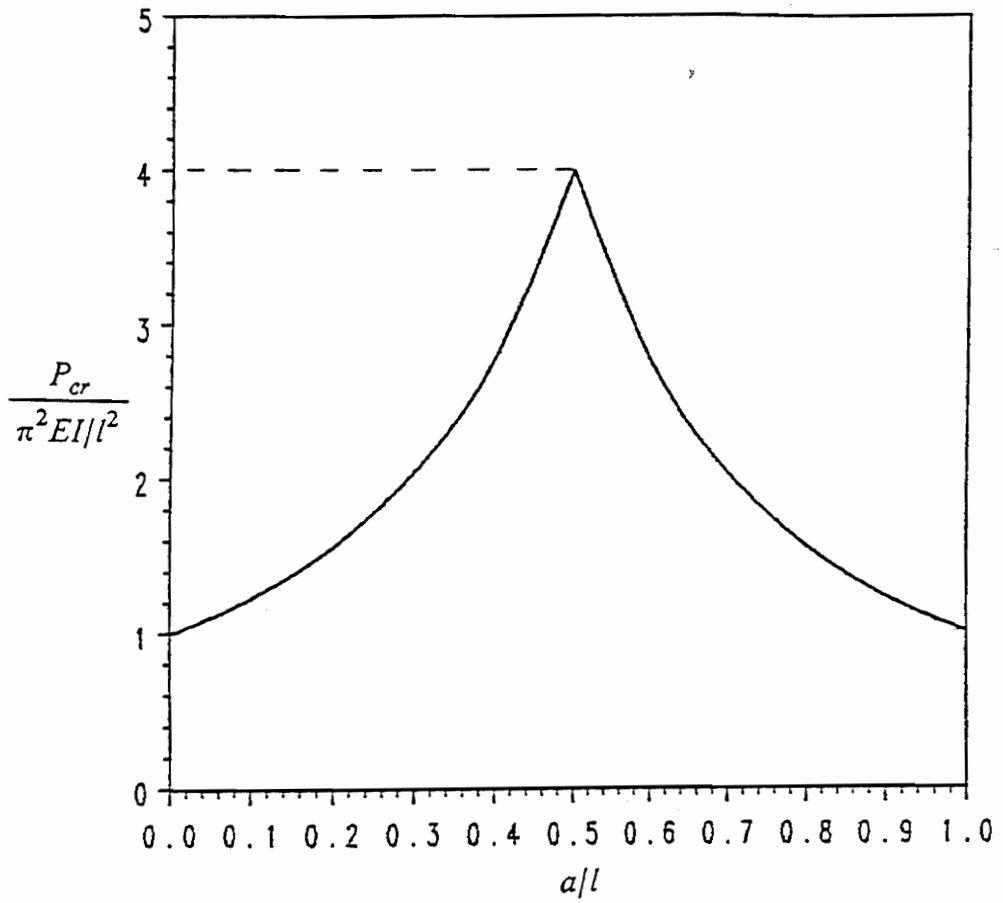

Figure 4.5 Change in buckling load with the location of the point on the beam through which the actuator passes.

Rogers, 1991).

Another interesting feature of this configuration is the buckling mode shapes of the beam. The buckling modes have the form

For $0 \le a/l \le 0.5$

$$w(x_1) = 0 \tag{16a}$$

$$w(x_2) = A_2(\sin kx_2 - kx_2) \tag{16b}$$

For $0.5 \le a/l \le 1$

$$w(x_1) = A_1(\sin kx_1 - kx_1) \tag{17a}$$

$$w(x_2) = A_1\{k(\cos ka - 1)x_2 + \sin ka - ka\} \tag{17b}$$

The mode shapes are indeed unique and most unusual. The buckling gets completely localized in the longer section with the other section remaining completely straight. It is as if the two sections act independently of one another. This phenomenon is similar to mode localization in disordered structures (Pierre, 1988). In structural dynamics, under conditions of weak internal coupling (weak disorder) the vibration mode shapes undergo dramatic changes to become strongly localized when small disorder is introduced, thereby confining the energy associated with a given mode to a small geometric region. Recently Pierre and Plaut (1989) have shown that similar phenomenon occur in buckling problems as well. Although in this configuration there is no eigenvalue veering, and the buckling

is completely localized, the two phenomenon are similar. In this configuration what causes the two sections of the beam to behave independently is the fact that the moment of the actuator force about the point on the beam through which it passes is zero.

This phenomenon, considered drastic from the point of view of structural stability, offers many new possibilities of shape control. Simply by changing the location of the point through which the actuator passes, a totally different shape can be obtained.

4.4.2 Experimental Verification of Mode Shapes and Critical Buckling Load

Since our interest is in bending control, a beam with eccentric actuators was used to verify the change in the critical buckling load as a function of the location of the point through which the actuator passes. The experimental set-up is shown in Figure 4.6, and the load versus beam tip displacement is shown in Figures 4.7 and 4.8. In Figures 7 and 8 the solid lines represent the solution obtained using Equations (10,11). There is good correlation between the experimental and theoretical results. The experimental results in the highly nonlinear range are not as accurate because at these load levels a small amount of friction at the contact points will change the beam response substantially.

To experimentally verify the mode shapes of the 'perfect' beam, a beam actuator design which minimizes eccentricity was chosen. To keep the eccentricity of the actuators as

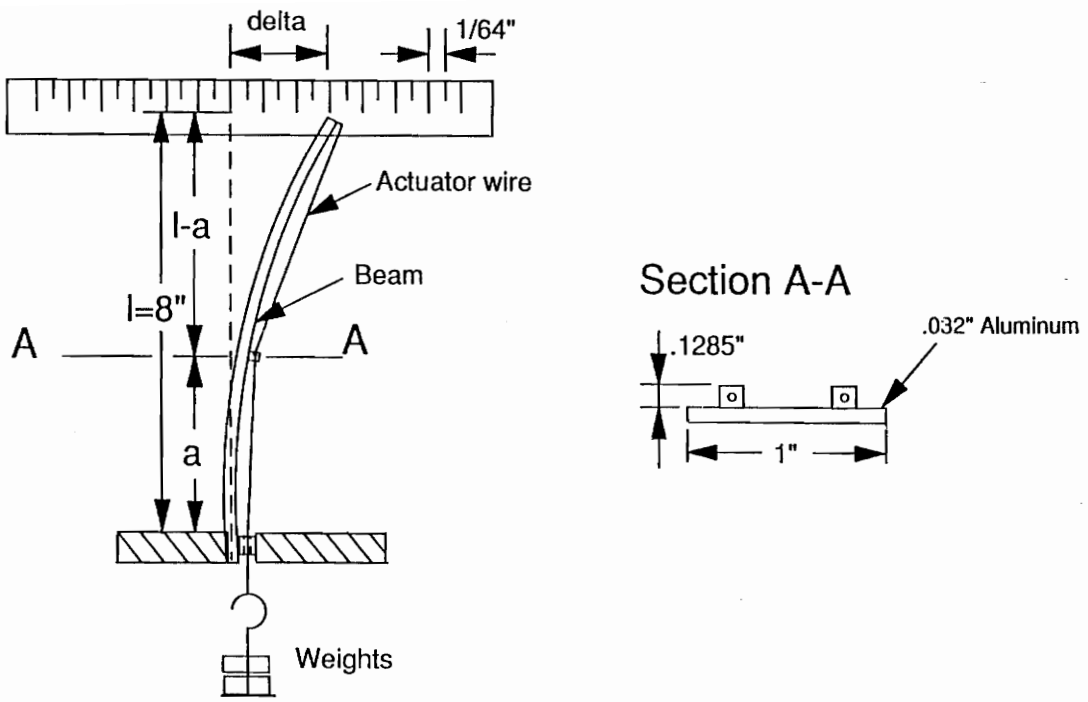

figure 4.6. Experimental setup to verify the response of tilt buckling variant configuration.

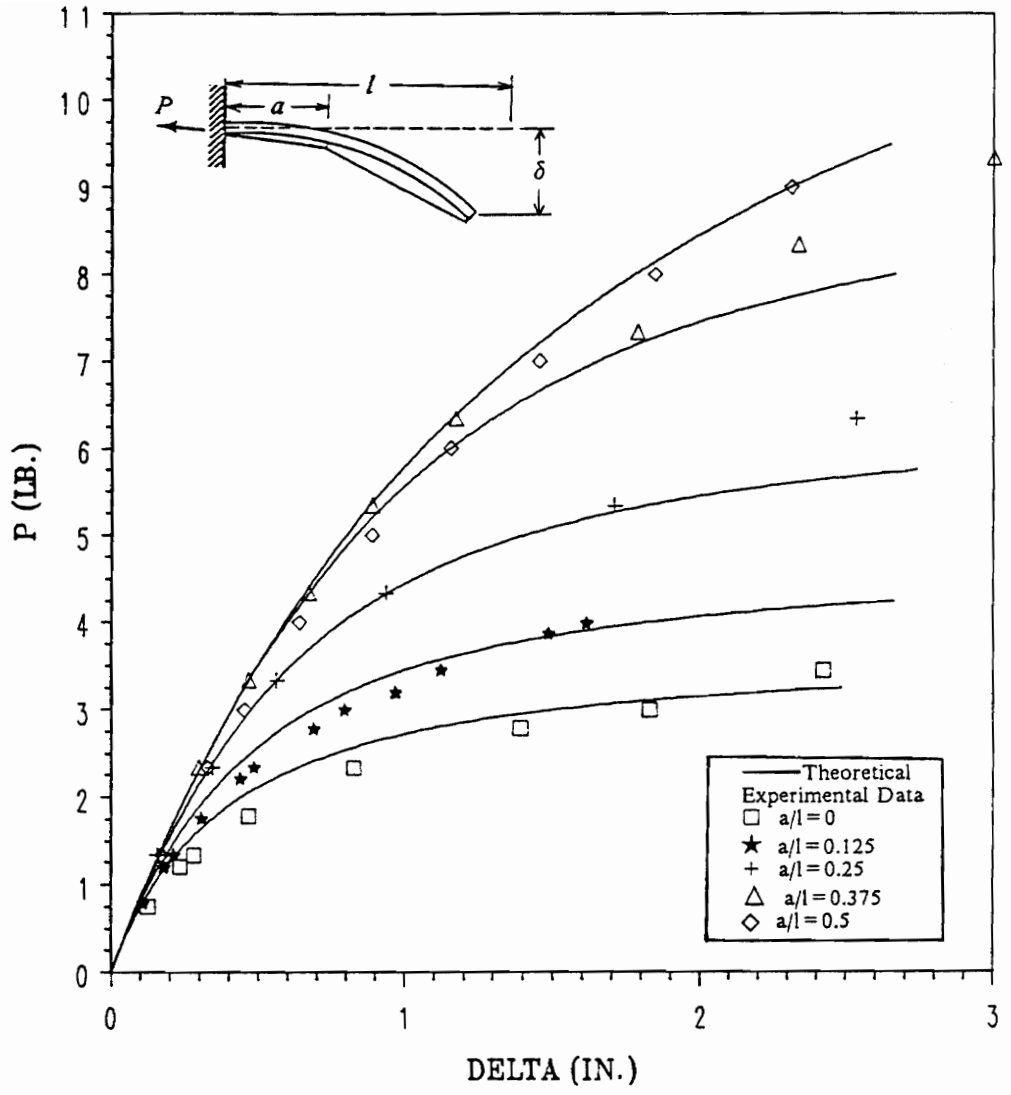

Figure 4.7 Applied load (weight) versus beam tip deflection for various values of *a/l*. Comparison of experimental and theoretical results.

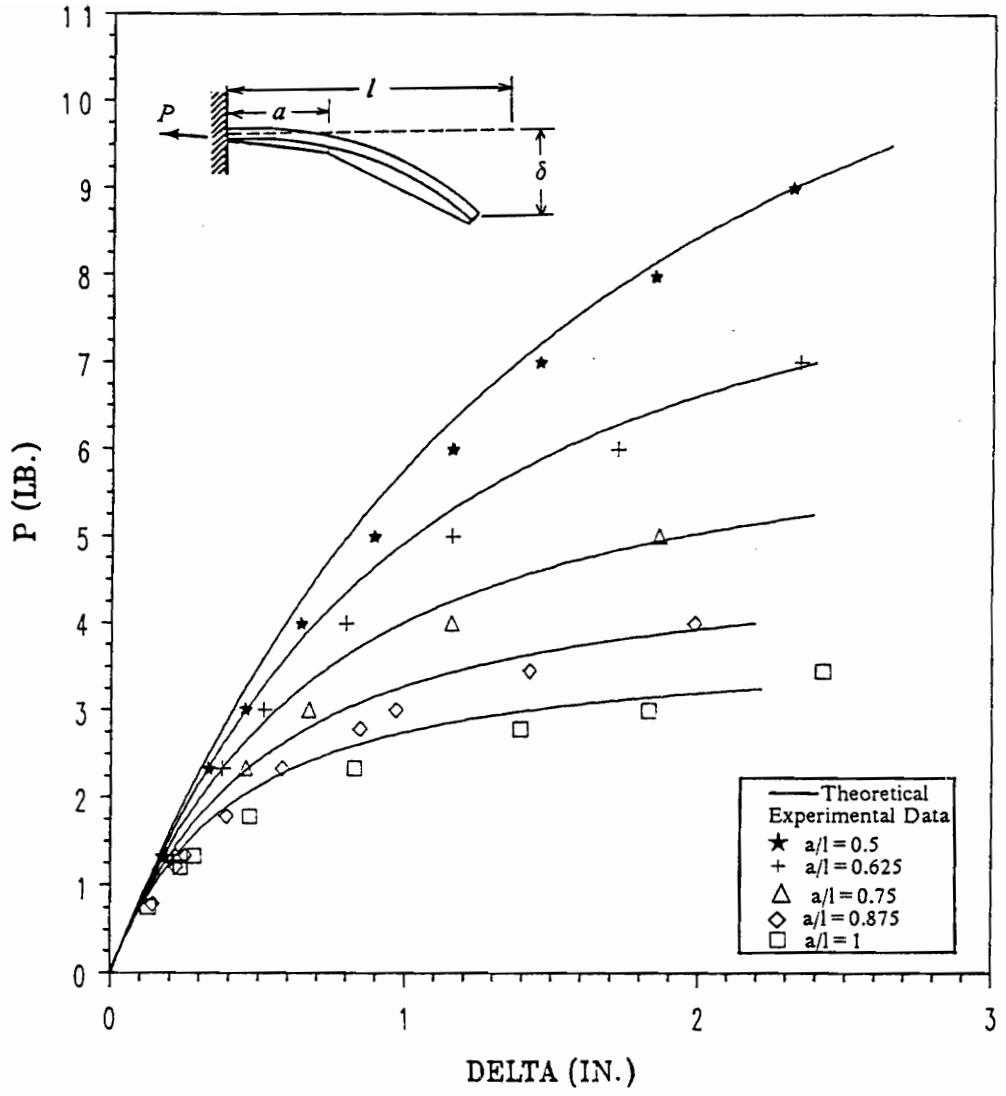

Figure 4.8 Applied load (weight) versus beam tip deflection for various values of *a/l*. Comparison of theoretical and experimental results.

close as possible to zero the actuators were attached to the side of the beam as shown in Figure 4.9. For $0.48 \leq a/l \leq 0.52$ it was not possible to see the total localization of buckling in the longer section. This is perhaps due to the fact that the structure has some inherent eccentricity and other imperfections. However, for values of $a/l < 0.48$ or $a/l > 0.52$ the buckling localization was complete, with the shorter section remaining absolutely straight as can be seen in the time lapsed pictures of the beam in Figures 4.10 and 4.11.

4.4.3 Advantages

For a given actuator force the bending control in this configuration (where the actuator passes through a point on the beam) is certainly less than the tilt buckling configuration. Then how is this configuration better? This question is simply answered by looking at Figure 4.7 where the experimental and theoretical results for various values of a/l are compared. A tip deflection of 2 in. with the tilt buckling configuration is achievable only by getting into the completely nonlinear (buckled) region, whereas for $a/l=0.5$ the same level of tip deflections can be achieved staying well within the bounded nonlinear region. Therefore, for longer sections to achieve a desired tip deflection it is better to divide it into smaller equal sections such that within each section the displacements are bounded, but resulting in an overall tip displacement which is quite large. The actuator strain for a given tip displacement is also smaller if the beam is divided into two or more sections.

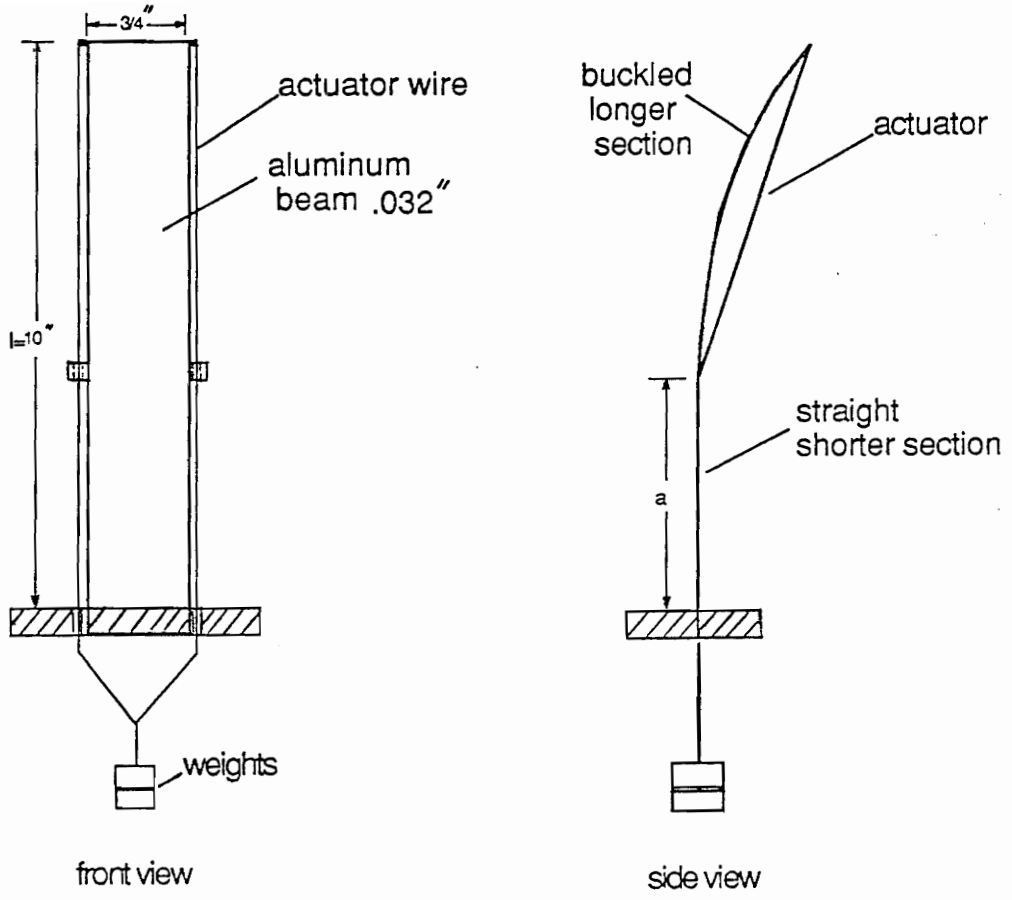

Figure 4.9 Experimental setup to verify mode shapes of perfect structure.

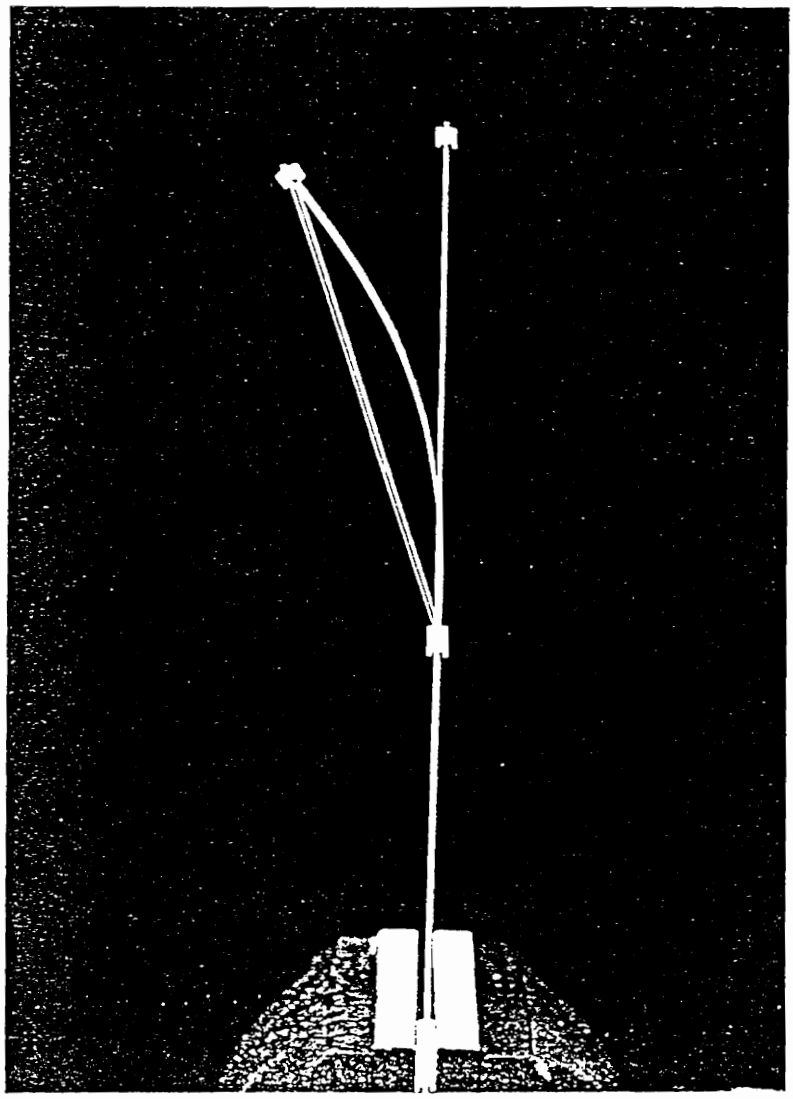

Figure 4.10 Time-lapsed picture of buckled beam a/l < 0.5.

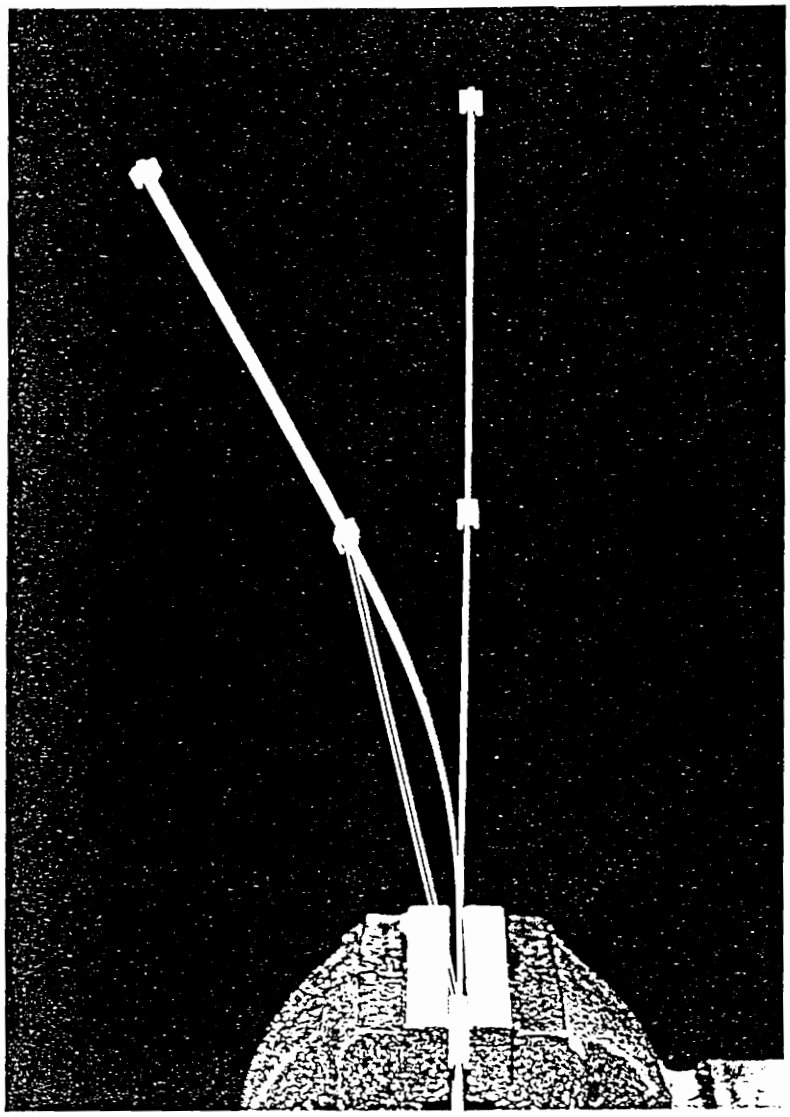

Figure 4.11 Time-lapsed picture of buckled beam $a/l > 0.5$.

Another advantage is the variety of shapes that the beam can achieve by changing the location of the point through which the actuator passes. Practically it may not be possible to change the location of the point on a real structure, but the same beam can have two sets of actuators passing through two different points. Activating one will result in one shape and activating the other will result in a different shape. Almost any desired shape can be achieved. Figure 4.12 shows the time lapsed photograph of the 'perfect' beam. To show the variety of shapes possible the point through which the actuator passes is made moveable in this configuration. Four distinct shapes of the beam can be seen, the first is the straight un-buckled beam, the second is the buckled beam with $a/l = 0.45$, the third is with $a/l=0$, and the fourth is with $a/l = 0.55$.

Also, this application is specially suitable when the actuator needs to be close to the beam.

4.5 A Configuration of Internal Actuators with Enhanced Bending

This configuration attempts to increase bending control with internal actuators. The basic idea is to increase the actuator offset distance with a minimal increase in the flexural stiffness of the beam. This is done by placing a thicker flexible tube next to the parent beam such that it is free to slide with respect to the parent beam, and the actuator connected to the end of the parent beam passing through the tube. The tube is constrained

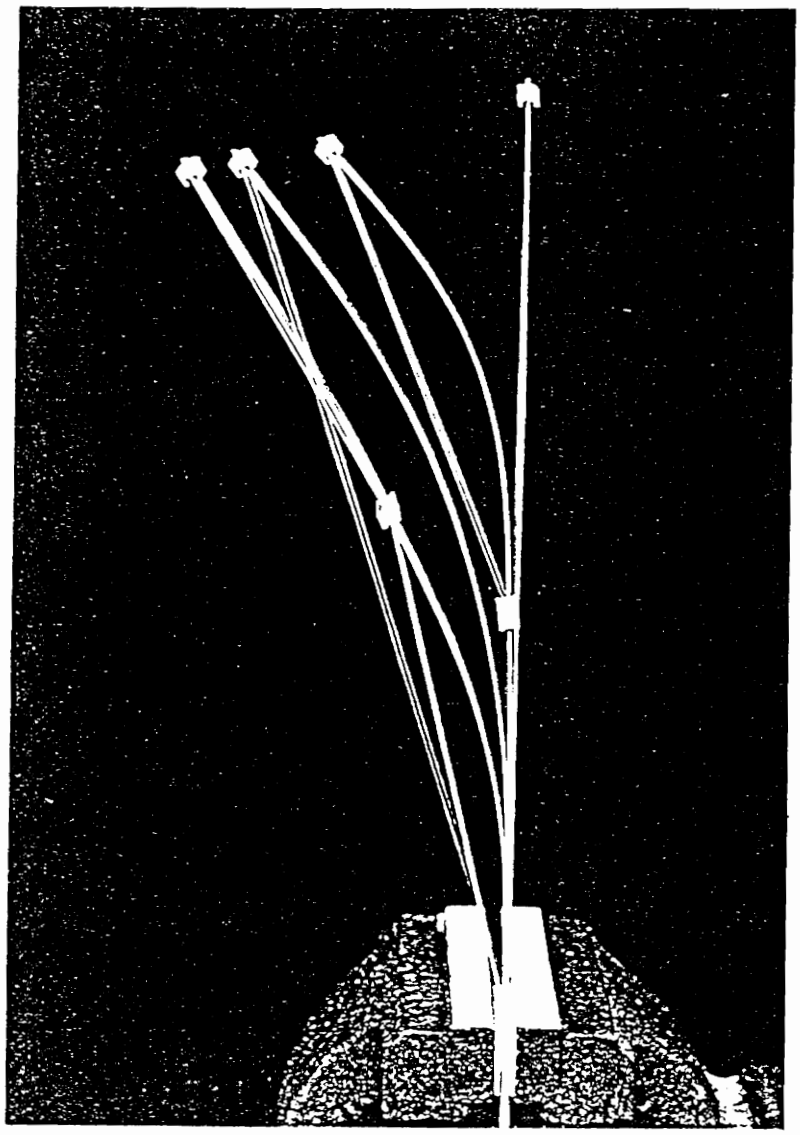

Figure 4.12 Time-lapsed picture of the beam where the point through the actuator passes is moveable. Picture shows variety of shapes possible.

to deform along with the beam by evenly spaced brackets attached to the parent beam. In this scenario, the flexible tube or tubes deform along with the beam but since they are free to slide they add only minimally to the flexural stiffness. The tubes through which the actuator passes adheres closely to the parent beam and follows its shape, thus there is no differential movement between the parent beam and the actuator and no buckling. Although the parent beam and the tube slide with respect to each other but from a structural standpoint they can be regarded as one cantilever beam under the action of a tip moment.

4.5.1 Experimental Verification of Response

A beam specimen was prepared and tested to demonstrate the feasibility of this configuration, and to verify its response. A .032 in. thick, 1 in.wide, and 12 in. long aluminum beam was used as the parent beam, and flexible square plastic tubes with internal holes were used to carry the actuators within them. This configuration and the experimental set-up is shown in Figure 4.13.

The load versus beam tip displacement for this configuration is plotted in Figure 4.14. The response is purely due to the applied tip moment, i.e., $\delta = Ml^2/2EI$, and the correlation is good between the theoretical tip moment response and the experimental results. Because the flexible tubes carrying the actuator in them adhere closely to the parent

aluminum beam, there is no buckling action and hence no nonlinearity in response. There is some difference between the theoretical and experimental results at higher force levels because of increased friction between the sliding plastic tubes and the parent beam which increases the effective flexural stiffness of the beam. For comparison, a variant of the tilt buckling configuration (with the actuator passing through three points) is also plotted. Also the response of the same parent beam but with the same two plastic tubes bonded to the surface (instead of free to slide) is plotted. The parent beam and the actuator offset distance for all three curves is the same (i.e., .032 in. thick, 1 in. wide, and 12 in. long aluminum beam). By bonding the plastic tubes to the aluminum beam the flexural stiffness of the composite beam becomes approximately three times as much as when the plastic tubes are free to slide with respect to the beam. This plot illustrates the limitation of integrally embedded or bonded actuators. Although in the case where the plastic tubes are free to slide the response is still purely due to the tip moment; but, because the flexural stiffness has increased only minimally, it is possible to get much larger displacements for the same force.

As can be seen in Figure 4.14 the beam where the actuator passes through three discrete points is, of course, most efficient from the point of view of bending control. The theoretical response for this configuration is obtained in a manner similar to Equations (12) and (13).

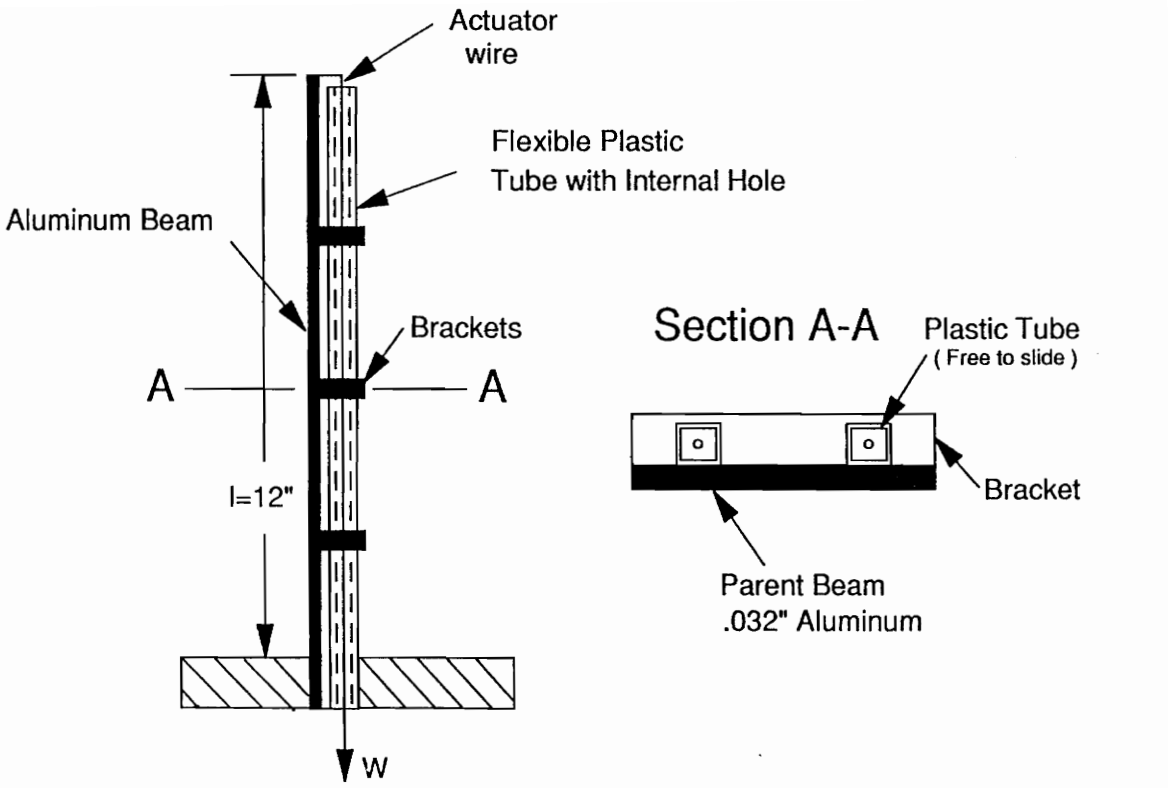

Figure 4.13 Configuration and experimental setup to verify response of enhanced bending configuration.

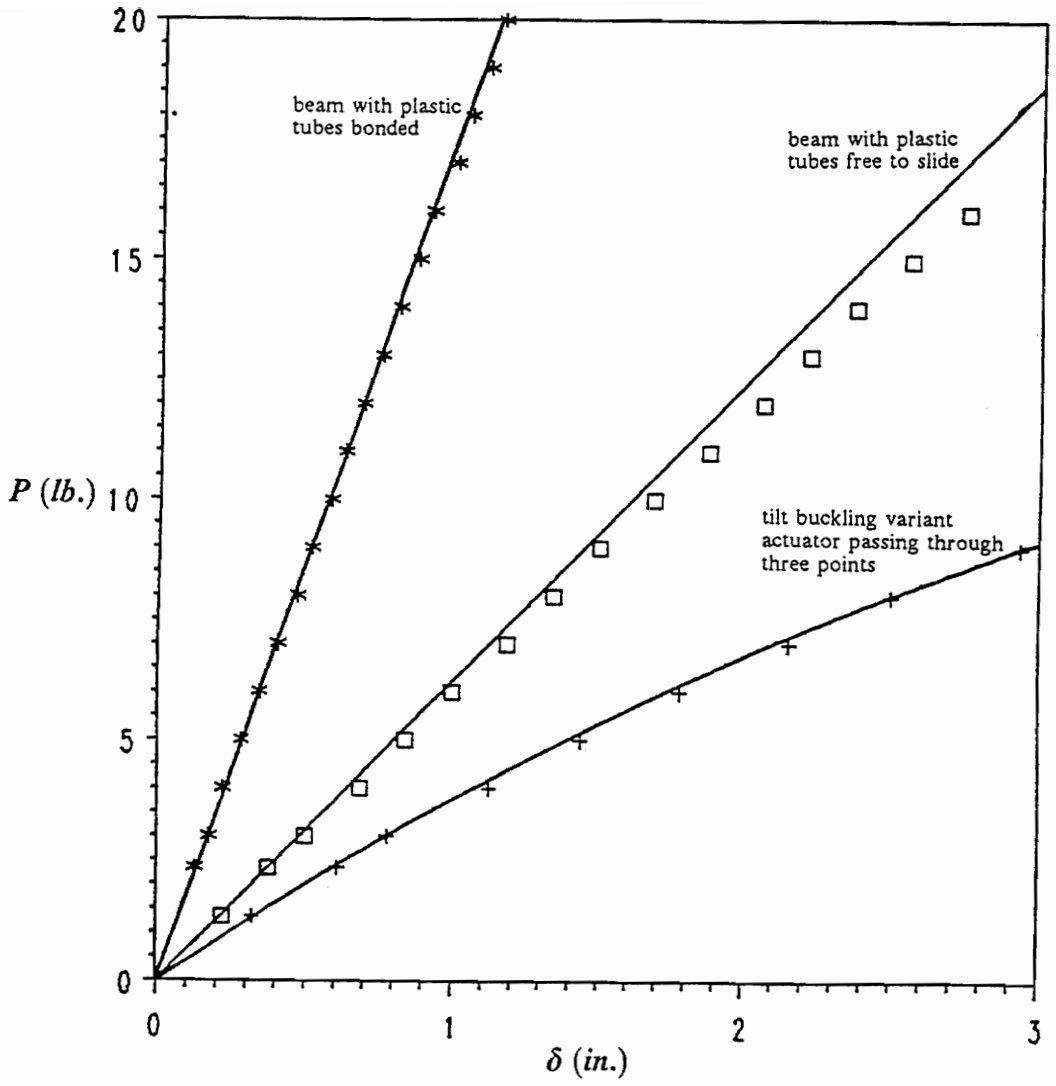

Figure 4.14 Load (weight) versus beam tip deflection. Comparison of three configurations of bonded tubes, sliding tubes, and actuator passing through three points.

4.6 Verification of Concept with Nitinol Actuators

In all the experimental work discussed so far ordinary weights were used to simulate the force exerted by the SMA actuators; similarly,ordinary flexible wire was used to represent the SMA actuators. To verify the response of the proposed configurations with SMA actuators,the ordinary wires and weights were replaced with .015 in. nitinol wires in the same beams described in the previous section. The nitinol wires were anchored to a terminal post at the base of the beam. The beam tip displacement versus the applied voltage for the two proposed configurations is plotted in Figures 15 and 16. The different curves are for different values of the pre-tension in the nitinol actuator wires. Further experimentation is being done to better understand these response curves and relate them to nitinol phase transition temperatures, power consumption, etc.

Figure 17 shows a time lapsed photograph of the beam where the nitinol actuator passes through three points. Any one of the desired shapes can be achieved by adjusting the voltage applied to the .015 in. nitinol actuator wire.

4.7 Possible Applications of the Concept

External SMA actuators used in the tilt buckling configuration or one of its variants have much greater control authority compared to embedded or bonded actuators. They have the

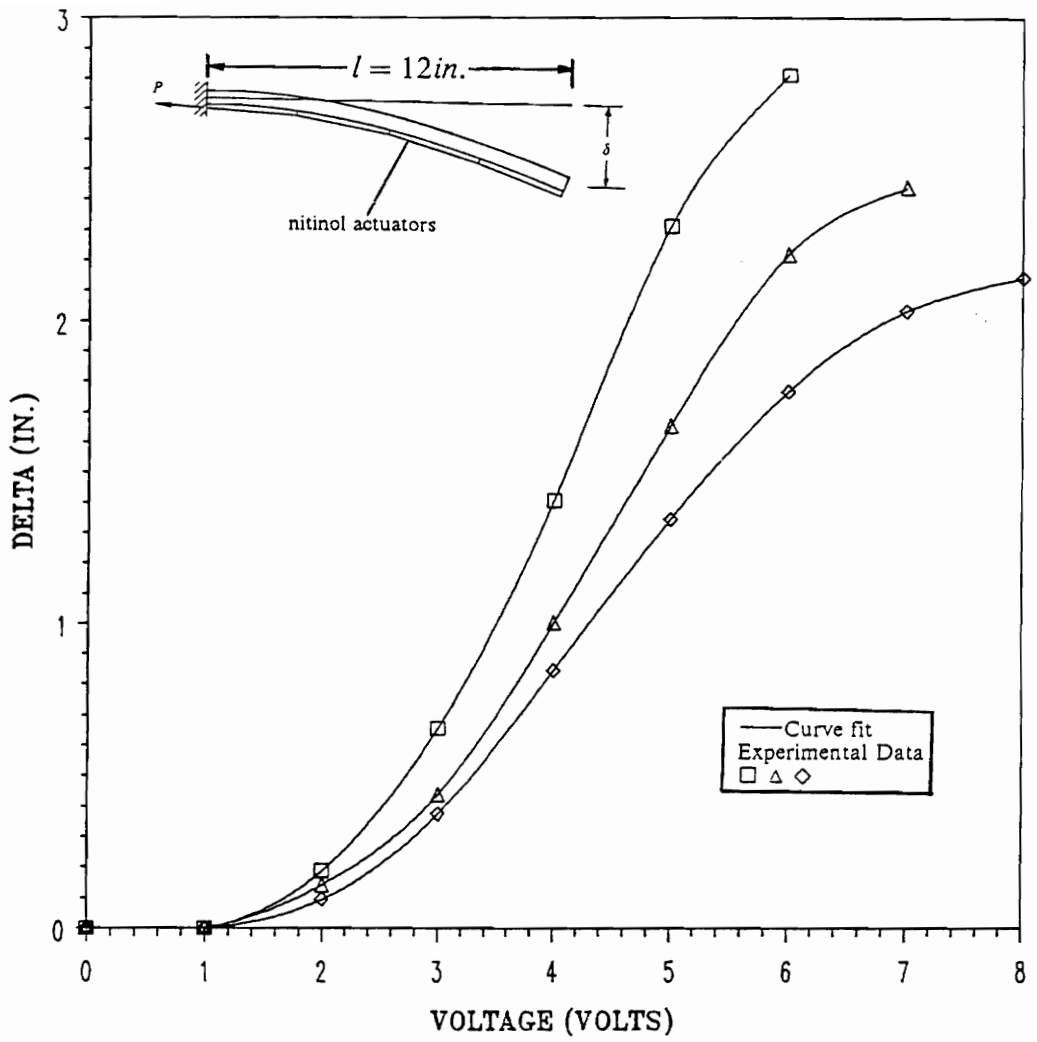

Figure 4.15 Beam tip deflection versus voltage applied to nitinol actuator wires. Tilt buckling variant configuration, actuator passing through three points. Different curves show response with different levels of pre-tension applied to the nitinol wires.

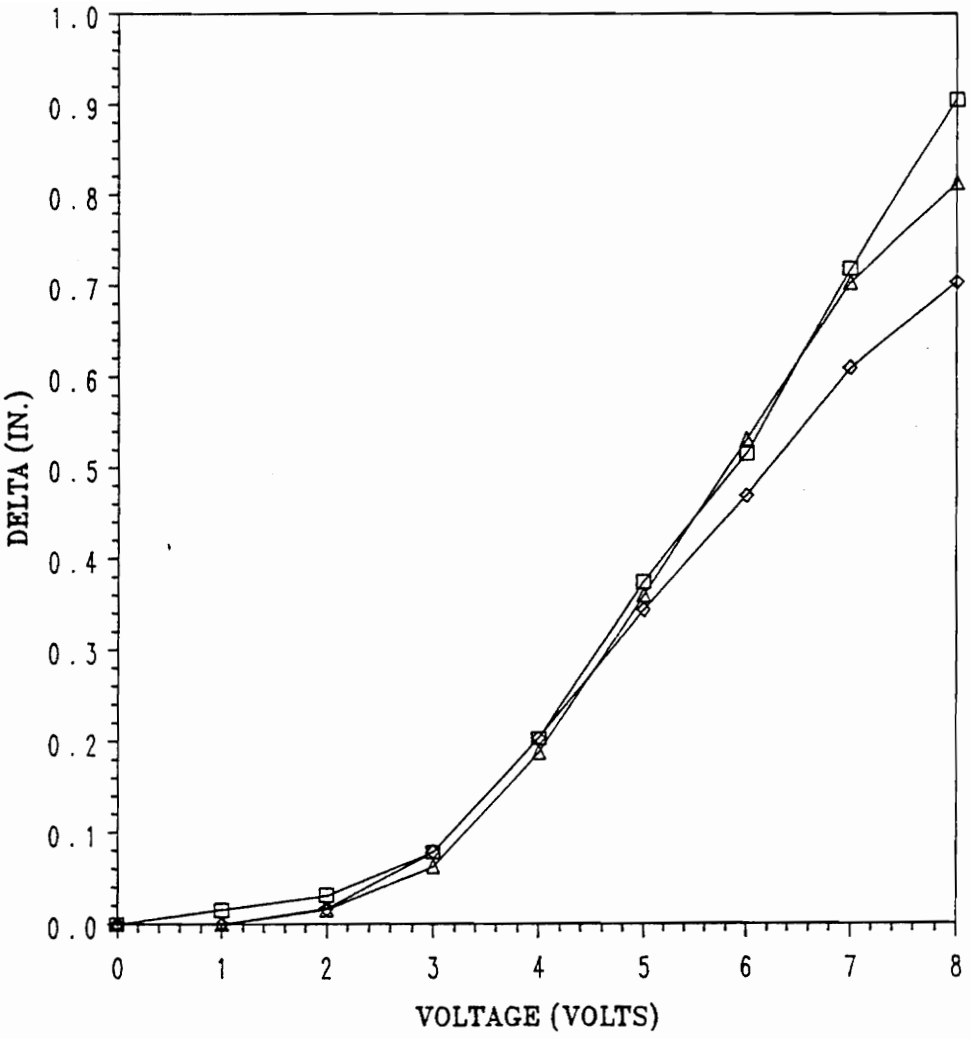

Figure 4.16 Beam tip displacement versus voltage applied to nitinol wires. Enhanced bending with internal actuator configuration.Different curves show response with differnt levels of pre-tension applied to the nitinol wires.

force capability to cause small shape changes in stiff structures, and they have the stroke capability to effect major shape changes in flexible structures. To use SMA actuators in these configurations all that is required is a select number of discrete points where the actuator is to be connected to the structure and electrical leads to supply the electric current. Where applicable the convenience they offer compared to conventional hydraulic or electrical actuators is overwhelming.

In the large force category, they could be used to produce minor shape changes in the sensitive areas of an airfoil section for boundary layer control or aeroelastic control. Another possible application is the continuous surface deformable mirrors. The SMA actuators can be used as bending moment actuators to achieve mirror deformations as shown in Figure 4.18. This technique which was first suggested by Scott (1975) allows the mirror shape to be adjusted without applying external forces from a back plate. The band width limitation of SMA actuators can be overcome by using them in conjunction with piezoelectric actuators, where the SMA actuators would be used to effect larger shape changes and the PZT's for finer shape control.

External SMA actuators in the tilt buckling configuration or one of its variants also offer great promise in such applications as the variable camber wing. From this preliminary investigation they appear to have the force and stroke capability necessary to incorporate them into the mission adaptive wing. If the direct transverse load to which these devices

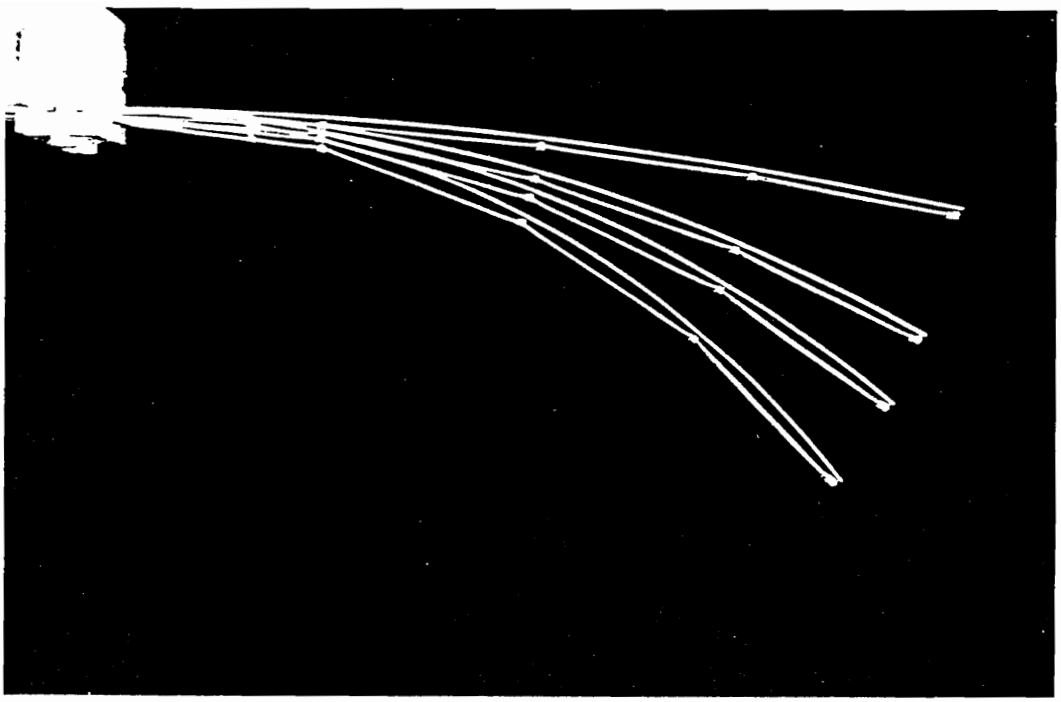

Figure 4.17 Time-lapsed picture of tilt buckling variant configuration where actuator passes through three points on the beam. Actuation with .015 in. nitinol wires.

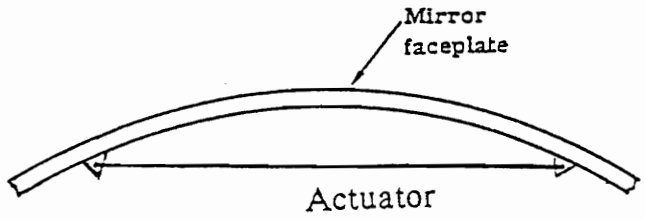

Figure 4.18 SMA actuator for mirror shape control.

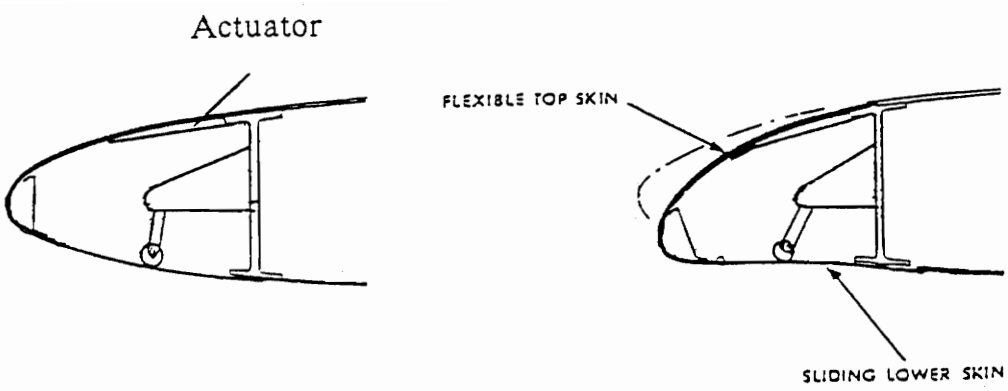

Figure 4.19 A possible configuration of moving leading edge with SMA actuators.

are subjected can be reacted by some other means, the SMA actuators can be used to provide the necessary bending control. A possible configuration similar to that suggested by Chacksfield (1980) is shown in Figure 4.19.

4.8 Conclusions

The theoretical and experimental study of external SMA actuators for bending and shape control of beams indicates that SMA actuators used in this configuration are much more efficient compared to embedded actuators. The SMA actuator strain in this configuration is well within the useful limit of SMA actuators. Several variants of this configuration along with their advantages are discussed.

The theoretical beam response for all configurations discussed has been checked against experimental results. The obtained results verify the theoretical model. Experiments with actual SMA actuators confirm their force and stroke capability for the proposed configurations.

A new configuration for internal actuators is also proposed. This configuration enhances bending control without any significant increase in the flexural stiffness of the beam.

4.9 References

Baz, A., and Tampe, L., 1989, "Active Control of Buckling of Flexible Beams", ASME Design Conference, Montreal, Canada.

Chacksfield, J. E., 1980, "Variable Camber Airfoils", Aeronautical Journal, May.

Chaudhry, Z., and Rogers, C. A., 1991, "Response of Composite Beams to an Internal Actuator Force", AIAA paper 91-1168.

Chirappa, D. J. and Claysmith, C. R., 1981, "Deformable Mirror Surface Control Techniques", J. of Guidance and Control, Vol. 4, No. 1.

Crawley, E. F. and de Luis, J., 1987, "Use of Piezoelectric Actuators as Elements of Intelligent Structures", AIAA Journal, Vol.25, No. 10.

Crawley, E. F. and Lazarus, K. B., 1989, "Induced Strain Actuation of Isotropic and Anisotropic Plates", AIAA Paper No. 89-1326, Proceedings of the 30 th SDM Conference, Mobile, AL.

Ehlers, S. M., and Weisshaar, T. A., 1990, "Static Aeroelastic Behavior of an Adaptive Laminated Piezoelectric Composite Wing", AIAA Paper No. 90-1078.

Gilbert, W. W., 1981, "Mission Adaptive Wing System for Tactical Aircraft", J. Aircraft Vol. 18 No. 7.

Ikegami, R., Wilson D. G., Anderson, J. R., and Julien, G. J., 1990, "Active Vibration Control using Nitinol and Piezoelectric Ceramics", J. of Intelligent Material Systems and Structures, Vol. 1, No. 2.

Jackson, C. M., H. J. Wagner, and R. J. Wasilewski., 1972, "55- Nitinol The Alloy with a Memory: Its Physical metallurgy, Properties, and Applications", NASA-SP-5110,91 p.

Kokorowski, S. A., 1979, "Analysis of adaptive optical elements made from piezoelectric bimorphs", J. Opt. Soc. Am., Vol. 69, No 1.

Lazarus, K. B., Crawley, E. F., and Bohlmann, J. D., 1990, "Static Aeroelastic Control using Strain Actuated Adaptive Structures", 1 st Japan U.S. Conference on Adaptive Structures.

Liang, C., and C. A. Rogers, 1991, "The Multi-Dimensional Constitutive Relations of

Shape Memory Alloys", AIAA paper 91-1165.

Pierre, C., 1988, "Mode localization and eigenvalue loci veering phenomenon in disordered structures", J. Sound & Vibration 126(3), 485-502.

Pierre, C., and Plaut, R. H., 1989, "Curve veering and mode localization in a buckling problem", J. of Applied Mathematics and Physics (ZAMP), Vol. 40.

Redeker, G., Wichmann, G., and Oelker, H. C., 1986, "Aerodynamic Investigations Toward an Adaptive Airfoil for Transonic Transport Aircraft", J. Aircraft, Vol. 23, No. 5.

Schetky, L. M., 1984, "Shape Memory Effect Alloys for Robotic Devices", Robotics Age July.

Scott, R. M., 1975, "New technique for controlling optical mirror shapes", Opt. Eng., Vol. 14, pp 112-115.

Simitses, G. J., 1976, An Introduction to the Elastic Stability of Structures, Prentice -Hall, Inc.

Sobieczky, H., Fung, K. Y., and Seebass, A. R., 1978, "A new method for designing Shock-free Transonic Configurations", AIAA Paper 78-1114.

Song, O., Librescu, L., and Rogers, C. A., 1991, "Static aeroelasticity behavior of adaptive aircraft wing structures modelled as composite Thin-walled beams", Presented at the International Forum on Aeroelasticity and Structural Dynamics, June 3-6, 1991, Aachen, Germany.

Chapter 5

Enhanced Structural Control with Discretely Attached Offset Induced Strain Actuators

5.1 Introduction

In structural control, induced strain actuators are utilized generally by bonding them or embedding them in a structure. With bonded or embedded actuators used for inducing flexure, the developed in-plane force contributes indirectly through a locally-generated moment. Control authority in this configuration is thus limited by actuator offset distance. In this chapter, a new concept of flexural or shape control is presented, whereby induced strain actuators such as piezoelectric ceramic patches or shape memory alloys are attached to a structure at discrete points (as opposed to being bonded). This chapter specifically addresses discretely attached induced strain actuators like piezoceramic and electrostrictive actuators which are available in the form of plates or patches, and includes actuator flexural stiffness considerations. This configuration is different from the bonded actuator configuration in two ways. One, because the actuator and the structure are free to deform independently, the in-plane force of the actuator can result in an additional moment on the structure and enhanced control. Second, the actuator can be offset from the structure

without an increase in the flexural stiffness of the basic structure. This allows for the optimization of the offset distance to maximize control. Enhanced control is demonstrated by comparing the static response of a discretely attached actuator beam system with its bonded counterpart system. The advantage of this configuration over the bonded configuration is also verified experimentally.

In recent years, there has been increased interest in the use of induced strain actuators for various types of structural control. A number of models have been developed to represent the induced strain actuator and substrate coupling. Models of strain actuators coupled with simple beams (Forward and Swigert, 1981; Hanagud and Obal, 1985; Crawley and de Luis, 1987; Burke and Hubbard, 1987; Lin and Rogers, 1992) and plates (Crawley and Lazarus, 1989; Wang and Rogers, 1991) have been introduced. Most of this work has focused on the development of accurate models to represent actuator and substrate coupling. In all these models, however, the actuators are either embedded or bonded to the surface of the structure. No other configuration for mounting the actuator on the structure has been considered.

The focus of this research has been to investigate various configurations for integrating induced strain actuators into structures and to determine an efficient way of utilizing induced strain actuators. The conventional method of bonding induced strain actuators to the surface is certainly the easiest, but may not exploit the full capabilities of the induced

strain actuators. By bonding or embedding an actuator in a structure, the actuator becomes part of the structure and as such, deforms along with it. The in-plane force of the actuator, which is the major force exerted by the actuator on the structure, does not contribute directly in any way to modifying the structural response. This is because of a balancing action between the compression and tension members in the structure (Chaudhry and Rogers, 1991). The in-plane force contributes only indirectly, i.e., in the development of a moment on the structure. The moment is a product of actuator force and actuator offset distance. Therefore, for a given available force, the actuator offset distance must be increased to increase the moment and, consequently the structural control. Increasing the actuator offset distance poses two problems — it increases the flexural stiffness of the structure and it increases the stroke requirement of the actuator. This is the dilemma regarding structural control with embedded or surface-bonded actuators.

To illustrate this dilemma, consider a simply-supported beam subjected to concentrated end moments, shown in Fig. 5.1. The displacement of the beam is given by:

$$w(x) = \frac{M}{2EI}(x^2 - xl), \tag{1}$$

where the moment of inertia I of the beam is given by:

$$I = \frac{bt^3}{12}, \tag{2}$$

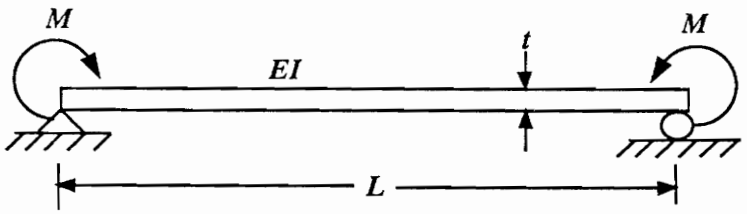

Figure 5.1 Beam under the action of a pure moment.

and the maximum strain which occurs at the outer most fibers of the beam is given by:

$$\varepsilon_{max} = \frac{t}{2}\frac{M}{EI}. \tag{3}$$

Using Eq. (1) the moment (M^*) required to cause a one-thickness deflection at the center of the beam is:

$$M^* = \frac{2}{3}\frac{Ebt^4}{l^2}. \tag{4}$$

Substituting the above moment into Eq. (3), we can express the maximum strain (which will develop in the beam for a one-thickness deflection at the center) as a function of the thickness t and the length l of the beam:

$$\varepsilon_{max} = \frac{4t^2}{l^2}. \tag{5}$$

Maximum strain which is proportional to the square of the thickness, is plotted versus the thickness-to-length ratio t/l in Fig. 5.2. From this figure, it is clear that achieving a one-thickness deflection in a thicker beam requires much higher strain in the outermost fibers. For surface-bonded actuators, the scenario is similar to a beam with concentrated end moments, as described above. Therefore, for bonded induced strain actuators inducing flexure, as the thickness of the basic substrate increases, the strain which they must induce on the outer surface increases as a square of the thickness of the substrate. This is of course assuming that the actuator has the force and capability to develop the one thickness deflection in the thicker substrate.

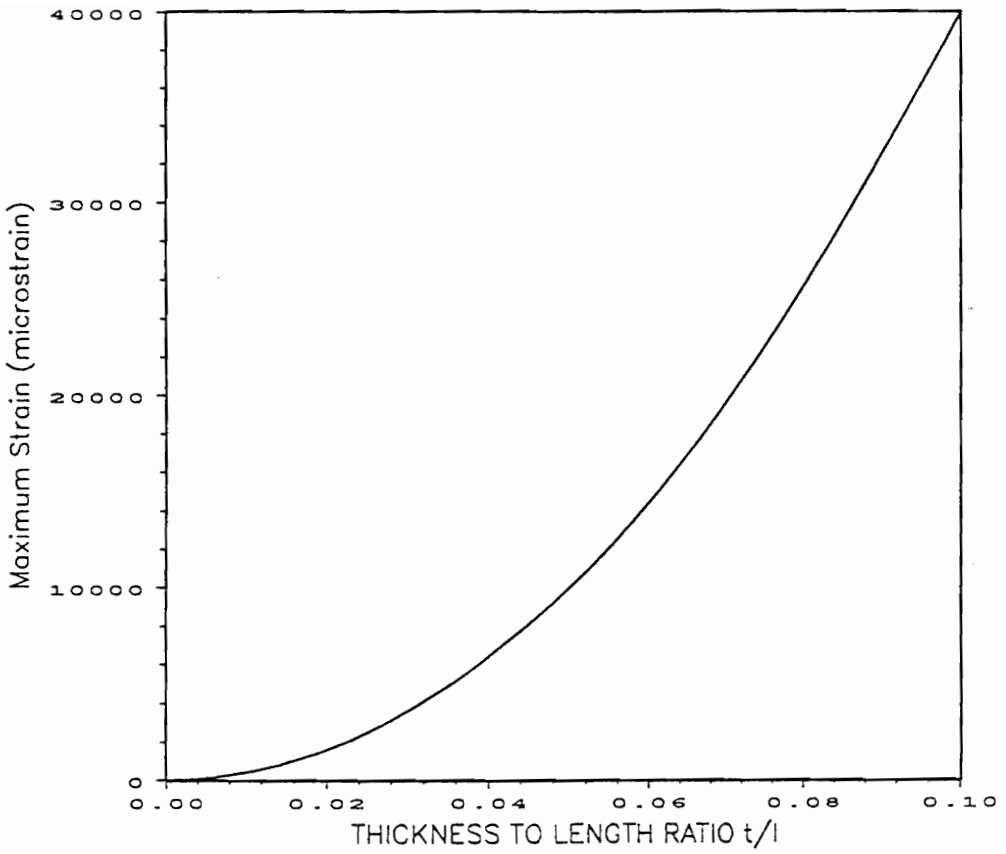

Figure 5.2 Maximum strain versus beam thickness.

Faced with this dilemma, a new configuration in which the actuator is attached to the structure at discrete points is proposed. This configuration is fundamentally different from the bonded/ embedded configuration. In this configuration, the structure and actuator between the two discrete points can deform independently, and the in-plane force of the actuator which is dormant in case of the bonded actuator, can cause out-of-plane displacements of the structure. Also, because now the actuator offset distance can be increased without any increase in the basic flexural stiffness of the structure, this distance can be optimized for maximum control.

Two implementations of this concept are possible. In the first, the actuator (e.g., shape memory alloy actuator wires) does not possess any flexural stiffness and, therefore, force exerted by the induced strain actuator on the structure is directed along a straight line joining the two attachment points. This configuration is the most efficient, and results in much greater control compared to the bonded configuration. The formulation and experimental results for this configuration and its variants have already been investigated and have been reported in an earlier paper (Chaudhry and Rogers, 1991). In this chapter the second implementation, where the actuator (like PZTs and electrostrictive actuators) possesses flexural stiffness, is analyzed. In this configuration, structural control is again enhanced, but is limited by the stroke capability of the actuator.

5.2 Formulation

Consider a simply-supported beam with an induced strain actuator attached at two discrete points, as shown in Fig. 5.3. When the actuator contracts in response to an applied electric field or temperature gradient, it exerts a compressive force on the beam and the actuator itself goes into tension. Tensile force in the actuator is exactly equal and opposite to compressive force in the beam. The form of the governing equation for both beam and actuator is the same:

$$EI w_{,xxxx} \mp P w_{,xx} = 0 \tag{6}$$

The form of the solution of the above equation is, of course, different for the actuator and the beam. For the beam, the force P is compressive and for the actuator, the force P is tensile. In general, the flexural stiffnesses EI of the beam and the actuator are also different. The solution of the differential equation for the beam is:

$$w_1(x_1) = A_1 \sin kx_1 + B_1 \cos kx_1 + C_1 x_1 + D_1 , \tag{7}$$

and for the actuator:

$$w_2(x_2) = A_2 \sinh \bar{k} x_2 + B_2 \cosh \bar{k} x_2 + C_2 x_2 + D_2 , \tag{8}$$

where

$$k = \sqrt{\frac{P}{EI_1}} \tag{9}$$

and

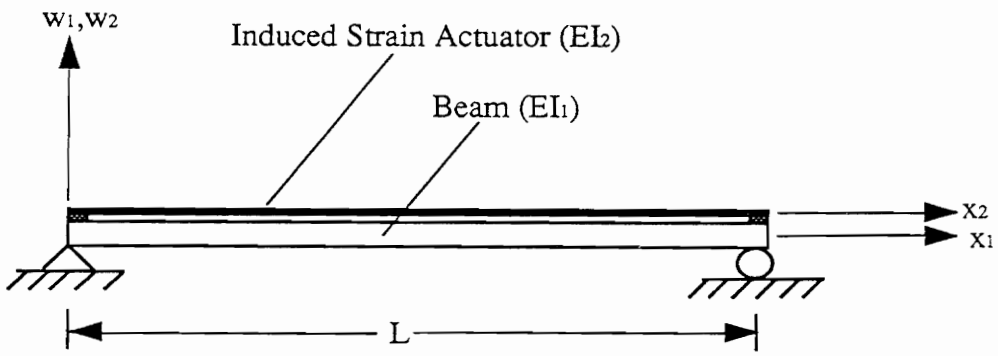

Figure 5.3 Geometry of the problem.

$$\bar{k} = \sqrt{\frac{P}{EI_2}} \quad . \tag{10}$$

The eight constants A_i , B_i , C_i , and D_i ($i=1,2$) are solved from the following eight boundary and matching conditions:

at $x_1=0$, and $x_2=0$:

$$w_1 = w_2 = 0 \tag{11}$$

$$w_{1,x_1} = w_{2,x_2} \tag{12}$$

$$-EI_1 w_{1,xx} - EI_2 w_{2,xx} = -P d \, . \tag{13}$$

and at $x_1=l$, and $x_2=l$:

$$w_1 = w_2 = 0 \tag{14}$$

$$w_{1,x_1} = w_{2,x_2} \tag{15}$$

$$-EI_1 w_{1,xx} - EI_2 w_{2,xx} = -P d \, . \tag{16}$$

5.3 Critical Buckling Load

The true input in such problems is applied electric field or free induced strain of the actuator (e.g., $\Lambda=d_{31}E$), but before addressing the question of the relationship between the

free induced strain and the force P, the eigenvalue problem is analyzed. The characteristic equation for the critical buckling load can be obtained by simply setting the actuator offset distance d to zero:

$$2(1-\cos kl\cosh \bar{k}l)+\frac{\bar{k}^2-k^2}{k\,\bar{k}}\sin kl\sinh \bar{k}l=0\,. \qquad \textbf{(17)}$$

The critical buckling load, as it changes with the flexural stiffness ratio of the actuator and beam (EI_1/EI_2), is shown in Fig. 5.4. The critical buckling load has been normalized by EI_1/l^2. Also, only flexural stiffness ratios greater than one are considered because in most applications the structure is stiffer than the actuator.

At higher values of flexural stiffness ratios, the value of the critical buckling load is asymptotic to π^2EI_1/l^2, which is the critical buckling load of a column with both ends pinned. This is perfectly logical, because as the flexural stiffness ratio increases, the flexural stiffness of the actuator becomes less and less significant compared to the beam, until finally the actuator behaves like a cable (with negligible flexural stiffness) tied to the two ends of the beam.

It is important to realize that buckling in such a configuration is possible, but for practical real-time induced strain actuators, which have limited stroke capability, it does not pose any problem. This is because, catastrophic buckling (i.e., large displacements) not only requires a force greater than the critical buckling load but also requires that the force

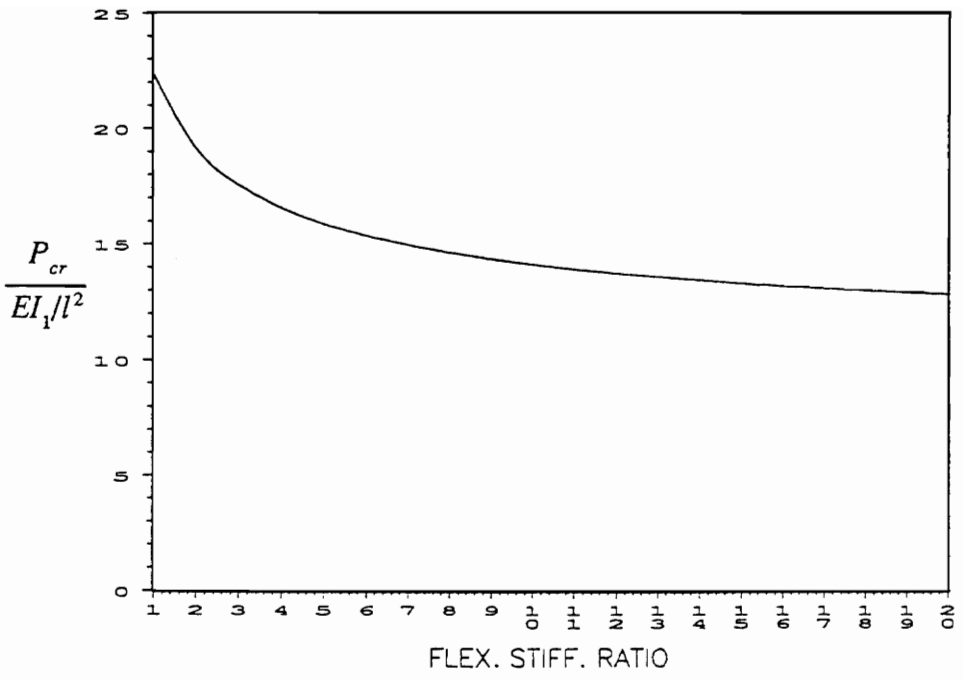

Figure 5.4 Critical buckling load versus flexural stiffness ratio EI_1/EI_2.

remain constant regardless of the displacement of the structure. This is of course not the case with induced strain actuators; they have limited stroke, after which they exert only a negligible force on the structure. Theoretically, buckling can take place with induced strain actuators, but displacements will still depend on the stroke capability of the actuators. Generally speaking, for any significant structural buckling, the actuator strain must be greater than 1%, which is possible only in the case of SMA actuators. But as stated earlier SMA actuators, which are available in the form of wires, have negligible flexural stiffness and therefore do not fall into this category of problems.

5.4 Force-Free Induced Strain Relationship

The free induced strain Λ, which is the true primary input variable, can be computed for a given force P using the following equation:

$$P = EA_2(\varepsilon^0_{x_2} - \Lambda)\,, \tag{18}$$

where

$$\varepsilon^0_{x_2} = \frac{du_2}{dx_2} + \frac{1}{2}\left(\frac{dw_2}{dx_2}\right)^2 . \tag{19}$$

Substituting for $\varepsilon_x{}^0$ in Eq. (18) and rearranging,

$$\frac{du_2}{dx_2} = \frac{P}{EA} - \frac{1}{2}\left(\frac{dw_2}{dx_2}\right)^2 + \Lambda . \tag{20}$$

Integrating the above expression yields the following expression for u_2:

$$\begin{aligned} u_2 = -\frac{1}{2}\Bigg\{ & A_2^2\bar{k}^2\left(\frac{\sinh 2\bar{k}x_2}{4\bar{k}} + \frac{x_2}{2}\right) + B_2^2\bar{k}^2\left(\frac{\sinh 2\bar{k}x_2}{4\bar{k}} - \frac{x_2}{2}\right) + C_2^2 x_2 \\ & + A_2B_2\bar{k}\left(\frac{\cosh 2\bar{k}x_2}{2}\right) + 2A_2C_2\sinh\bar{k}x_2 + 2B_2C_2\cosh\bar{k}x_2\Bigg\} \\ & + \left(\frac{P}{EA} + \Lambda\right)x_2 + F \end{aligned} \tag{21}$$

two unknowns, Λ and the constant of integration F, can now be evaluated by enforcing the following two boundary conditions on the u_2 displacement at $x_2=0$, and $x_2=l$ (Note, at this stage the coefficients A, B, C, and D are all known.):

$$u_2(0) = d.w_{1_x}(0) \tag{22}$$

$$u_2(l) = d.w_{1_x}(l) . \tag{23}$$

From the above equations, free induced strain Λ can be computed for a given force P. It is noted that the problem could have also been formulated with the free induced strain as the referenced variable instead of the force P. But since in most stability-type problems the primary variable is force, this problem was formulated accordingly.

5.5 Beam Response

With the above equations it is now possible to examine the beam response as a function of both the actuator-induced force P or the free induced strain Λ. Other variables which influence the response are flexural stiffness ratio EI_1/EI_2, and actuator offset distance d.

The effect of flexural stiffness ratio on the beam response is shown in Figs. 5.5, 5.6, and 5.7. Figure 5.5 shows the response for $EI_1/EI_2=1$, Fig. 5.6 for $EI_1/EI_2=5$, and Fig. 5.7 for $EI_1/EI_2=10$. Although the force has been normalized by the critical buckling load (for the specified flexural stiffness ratio), it is necessary to show a different plot for each of the values of the flexural stiffness ratios because of the nonlinear relationship between force and free induced strain. In all three figures, the normalized force is plotted versus the beam center point displacement, normalized by beam length. The free induced strain corresponding to values of actuator force is plotted on the right vertical axis. For comparison, the response of the beam to a pure moment ($M=Pd$) is also plotted in each figure. Note that the free induced strain on the right vertical axis does not correspond to this linear, moment response curve.

One thing to notice from all three figures is the enhanced bending compared to the bonded actuator case. But, to take advantage of the nonlinear region of enhanced bending, a certain minimum force and free induced strain are required. For example, in Fig. 5.5,

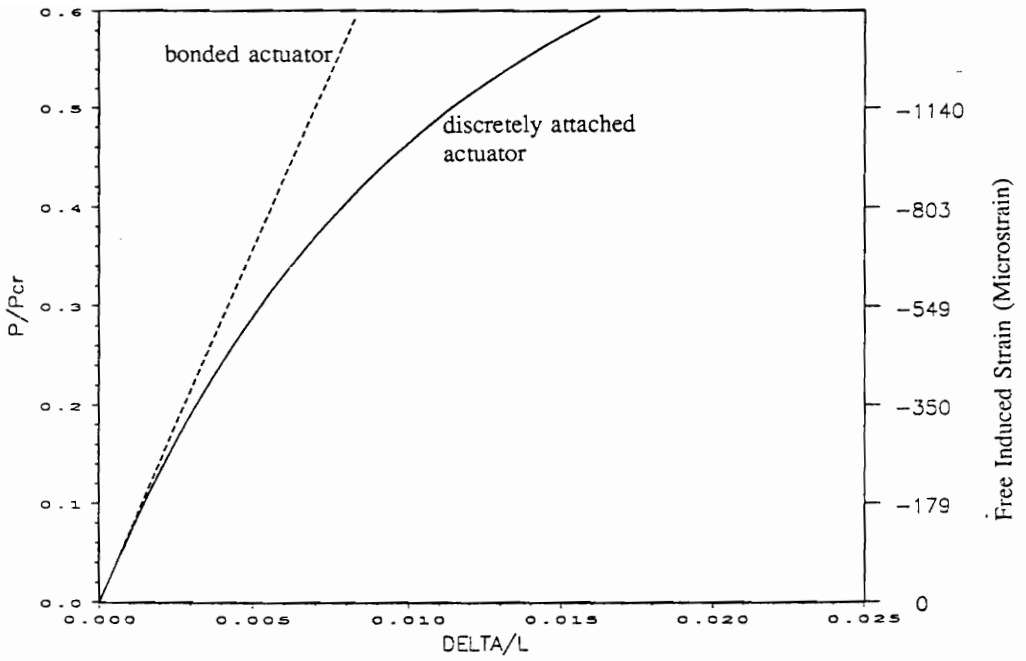

Figure 5.5 Beam response for a flexural stiffness ratio of 1. The right vertical axis shows the free induced strain corresponding to the force.

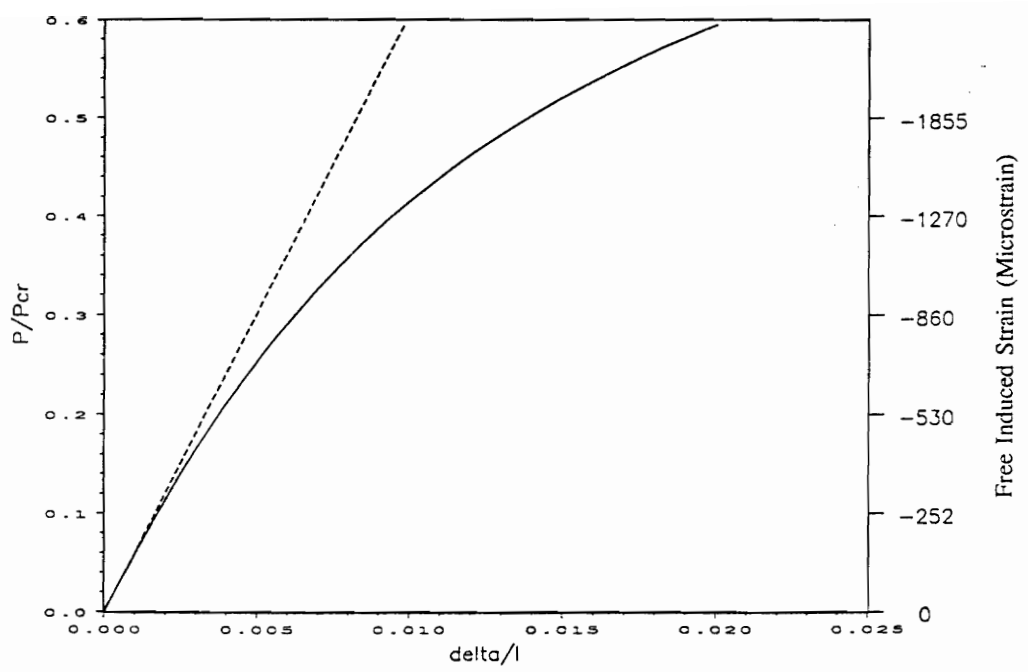

Figure 5.6 Beam response for a flexural stiffness ratio of 5.

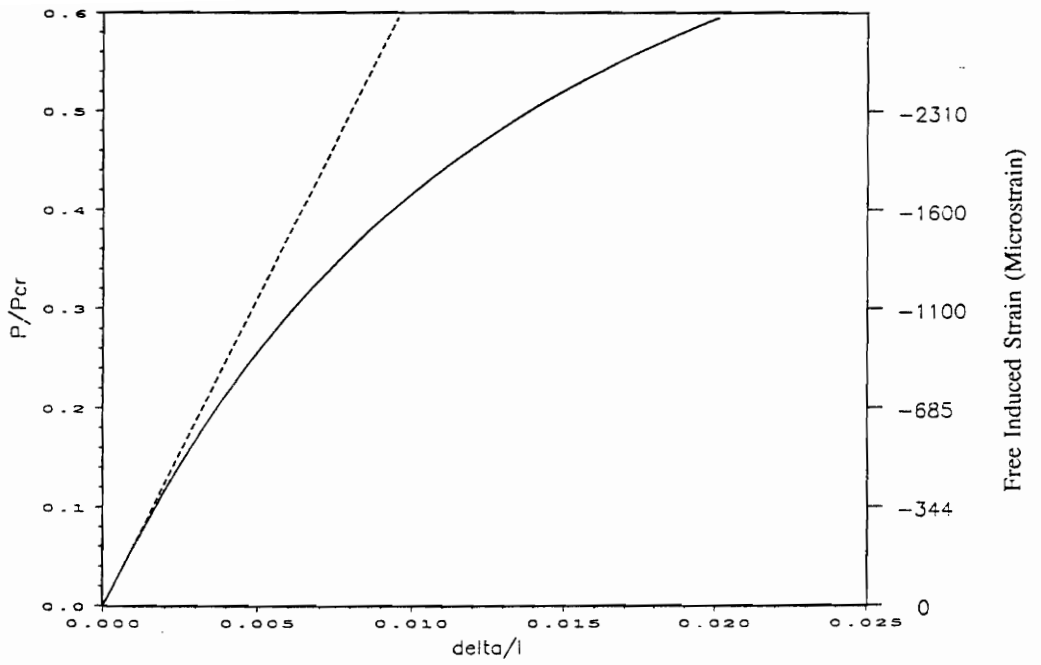

Figure 5.7 Beam response for a flexural stiffness ratio of 10.

where the flexural stiffness ratio is 1, a free induced strain greater than 1000 microstrain will result in a substantial increase in displacement, compared to that obtained with a bonded actuator.

As the flexural stiffness ratio is increased, the beam becomes stiffer compared to the actuator, and an even greater free induced strain is required to get into the nonlinear region of enhanced bending, as can be seen in Figs. 5 and 6. But, as the flexural stiffness ratio increases beyond 10, the free induced strain required to achieve a certain fraction of the critical buckling load becomes almost a constant. This is consistent with the fact that the normalized critical buckling load becomes insensitive to the flexural stiffness ratio as this ratio becomes greater than 10.

Therefore, for most practical structures, where the flexural stiffness ratio is likely to be higher than 10, an actuator with an induced strain capability greater than 1000 microstrain can result in substantially enhanced bending control.

Length of the beam, or distance between the two points where the actuator is attached to the structure, is also an important factor which controls the beam response. In all figures, the force P has been normalized by the critical buckling load, and the critical buckling load is inversely proportional to the length of the beam. Therefore, a longer distance between the two points where the actuator is attached to the structure reduces the critical

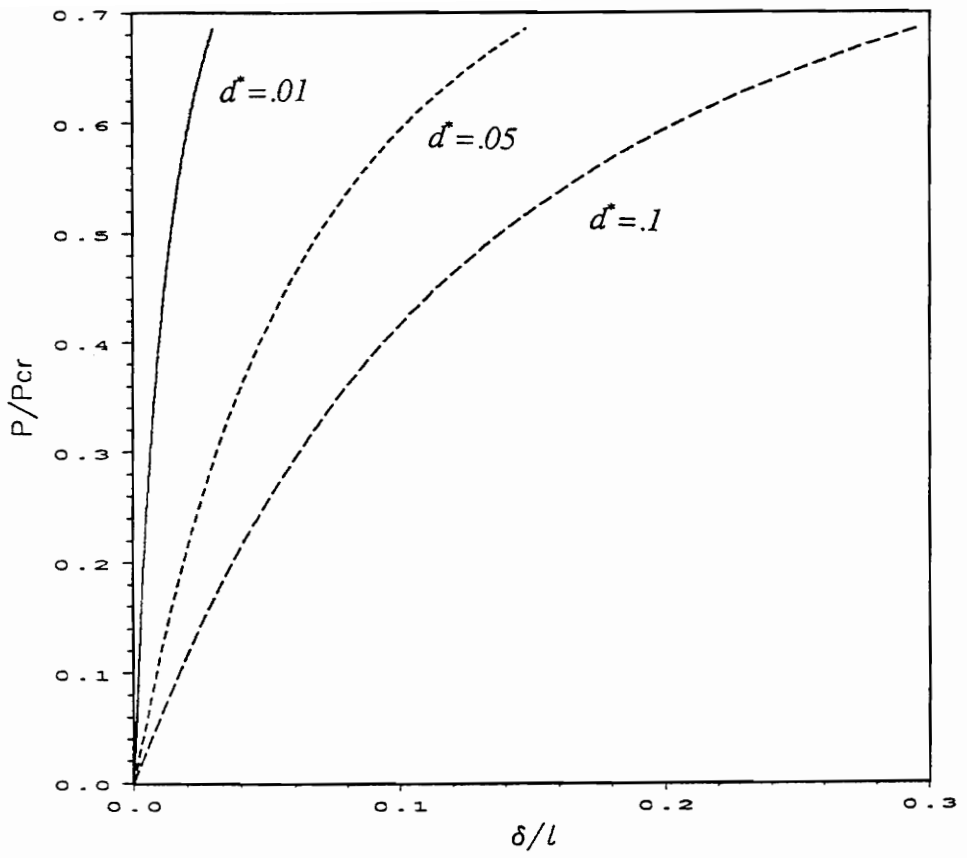

Figure 5.8 Beam response for different values of actuator offset distance.

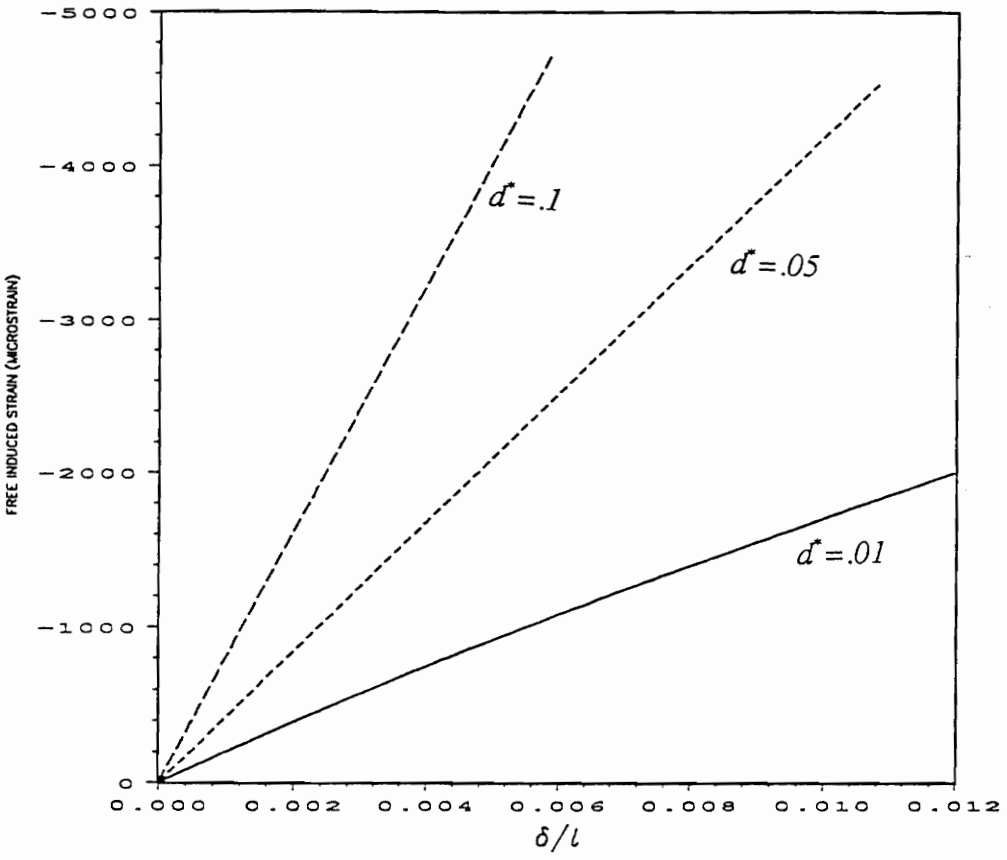

Figure 5.9 Beam response for different values of actuator offset distance. Figure shows the increasing stroke requirement for higher values of actuator offset distance.

buckling load and hence the force required to cause nonlinear effects.

5.6 Optimization of offset distance for enhanced control

Within the region of linear response, the most important parameter which influences response is the actuator offset distance. This parameter, as will be shown, if used properly can result in a substantial increase in bending control. As seen in Fig. 5.8 for a given value of P/P_{cr} a higher value of the offset distance beneficially decreases the force required (out of the actuator) to achieve a certain displacement, but at the same time, as seen in Fig. 5.9, increasing the actuator offset distance increases the stroke requirement. Mechanically when the actuator is close to the surface, the structure to which it is attached provides a greater constraint to the actuator's expansion and contraction, and in turn a greater force is developed in the actuator and applied to the structure and this leads to force saturation in the actuator. On the other hand if the actuator offset distance is increased the constraint offered to the actuator by the structure is reduced, this lets the actuator contract or expand more freely, and in the extreme case can lead to strain saturation. Between the two extremes of force saturation and strain saturation, there is in fact, an optimum offset distance which maximizes the moment applied to the substrate.

To study the effect of variation of offset distance on the beam displacements, the offset distance is normalized as follows:

$$\textit{normalized offset distance}\quad \bar{d} = \frac{d}{t_b/2}\ ,$$

and the beam displacement at the center δ is normalized by the displacement when the offset distance is a minimum, i.e., $\bar{d}=1$ or $d=t_b/2$

$$\textit{normalized displacement}\quad \bar{\delta} = \frac{\delta}{\delta)_{\bar{d}=1}}\ .$$

This normalizing scheme is physically meaningful and also allows us to study the effect of variation of the offset distance in the most general manner. The minimum value of the normalized offset distance is 1 and this corresponds to when the actuator is on the surface of the beam with minimum offset distance (i.e., $d=t_b/2$). For values higher than 1, it represents the offset distance as a fraction of half of the substrate thickness. Similarly the normalized beam displacement represents the ratio of the beam displacements with the actuator offset to when the actuator has no offset and lies on the surface.

Figure 5.10 shows the normalized beam displacement plotted versus the normalized offset distance for two different values of the beam-actuator thickness ratio t_b/t_a, and $E_1/E_2=1$. Figure 5.11 shows a similar plot for $E_1/E_2=3$. As expected the beam displacement increases with increasing offset distance until it reaches a maximum, after which it begins to decrease again. This behavior is consistent with the physical explanation presented earlier. As seen in Fig. 10 as the substrate becomes thicker relative to the actuator the

optimum offset distance also increases. As the thickness ratio is increased from 10 to 20 the normalized optimum offset distance changes from 2 to 2.6. In this figure where the modulus of the beam and the actuator are the same, the beam displacement can be increased by as much as 50% compared to bonded actuator.

If the substrate stiffness is greater than the actuator stiffness, the advantage of increasing the offset distance is even greater as seen in Fig. 11 where the beam-actuator modulus ratio is 3. For this stiffness ratio optimally offsetting the actuator can result in more than 100% increase in displacements compared to bonded actuator (It will be shown later that the bonded actuator configuration is indeed the degenerate case for this discretely attached actuator configuration).

It is important to point out that in both Fig. 5.10 and 5.11 the beam response is in the linear region and the only factor which is changing with the change in offset distance is the moment applied to the beam (the in-plane force of the actuator does not contribute to the beams transverse displacements). However, if the distance between the two points where the actuator is attached to the beam is long or if the force of the actuator is a significant fraction of the critical buckling load and the nonlinear effects are prominent, the optimum offset distance also becomes a function of the actuator activation level.

5.7 Relationship between bonded and discretely attached actuator configurations

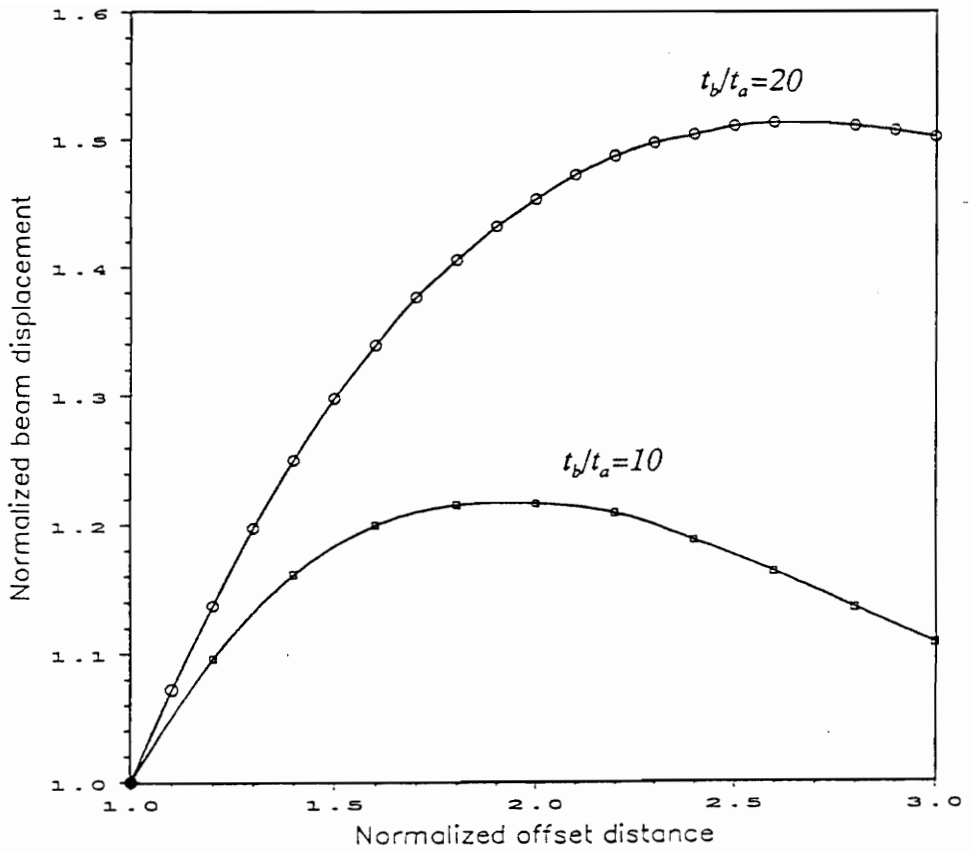

Figure 5.10 Normalized beam displacement vs. normalized offset distance ($E_1/E_2=1$).

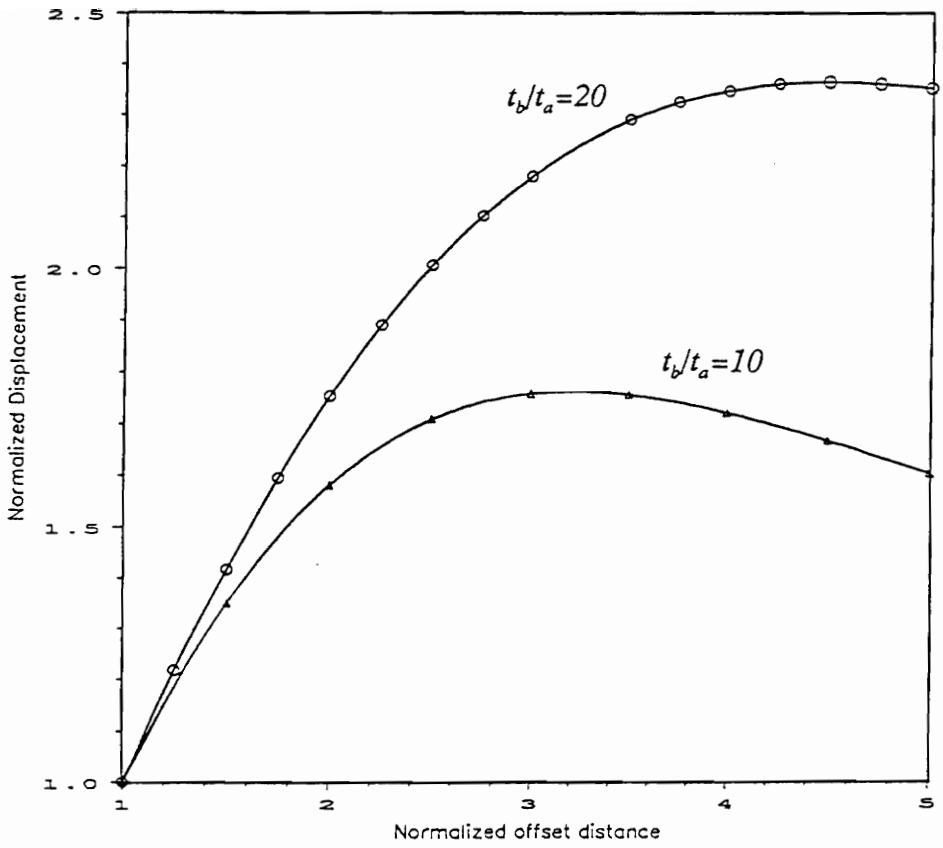

Figure 5.11 Normalized beam displacement vs normalized offset distance (E_1/E_2=3).

As stated in the discussion on the optimum offset distance, the enhanced displacements in the linear region are due to the increased bending moment and not because of the nonlinear structural response. In the model for the discretely attached actuator the beam and the actuator are subjected to concentrated moments applied at the two points where the actuator is attached to the beam. For bonded actuators, also, the action of the actuators is represented by concentrated moments applied at two ends of the actuator. Thus in both cases the response is basically due to end moments. Then how does the discretely attached actuator formulation with minimum offset distance compare with the bonded actuator formulation? The two formulations do in fact give exactly the same response within the linear regime and the bonded configuration is a degenerate case of the discretely attached actuator configuration. In fact it is possible to derive the Bernoulli-Euler expression for the beam curvature from considerations similar to the one used in the discretely attached formulation (this work is presented in the next chapter).

Thus the observations regarding the optimum offset distance can be directly applied to bonded actuators with one restriction. The restriction being that increasing the offset distance should not add to the basic flexural stiffness of the structure. This can be done by filling the area created by the offset with a honeycomb type structure which only provides a filler and no increase in flexural stiffness. In case the actuator offset distance is increased by increasing the basic thickness of the substrate, obviously none of the

above advantages apply because it is well known that increasing the substrate thickness increases the flexural stiffness as a square of the offset distance whereas the actuation moment increases only linearly.

The above discussion also implies that for thinner and softer substrates it would be advantageous to embed actuators below the surface rather than surface mount them.

This problem has been specifically formulated for the case where the actuator is contracting and applying a compressive force to the beam. Within the linear region, where the response is essentially due to the concentrated end moments, all the observations regarding the optimum offset distance also apply to a situation where the actuator is expanding and applying a tensile force to the beam. In such a situation, however, the discretely attached actuator is likely to bend itself and transmit minimal force to the structure, specially if the substrate is thick. This situation can be alleviated by having a honeycomb type filler between the actuator and the substrate. The honeycomb would ensure that the actuator itself does not bend and transfers all the force to the substrate.

5.8 Experimental Procedure and Results

To demonstrate enhanced control experimentally a relatively thick beam was chosen. As stated earlier increasing the offset distance is most beneficial for thicker substrates. The

actuators used were 0.25 mm-thick (10 mils) Piezoelectric Products G-1195 piezoceramic plates. A PZT patch was attached to a 1/8 in. thick, 3/4 in. wide and 6 in. long aluminum beam as shown in Fig. 5.12. Spacers .075-in. thick were placed at the two ends of the PZT to provide the necessary offset. To contrast the response of the discretely attached actuator with the bonded actuator, a second specimen with bonded PZT actuator patch was prepared. Geometric and material properties of the PZT actuator and the beam were identical for both specimen. In preparing the discretely attached actuator specimen, it was important that the actuator be absolutely straight. If there is a slight curvature, the actuator will quickly saturate by overcoming the slack due to the initial curvature and very little force will be transmitted to the structure.

Beam displacements were measured in the cantilever configuration at a point 1 in. from the right end of the PZT patch as shown in Fig. 12. An LVDT-type miniature displacement transducer type DFg-5 (Manufactured by Sangamo Schlumberger Industries), with a sensitivity of 1070 mV/mm, was used. As shown in Fig. 12, the armature of the LVDT transducer rested on the beam, and ensured positive contact between the beam and the armature at all times. The armature of the displacement transducer weighs only 1.14 gms. and was assumed to have negligible effect on the system response.

DC voltage applied in the poling direction of the PZT actuator was varied manually from 0 to 250 Volts. A personal computer equipped with an A/D board was used to record the

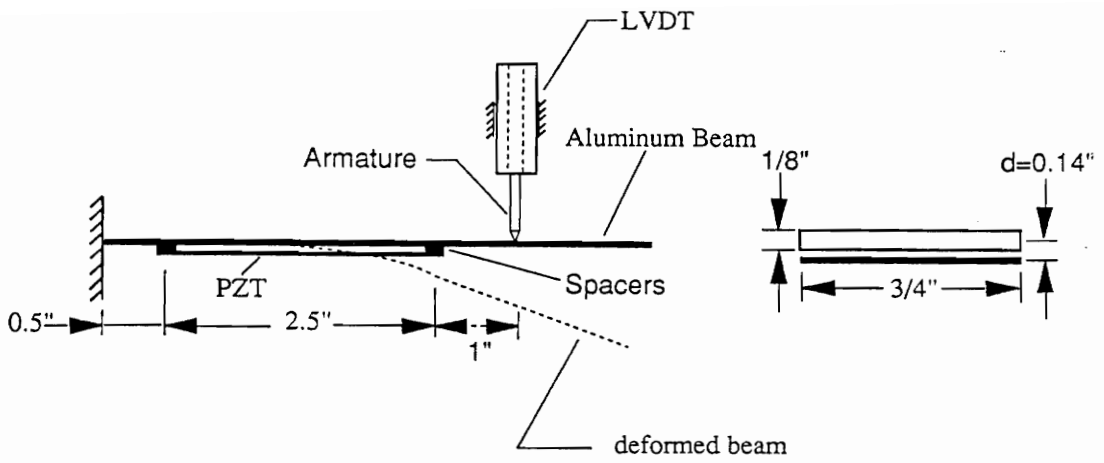

Figure 5.12 Figure showing the discretely attached beam-actuator specimen and experimental setup used to measure displacements.

voltage being applied to the actuator and the voltage output from the displacement transducer. The voltage output from the transducer was fed directly to the A/D board, but the voltage applied to the PZT was stepped down through a voltage divider and then fed to the A/D board. The voltage and displacements were recorded at increments of 10 Volts in the applied voltage.

Figure 5.13 shows the results of the experiment; applied electric field is plotted on the vertical axis and displacement is on the horizontal axis. In the figure there are two sets of experimental data points, for both the bonded and the discretely attached beam-actuator specimen. Agreement between the theoretical response and the experimental data is generally good, except at high field levels, where the theoretical response overpredicts displacements.

A theoretical solution for the bonded beam-actuator specimen is obtained using the pin-force model formulation because for high beam-actuator thickness ratios, as is the case in this experiment, this model is as accurate as the Bernoulli-Euler model. In the computation of the theoretical response for both configurations a strain dependent mechanical/electrical coupling coefficient d_{31} is used. The method suggested by Anderson and Crawley (1989) is used to compute d_{31}^* (secant definition of d_{31}). The following second order curve fit of the reported experimental data was used to compute the value of d_{31}^* iteratively:

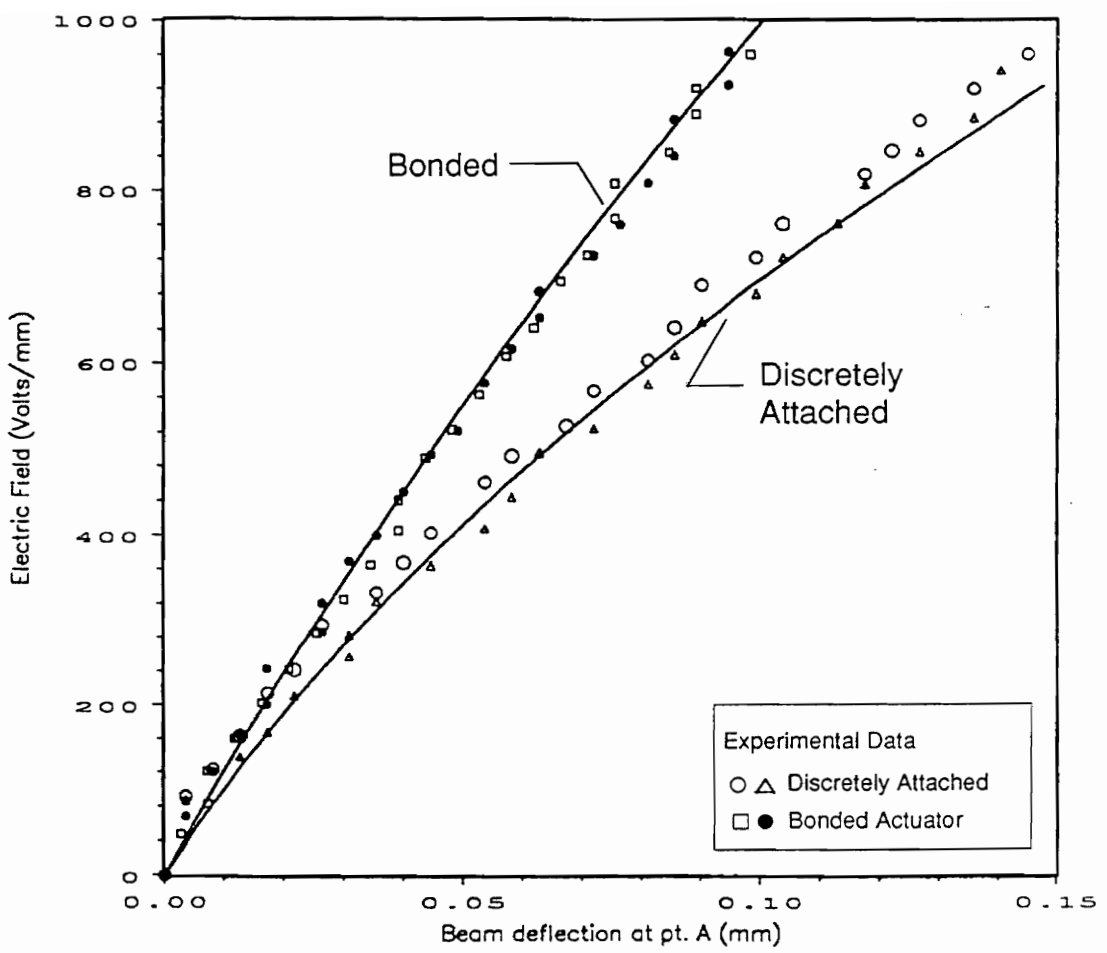

Figure 5.13 Experimental results, comparison of bonded and discretely attached actuator configuration.

$$d_{31}^{*} = 200 + .0012\varepsilon - 2\varepsilon^{2}$$

It is important to recognize that the nonlinearity in the response in Fig. 5.13 is not due to structural nonlinearity but is completely due to the nonlinear field-strain behavior of the PZT actuator.

It is interesting to note the predicted force in the actuator at different field levels and the resulting moment applied to the beam-actuator structure. Results of the predictions for some representative values are shown in Table 5.1. At 1000 V/mm, the predicted force in the discrete actuator is 16% less than the bonded actuator, but the moment is 40% greater. The difference in values of d_{31}^{*} used for predicting the response of the bonded actuator and the discretely attached actuator is also apparent. With an offset piezoelectric actuator, structural control authority is enhanced as a result of the nonlinear field-strain relationship of PZT.

5.9 Conclusions

To increase the realm of applications of induced strain actuators beyond vibration control and micropositioning, it is necessary to examine configurations other than the standard bonded/embedded configuration. In this chapter, a new configuration of discretely attached induced strain actuators to enhance structural control is developed and verified

Table 5.1 Experimental results.

Type	Field (V/mm)	d_{31}^* (pm/V)	Displacement (mm)		Predicted Force (lb.)	Predicted Moment (in. lb.)
			Predicted	Data		
Discretely Attached	500	273	.0646	.0605	4.7	0.611
	1000	349	.1640	.1450	11.8	1.534
Bonded	500	223	.0451	.0445	6.16	0.3853
	1000	249	.1000	.1050	13.767	0.86

experimentally. As a first step, a simple beam/actuator system is analyzed. The equations necessary to predict the response for such a system are derived. While buckling is possible in this configuration, it does not pose any problems, because of the limited stroke capability of most induced strain actuators. Aside from the distance between the two discrete points where the actuator is attached to the beam, the beam response is basically a function of two variables, the ratio of the flexural stiffnesses of the beam and actuator and the actuator offset distance.

This proposed configuration can enhance the response above that of the bonded actuator configuration by two mechanisms. One is by taking advantage of the nonlinear enhanced structural response. For most practical structures where the beam actuator flexural stiffness ratio is greater than 10, this would require an actuator with a free induced capability greater than 1000 microstrain. The second mechanism is that of optimally increasing the distance through which the actuator is offset from the structure at the two points of attachment. This mechanism enhances control in both the linear and nonlinear regions of structural response and does not require any minimum stroke capability of the actuator.

The increase in control achieved by offsetting the actuator depends on the beam-actuator thickness and modulus ratio. For thicker or high modulus substrates, optimal increase in the actuator offset distance results in a substantial increase in flexural control. In

experimental work with PZT actuators and aluminum beams a 40% increase in displacements over the bonded configuration was observed.

5.10 References

Crawley, E. F. and de Luis, J., 1987, "Use of Piezoelectric Actuators as Elements of Intelligent Structures," AIAA Journal, Vol. 25, No. 10.

Crawley, E. F. and Lazarus, K. B., 1989, "Induced Strain Actuation of Isotropic and Anisotropic Plates," AIAA Journal, Vol. 29, No. 6.

Chaudhry, Z. and Rogers, C. A., 1991, "Response of Composite Beams to an Internal Actuator Force," AIAA Paper No. 91-1168, Proceedings of the 32nd SDM Conference, Baltimore, MD.

Chaudhry, Z. and Rogers, C. A., 1991, "Bending and Shape Control of Beams using SMA Actuators," Journal of Intelligent Material Systems and Structures, Vol. 2, No. 4.

Forward, R. L. and Swigert, C. J., 1981, "Electronic Damping of Orthogonal Bending Modes in a Cylindrical Mast theory," J. of Spacecraft and Rockets, Jan-Feb.

Hanagud, S., Obal, M. W., and Meyyappa, M., 1985, "Electronic Damping Techniques and Active Vibration Control," AIAA Paper No. 85-0752, Proceedings of the 26th SDM Conference.

Wang, B. T. and Rogers, C. A., 1991, "Modelling of Finite Length Spatially Distributed Induced Strain Actuators for Laminate Beams and Plates," AIAA Paper No. 91-1258, Proceedings of the 32nd SDM Conference, Baltimore, MD.

Lin, M. W. and Rogers, C. A., 1992, "Analysis of a Beam Structure with Induced Strain Actuators Based on an Approximated Linear Shear Stress Field," Proceedings,Conference on Recent Advances in Adaptive and Sensory Materials and Their Applications, Virginia Polytechnic Institute and State University, Blacksburg, Virginia April 27-29, 1992; in press.

Chapter 6

A Mechanics Approach to Induced Strain Actuation of Structures

6.1 Introduction

In this chapter, a mechanics-based formulation for induced strain actuation of beam-like structures is presented. Two configurations are considered, one in which the actuators are symmetrically bonded on the surface of the beam and activated out of phase, and one in which the actuator is bonded to one side of the beam only. The pin-force model for a symmetric patch is first examined. Then the corrections necessary to upgrade this model to the level of the Bernoulli-Euler model are discussed. The same procedure is then applied to a beam with a single patch on one side. The static beam response equations developed for both cases are shown to be identical to those obtained from the more rigorous Bernoulli-Euler model. This work, thus, forms a bridge between the relatively simple pin-force model and the Bernoulli-Euler model and illustrates the use of mechanics principles in the treatment of structures with active members such as induced strain actuators.

To date, a number of models predicting the interaction between induced strain actuators

and the structure to which they are bonded have been developed. These models can be divided into three broad categories. In the first category are the relatively simple models like the pin-force model (Bailey and Hubbard, 1985; Crawley and Anderson, 1990). In the second category are the more advanced models based on assumed strain field. The consistent plate model (Crawley and Lazarus, 1989), the strain energy model (Wang and Rogers, 1991), and the models proposed by Dimitriadis and Fuller (1989), and Lee (1990) fall into this category. In the third category are the more accurate and relatively complex models which account for transverse shear effects. The most recent among them are the fully nonlinear model proposed by Pai, Nayfeh and Oh (1992), and the linear shear stress variation model proposed by Lin and Rogers (1992). In addition, a finite element formulation incorporating constitutive equations for piezoelectric materials has also been proposed recently by Shah, Chan and Joshi (1992).

The pin-force model, which is one of the earliest models, was derived from mechanics considerations. Although this model does not correctly predict the actuator/substrate response for thin structures, it is invaluable in understanding the physics of induced strain actuation. The other more refined models like the consistent plate model (based on classical lamination theory), although more accurate, do not provide insight into the mechanics of interaction between the actuator and substrate.

In this chapter, the solution to a beam with symmetric induced strain actuator patches is

developed from mechanics considerations. The solution of a beam with an induced strain actuator patch on one side is also developed and presented. First, the simple pin-force model is considered, and the reason for it being inaccurate for thin structures is discussed. By applying a certain correction to this model, its performance for thin structures is enhanced; this model is referred to as the "enhanced pin-force model". Then, the exact formulation based on mechanics considerations is presented and contrasted with the Bernoulli-Euler model. The same procedure is then repeated for the beam with an actuator patch on one side only.

6.2 Beam with Symmetric Actuator Patches

6.2.1 The Pin-Force and Enhanced Pin-Force Model

First, the pin-force model is examined to determine why it fails to predict the correct structural response for thin structures. In this model, the actuators and the substrate are modeled as separate structures, linked together by pins at the edges of the actuator. Figure 6.1 displays the idealized "pin"-force model concept. This model of force transfer from actuator to substrate is consistent with the assumption of perfect bonding between the actuator and substrate. Under this condition the shear stress is concentrated in a small zone at the end of the actuator modeled by the "pins". The pin connection allows for the strain in the actuator and the substrate to be modeled independently; however, the strains

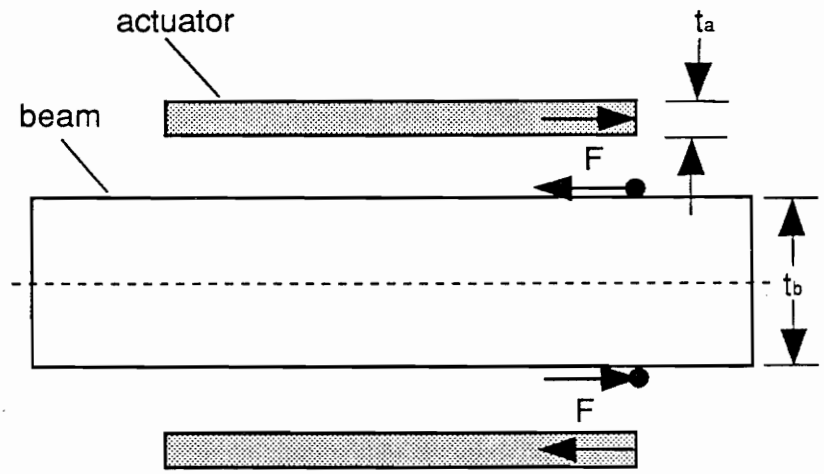

Figure 6.1 Pin-force model for a patch of symmetric actuators.

must be compatible at the interface, which is the pin location.

Only the actuation resulting in bending is considered because it is in this mode that the pin-force model fails for thin structures. The strain in the substrate is assumed to vary linearly through the thickness, as in Bernoulli-Euler beam theory; however the strain in the actuator is assumed to remain constant through the thickness. The curvature induced in the beam is computed by using the stress-strain relationship for the actuator:

$$\varepsilon_a = \frac{\sigma_a}{E_a} + \Lambda \ , \tag{1}$$

the moment curvature equation for the beam:

$$M = F t_b = (EI)_b \kappa \ , \tag{2}$$

and the compatibility of strain at the interface:

$$-\frac{t_b}{2}\kappa = \varepsilon_a = \frac{F}{(AE)_a} + \Lambda \ . \tag{3}$$

Substituting for the force F from Eq. (3) into Eq. (2), we can solve for the curvature induced in the beam:

$$\kappa = \frac{12\,\Lambda}{t_b(6+\psi)} \ . \tag{4}$$

In Fig. 6.2, the normalized curvature predicted by the above equation is plotted as a

function of the beam-actuator thickness ratio t_b/t_a, for a modulus ratio E_b/E_a of one. For small thickness ratios the pin-force model incorrectly predicts structure surface strains approaching the actuation strains. The important thing to notice here is that the discrepancy in the pin-force model is not because of the assumed uniform strain distribution in the actuator, as stated in the literature, but because of the incorrect moment curvature equation (Eq. (2)). In Eq. (2), the moment due to the pin forces of the actuators has been applied to the beam alone, whereas the actuators also bend along with the beam and their flexural stiffness must be appropriately represented in this equation. How to account for the flexural stiffness for such active members in a structure is a question which has eluded many a researchers and is a key part of this mechanics type formulation.

The correct moment curvature expression for the beam is:

$$M = F t_b - 2M_a = (EI)_b \kappa \ . \tag{5}$$

In the above equation, the moment M_a applied to each actuator is subtracted from the moment Ft_b applied to the beam (see Fig. 6.3). The above equation can be rewritten as:

$$M = F t_b = \{(EI)_b + 2(EI)_a\} \kappa \ , \tag{6}$$

where

$$(EI)_b = E_b \frac{b t_b^3}{12} \ , \tag{7}$$

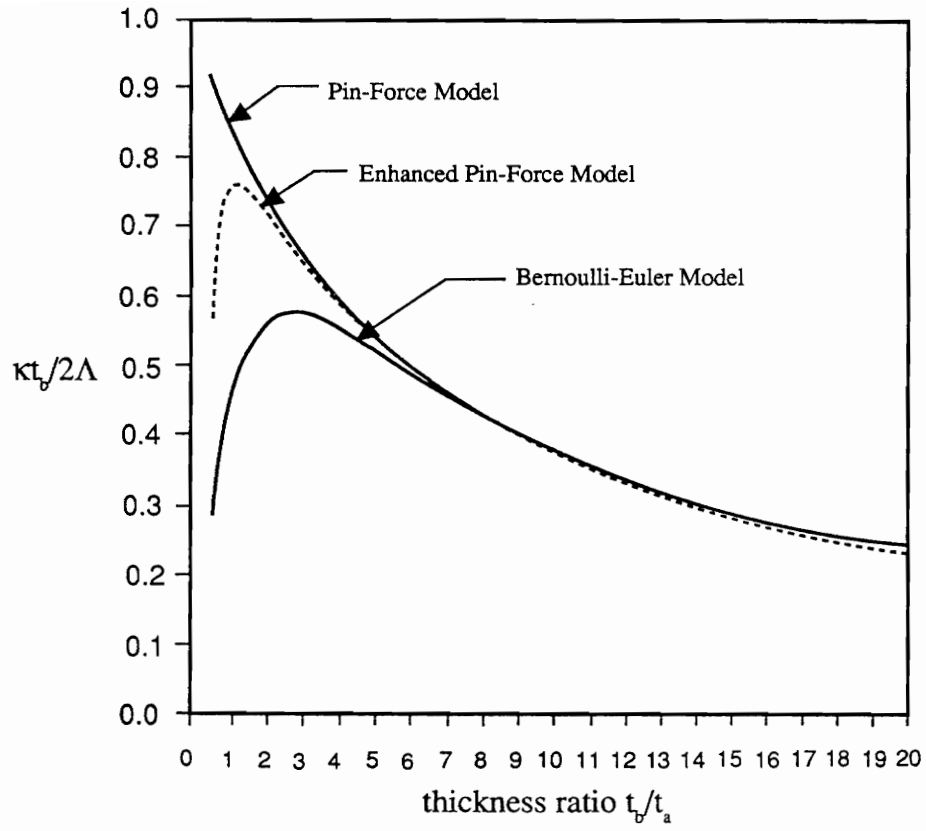

Figure 6.2 Normalized curvature vs. beam-actuator thickness ratio for a symmetric patch of actuators.

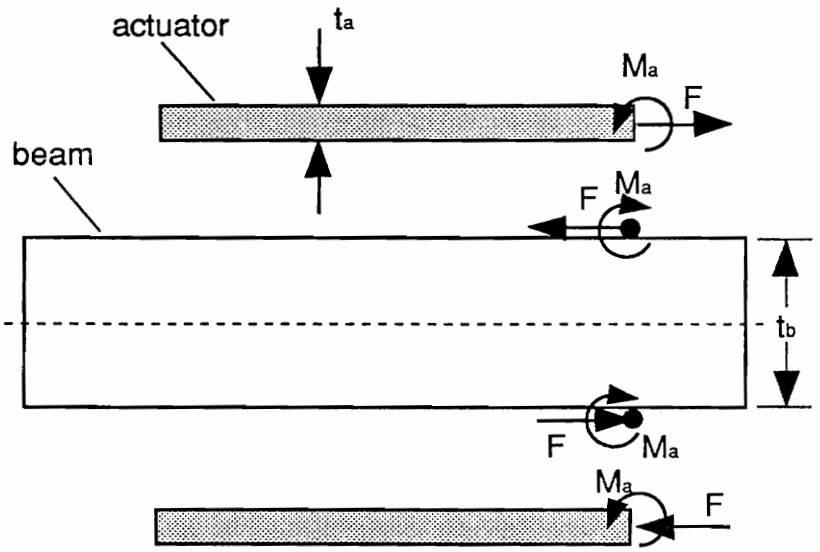

Figure 6.3 Pin-force model for a symmetric actuator patch. Figure shows the moments applied to the beam.

and

$$(EI)_a = E_a \frac{b t_a^3}{12} \ . \qquad \textbf{(8)}$$

The factor of 2 with $(EI)_a$ is simply to account for the two actuators, one on the top and one on the bottom surface. The physical explanation for such an addition of flexural stiffnesses is rather simple. The top and bottom actuators not only contract and expand, but also bend. If the actuators were attached to the beam at two points with pin connection (free to rotate), they would only contract and expand but not bend. Further they would apply point forces to the beam and the line of action of the forces would be directed along a straight line joining the two pins as is the case with discretely-attached external shape memory alloy actuators (Chaudhry and Rogers, 1991). In such an event, the beam would experience only point forces and the flexural stiffnesses of the actuators would not enter the moment curvature equation. But this is not the case for bonded actuators; in addition to contraction and expansion, they also bend. The contraction and expansion takes place in response to an external stimulus like an electric field or temperature, unlike the bending. Therefore, the individual flexural stiffnesses of the actuators get added to the flexural stiffness of the beam as in Eq. (6).

At this stage, it is important to distinguish the actuator force F used to compute the moment in Eq. (5) from the equivalent thermal load, usually designated by P_A. These two

quantities are by no means the same for induced strain actuators. They are related to each other through the following equation:

$$F = (EA)_a \varepsilon - P_\Lambda \ . \tag{9}$$

It is clear from the above equation that the force F used to calculate the moment on the composite beam-actuator structure is the actual resultant mechanical force in the actuator and is equal to P_Λ only for the case of perfect restraint.

By simply replacing Eq. (2) by Eq. (5) in the pin-force model formulation, the following expression for curvature for the enhanced pin-force model is obtained:

$$\kappa = \frac{12\Lambda}{t_b(6+\psi) + \dfrac{1}{T^2}} \ . \tag{10}$$

The normalized curvature predicted by the above equation is also plotted in Fig. 2 along with the original pin-force model. As is clearly evident, this formulation does not suffer from the predicament of the simple pin-force model. It does not wrongly predict the substrate surface strains approaching the actuation strains for thin structures.

In such an approach where the actuator and the substrate are considered to be separate elastic bodies, one is prone to include the effect of the in-plane axial force of the actuator on the out-of-plane displacements of the beam, and to treat the problem as a beam-column problem (Im and Atluri, 1989). But in reality, in such a configuration where the actuator

and the beam deform together, there is no column action (Chaudhry and Rogers, 1991), and the in-plane force contributes to out-of-plane displacements only through a moment due to actuator offset.

The extended pin-force model has a bit of contradiction in it from a theoretical standpoint. By assuming a constant strain distribution in the actuator, we are in fact specifying that the actuator does not bend, and therefore no moment is applied to it. Whereas, in Eq. (5) we are subtracting the moment applied to the actuator from the moment applied to the beam. As can be seen the assumption of constant strain in the actuator is not so bad, but not accounting for the actuator flexural stiffness is what really leads to the discrepancy in the pin-force model for thin structures.

6.2.2 Bernoulli-Euler Model

The Bernoulli-Euler Model, which is the one-dimensional version of the consistent plate model, is now examined. First, the conventional derivation is summarized; this is followed by the derivation based on mechanics considerations. It is pointed out that the Bernoulli-Euler model predicts the correct curvature for the complete range of actuator-to-substrate thickness ratios (Crawley and Anderson, 1990).

Consider the symmetrically bonded actuator arrangement shown in Fig. 6.4. Substituting

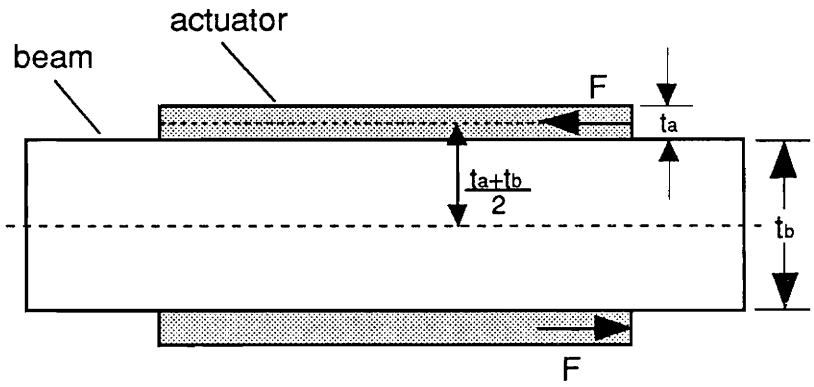

Figure 6.4 Symmetrically bonded actuators.

the assumed linear strain distribution into the stress-strain relationship of each layer, premultiplication by z, and integration yields:

$$(EI)_{Total}\,\kappa = M_{\Lambda}\ . \tag{11}$$

The $(EI)_{Total}$ in the above equation is the equivalent of D_{11} in CLT, and M_{Λ} is given by:

$$M_{\Lambda} = \int_{z} E(z)\,\Lambda\, b\, z\, dz\ . \tag{12}$$

Substituting the geometric and material properties of the actuator and beam into Eqs. (11) and (12) yields the following expression for curvature:

$$\kappa = \frac{6(1+\frac{1}{T})(\frac{2}{t_b})\Lambda}{(6+\psi)+\frac{12}{T}+\frac{8}{T^2}}\ , \tag{13}$$

where

$$\psi = \frac{t_b E_b}{t_a E_a}\ , \tag{14}$$

and

$$T = \frac{t_b}{t_a}\ . \tag{15}$$

Now, the above expression for curvature based on mechanics considerations is derived. The mechanics derivation proceeds in exactly the same way as the pin-force model, except now the strain distribution in the actuator is no longer constant. Note the stress-

strain relationship for the actuator is:

$$\varepsilon_a^0 = \frac{\sigma_a}{E_a} + \Lambda = \frac{F}{A_a E_a} + \Lambda \ . \tag{16}$$

Notice the middle-surface superscript on the actuator strain, which does not appear in the case of the pin-force model. The moment-curvature equation is also slightly different:

$$M = F(t_a + t_b) = \left\{2(EI)_a + (EI)_b\right\} \kappa \ . \tag{17}$$

The moment arm now includes half the actuator thickness on each side, resulting in a total moment arm of (t_a+t_b). The continuity of strain at interface equation is also slightly different due to the variation of strain within the actuator:

$$-\frac{t_b}{2}\kappa = \varepsilon_a^0 + \frac{t_a}{2}\kappa \ . \tag{18}$$

Substituting for ε^0 from Eq. (16) into Eq. (18) we can solve for the curvature from Eqs. (17) and (18):

$$\kappa = \frac{6(1+\frac{1}{T})(\frac{2}{t_b})\Lambda}{(6+\psi)+\frac{12}{T}+\frac{8}{T^2}} \ , \tag{19}$$

which is exactly the same expression as obtained from the Bernoulli-Euler model.

The above expression for curvature can also be obtained using the moment equilibrium condition (Kim and Jones, 1991). This condition simply states that in the absence of

externally applied moments, there must be moment equilibrium at all sections of the beam-actuator structure. But if we look closely, Eq. (11) used in the development of the Bernoulli-Euler model is also a statement of moment equilibrium and, in fact, the expression for effective bending moment (for the case of zero bonding layer) developed by Kim and Jones is exactly the same as would be obtained using the Bernoulli-Euler model.

Once again, it is important to realize that the forces and moments used in the mechanics formulation are the actual mechanical forces and moments and not the equivalent thermal loads.

6.3 Beam with Actuator Patch on One Side Only

6.3.1 Pin-Force and Enhanced Pin-Force Model

For a beam with an actuator patch on one side only, the formulation for the pin-force model proceeds in much the same way as a beam with symmetric actuator patches. Once again, the strain in the actuator is assumed to remain constant:

$$\varepsilon_a = \frac{\sigma_a}{E_a} + \Lambda \ . \tag{20}$$

The moment-curvature equation is different because now the moment arm, as seen in Fig.

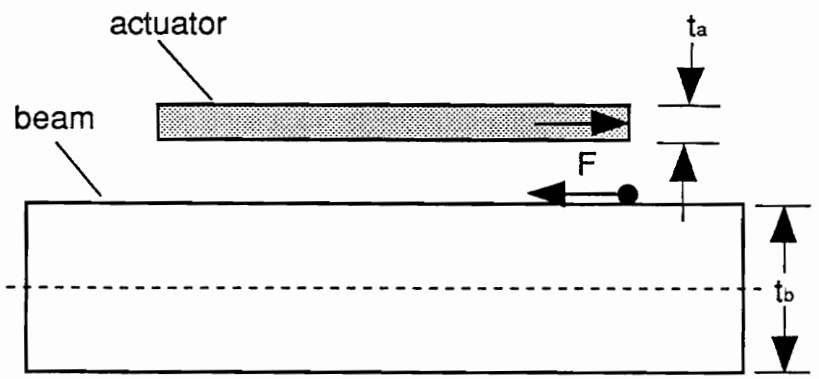

Figure 6.5 Beam with an actuator patch on one side only.

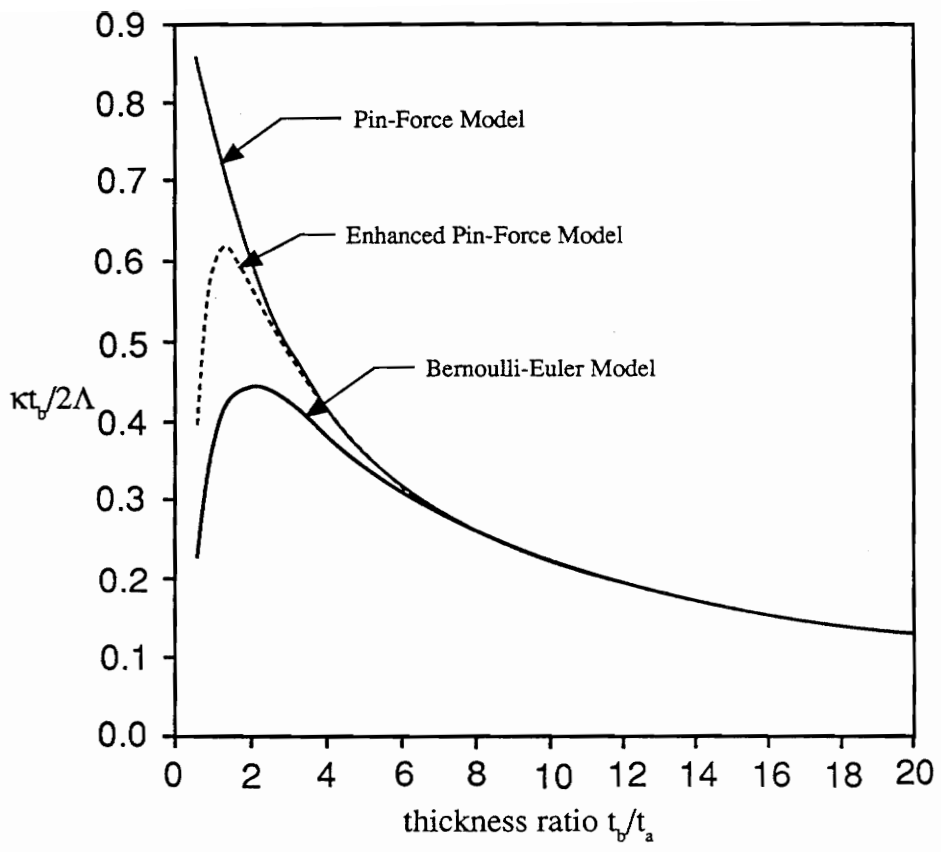

Figure 6.6 Normalized curvature vs. beam-actuator thickness ratio for an actuator patch on one side of beam only.

6.5, is only half the beam thickness, i.e.,

$$M = F\frac{t_b}{2} = (EI)_b \kappa \ . \tag{21}$$

The equation for continuity of strains is the same as for a symmetric patch:

$$-\frac{t_b}{2}\kappa = \varepsilon_a = \frac{F}{(EA)_a} + \Lambda \ . \tag{22}$$

Solving for the curvature from Eqs. (21) and (22):

$$\kappa = \frac{6}{t_b(3+\psi)}\Lambda \ . \tag{23}$$

Again we rewrite Eq. (21) to include the flexural stiffness of the actuator:

$$M = F\frac{t_b}{2} = \{(EI)_b + (EI)_a\}\kappa \ . \tag{24}$$

With this change in the moment-curvature equation, we get the following expression for curvature for the enhanced pin-force model for this configuration:

$$\kappa = \frac{6}{t_b(3+\psi+\frac{1}{3T^2})}\Lambda \ . \tag{25}$$

The normalized curvatures obtained from Eqs. (23) and (25) are plotted as a function of the thickness ratio in Fig. 6.6. Once again, the extended pin-force model does not incorrectly predict the surface strain approaching the actuator strain for thin structures.

6.3.2 Bernoulli-Euler Model

The development of the Bernoulli-Euler model is different in this case because the structure is no longer symmetric (see Fig. 6.7), and the bending and extension equations are coupled. Starting with the assumed linear strain distribution:

$$\varepsilon = \varepsilon^0 - z\,\kappa \ , \tag{26}$$

and the constitutive property of the materials in the cross-section:

$$E(z)\,\varepsilon(z) = \sigma(z) + E(z)\,\Lambda(z) \ . \tag{27}$$

Substituting Eq. (26) into Eq. (27) and integration with respect to z yields:

$$(EA)_{Total}\,\varepsilon^0 - (ES)_{Total}\,\kappa = P_\Lambda \ . \tag{28}$$

Substitution, premultiplication by z and integration yields:

$$(ES)_{Total}\,\varepsilon^0 - (EI)_{Total}\,\kappa = M_\Lambda \ . \tag{29}$$

Solving for the curvature from Eqs. (28) and (29) gives:

$$\kappa = \frac{6}{t_b}\,\frac{T(1+T)}{6T+4T^2+4+\psi T^2+\dfrac{1}{\psi}}\,\Lambda \ . \tag{30}$$

Next, the above expression for curvature is developed from mechanics considerations. The formulation proceeds the same way as the extended pin-force model, except now the strain in the actuator is not uniform. Thus, the strain variation within the beam and the

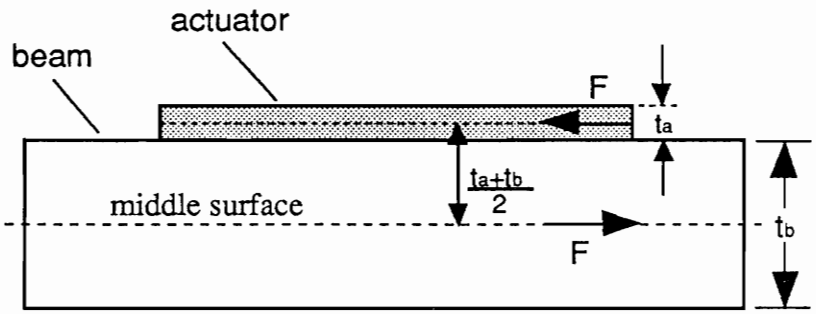

Figure 6.7 Actuator patch on one side of beam only.

actuator is now given by:

$$\varepsilon_b = \varepsilon_b^0 - z\,\kappa \ , \tag{31}$$

$$\varepsilon_a = \varepsilon_a^0 - z\,\kappa \ , \tag{32}$$

where $\varepsilon_a^{\,0}$ and $\varepsilon_b^{\,0}$ represent the middle-surface strains in the actuator and the beam, respectively. Using the stress-strain relationships, the middle-surface strains in the beam and the actuator can be written in terms of the force F as follows:

$$\varepsilon_b^0 = -\frac{F}{(EA)_b} \ , \tag{33}$$

$$\varepsilon_a^0 = \frac{F}{(EA)_a} + \Lambda \ . \tag{34}$$

The moment-curvature equation is written as:

$$M = F\frac{(t_a + t_b)}{2} = \left[(EI)_b + (EI)_a\right]\kappa \ . \tag{35}$$

Note that the above equation is exactly the same equation as the one used in the extended pin-force model, except now the moment arm also includes half the actuator thickness. Lastly, the continuity of strain at the interface equation can be written:

$$\varepsilon_b^0 - \frac{t_b}{2}\kappa = \varepsilon_a^0 + \frac{t_a}{2}\kappa \ . \tag{36}$$

Solving for the curvature from Eqs. (29-34) gives:

$$\kappa = \frac{6}{t_b} \frac{T(1+T)}{6T+4T^2+4+\psi T^2+\frac{1}{\psi}} \Lambda \ , \qquad (37)$$

which is again the same expression as developed from the Bernoulli-Euler formulation. The curvature predicted by the above equation is also plotted in Fig. 6.6. The curvature predicted by the above equation is different from the enhanced pin-force model for low thickness ratios for two reasons: one, the assumed strain distribution in the actuator, and two, the different moment arms used in the two formulations.

6.3.3 Finite Element Verification

The above formulation for the beam with an actuator patch on one side only was verified using finite element analysis. A typical finite element model is shown in Fig. 6.8. Two-dimensional linear plane stress isoparametric elements were used to model the beam and the actuator. The induced strain actuator was modeled with an isotropic thermoelastic material type. Extension was induced in the structure by specifying a coefficient of thermal expansion for the actuator and then applying a known temperature to the model. The solution was obtained using the ABAQUS finite element program.

Figure 6.9 shows the results obtained from the finite element analysis and the Bernoulli-

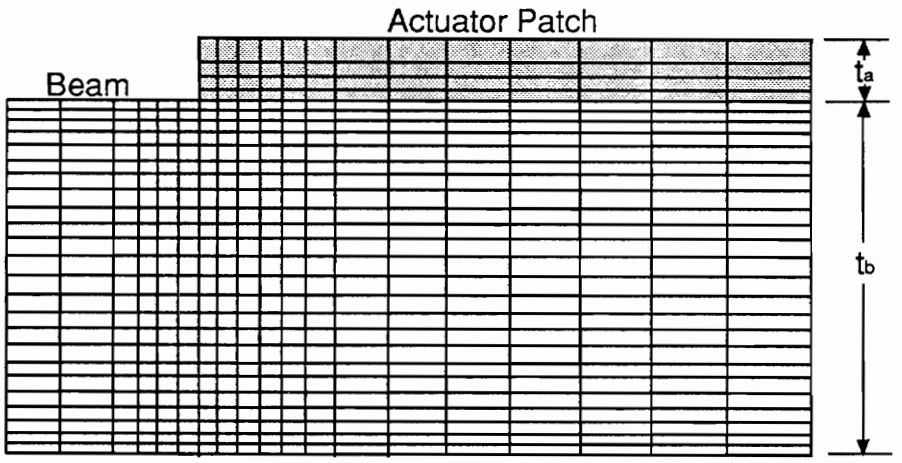

Figure 6.8 A typical finite element mesh.

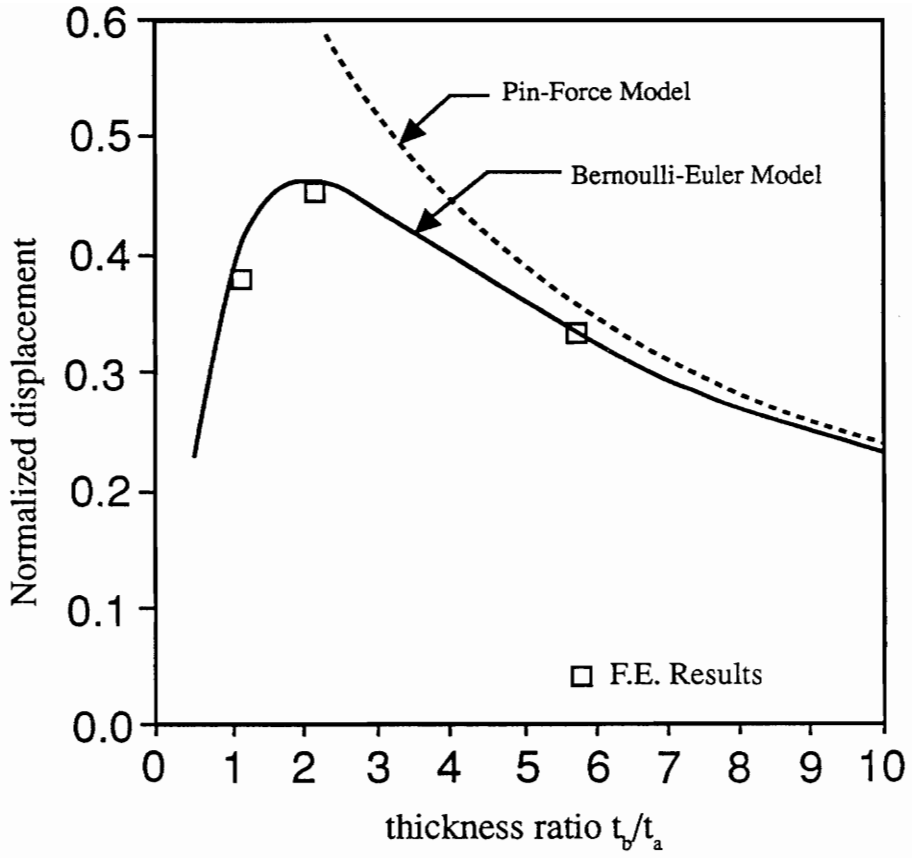

Figure 6.9 Normalized displacement vs. beam-actuator thickness ratio for an actuator patch on one side of beam only.

Euler model. The parameter used for comparison in the above figure is the normalized displacement of the beam middle surface at the center of the beam. Displacement is a better index to compare the analytical and the finite element results because: i) the output from the finite element program is directly available in terms of displacements, and ii) the displacements represent the integrated effect of the actuation over the whole patch. The agreement between the Bernoulli-Euler and finite element model is very good. The maximum difference which occurs for a thickness ratio of 1 is 3.9%. For a thickness ratio of 6, the difference is less than 0.2%. It also must be noted that if the actuator patch is small (with respect to actuator thickness) the correlation will not be as good due to the significant edge effects.

6.4 Conclusions

This paper presents an alternate derivation for the actuation of beams with induced strain actuators. The formulation which is based on mechanics considerations, provides a better understanding of the mechanics of interaction between the actuator and the substrate. The expressions developed for the response of a beam with symmetric actuator patches are identical to those obtained from the Bernoulli-Euler model. The equations necessary to predict the response of a beam with an actuator patch on one side only are also developed and presented. This derivation also provides rules to be followed in the use of moment-curvature equations in structures with active members like induced strain actuators.

6.5 References

Bailey, T., and Hubbard, J. E., 1985, "Distributed Piezoelectric-Polymer Active Vibration Control of a Cantilever Beam", Journal of Guidance, Control, and Dynamics, Vol. 8, No. 5, pp. 605-611.

Chaudhry, Z. and Rogers, C. A., 1991, "Response of Composite Beams to an Internal Actuator Force," Proceedings, AIAA/ASME/ASCE/AHS/ASC 32nd Structures, Structural Dynamics, and Materials Conference, (Baltimore, MD, 8-10 April 1991), AIAA, Inc., Washington, DC, Paper No. AIAA 91-1166, Part I, pp. 186-193.

Chaudhry, Z. and Rogers, C. A., 1991, "Bending and Shape Control of Beams using SMA Actuators," Journal of Intelligent Material Systems and Structures, Vol. 2, No. 4, pp. 581-602.

Crawley, E. F. and Anderson, E. H., 1990, "Detailed Models of Piezoceramic Actuation of Beams", J. of Intelligent Material Systems and Structures, Vol. 1, pp. 4-25.

Crawley, E. F. and de Luis, J., 1987, "Use of Piezoelectric Actuators as Elements of Intelligent Structures," AIAA Journal, Vol. 25, No. 10, pp. 1373-1385.

Crawley, E. F. and Lazarus, K. B., 1989, "Induced Strain Actuation of Isotropic and Anisotropic Plates," AIAA Journal, Vol. 29, No. 6, pp. 944-951 .

Dimitriadis, E. K., and Fuller, C. R., 1989, "Piezoelectric Actuators for Noise and Vibration Control of Thin Plates", 12th ASME Conference on Mechanical Vibration and Noise, Montreal, Canada.

Im, S. and Atluri, S. N., 1989, "Effects of a Piezo-Actuator on a Finitely Deformed Beam Subjected to General Loading", AIAA Journal, Vol. 27, No. 12, pp. 1801-1807.

Kim, S. J. and Jones, J. D., 1991, "Optimal Design of Piezoactuators for Active Noise and Vibration Control", AIAA Journal, Vol. 29, No. 12, pp. 2047-2053.

Lin, M. W. and Rogers, C. A., 1992, "Analysis of a Beam Structure with Induced Strain Actuators Based on an Approximated Linear Shear Stress Field," Proceedings, Conference on Recent Advances in Adaptive and Sensory Materials and Their Applications, Virginia Polytechnic Institute and State University, Blacksburg, Virginia April 27-29, 1992, Technomic Publishing Co., Inc., Lancaster PA.

Pai, P. F., Nayfeh, A. H., and Oh, K., 1992, "A Nonlinear Theory of Laminated Piezoelectric Plates," AIAA Paper No. 92-2407, Proceedings of the 33rd SDM Conference, Dallas, TX, pp. 577-585.

Shah, D. K., Chan, W. S., and Joshi, S. P., 1992, "Response of Piezoelectric Layer in Composite Laminates Due to Electromechanical Loads," AIAA Paper No. 92-2300, Proceedings of the 33rd SDM Conference, Dallas, TX, pp. 2918-2923.

Lee, C. K., 1990, "Theory of Laminated Piezoelectric Plates for the Design of Distributed Sensors/Actuators. Part I: Governing Equations and Reciprocal Relationships," Journal of Acoustical Society of America, Vol. 87, No. 3, pp. 1144-1158.

Wang, B. T. and Rogers, C. A., 1991, "Modelling of Finite Length Spatially Distributed Induced Strain Actuators for Laminate Beams and Plates," AIAA Paper No. 91-1258, Proceedings of the 32nd SDM Conference, Baltimore, MD, pp. 1511-1520.

Chapter 7

Results, Conclusions and Recommendations

The effectiveness of induced strain actuators for structural control in many applications has been established (Bailey and Hubbard, 1985; Crawley and de Luis, 1987; Baz and Poh, 1988; Rogers, 1990; Dimitriadis, Fuller and Rogers, 1991; Lee, Chiang and O'Sullivan, 1991; Fuller, Hansen and Snyder, 1991; Oh, Nayfeh and Pai, 1992). It is time now to critically examine the existing methods of integrating actuators into structures and to explore new actuator architectures which can enhance the authority of applied forces and moments without requiring additional energy input to the system. Here, architecture refers to discretely attaching induced strain actuators to the structure rather than bonding or embedding them.

Researchers working in the area of intelligent structures are becoming acutely aware of the need not only to maximize the electromechanical coupling of the actuators but also to mechanically enhance the performance of the actuators by correctly architecting them into the structure. Two designs very recently reported by Smith (1992) which illustrate the concept of mechanically enhancing the performance of induced strain sensors are presented.

The first example involves a hydrophone sensor using piezoelectric material. The figure of merit for hydrophone materials is the product of the hydrostatic piezoelectric charge coefficient (d_h) and the piezoelectric voltage coefficient (g_h). The geometry of hydrophone sensors, known as "moonies" because of the crescent-shaped cavities, is shown in Fig. 7.1. This sensor/material/structure arrangement, also referred to as a "composite piezoelectric", exploits the sensor-structure interaction to increase the sensitivity of the hydrophone. The hydrophone consists of a piezoceramic disk, electroded on its faces and poled through the thickness, sandwiched between two arched metal disks. When subjected to a compressive hydrostatic stress, the metal disks not only compress the ceramic where they touch it on its rim, but also push radially outward on the ceramic disk. Thus, the metal disks transform the vertical component of the hydrostatic stress into a tensile planar stress on the piezoceramic disk. The net stress on the piezoceramic disk is then a compressive stress transmitted directly to the rim of the disk, plus a tensile stress acting throughout the disk. For a typical PZT material, the values of both piezoelectric coefficients d_{33} and d_{31} are high (360×10^{-9} and -166×10^{-9} mm/Volt, respectively), but the hydrostatic charge coefficient d_h ($d_h = d_{33} + 2d_{31}$) is only about 28×10^{-9} mm/Volt because d_{33} and d_{31} have opposite signs. With this design, the hydrostatic stress is redirected in such a manner that d_{31} changes from negative to positive so that its contribution now adds to d_{33} rather than subtracting from it. The resulting electrical response is much larger than available from just the compression of the disk, and the figure of merit ($d_h g_h$) of this sensor is approximately 250 times that of pure PZT.

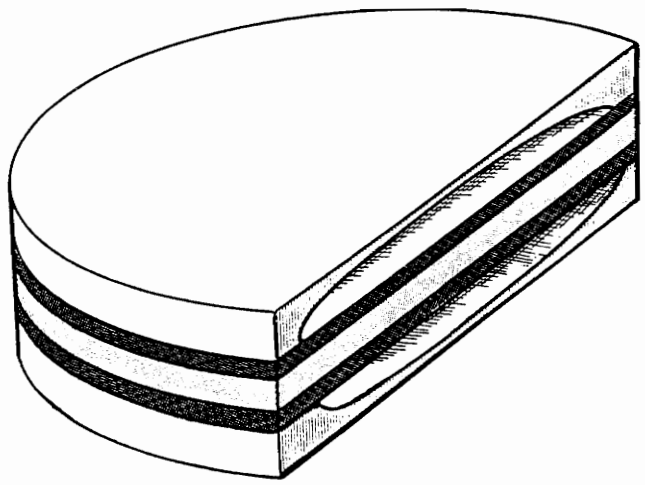

Figure 7.1 Hydrophone sensor using piezoelectric material.

The second example involves a pulse-echo transducer used in medical diagnostic imaging. In this application, thin plates of piezoceramic material are used at frequencies near the thickness-mode resonance to transmit short acoustic pulses and to detect their echoes. The transducer can be made of a solid block of piezoceramic or it can be in the form of a composite, as shown in Fig. 7.2. The piezocomposite consists of long, thin piezoceramic rods, poled along their longitudinal axis, held parallel to each other and perpendicular to the faces of the plate by a piezoelectrically passive polymer. In this configuration, the thin rods can expand or contract laterally; the large d_{33} is maintained while the d_{31} value is destroyed because of the series connection in the lateral dimension where the mechanical load is absorbed by the polymer and not transferred to the PZT rods. The resulting thickness-mode coupling constant d_{33} of the piezocomposite far exceeds that of its constituent ceramic alone. The resulting increased bandwidth and higher sensitivity are important advantages for pulse-echo transducers used in medical diagnostics. These advantages accrue because the external high frequency uniaxial stress of the ultrasonic waves are effectively coupled electrically within the rod composite.

Although the examples cited above relate to sensor applications, they clearly illustrate the importance of optimizing the sensor-material-structure interaction to maximize the overall electromechanical coupling of the system.

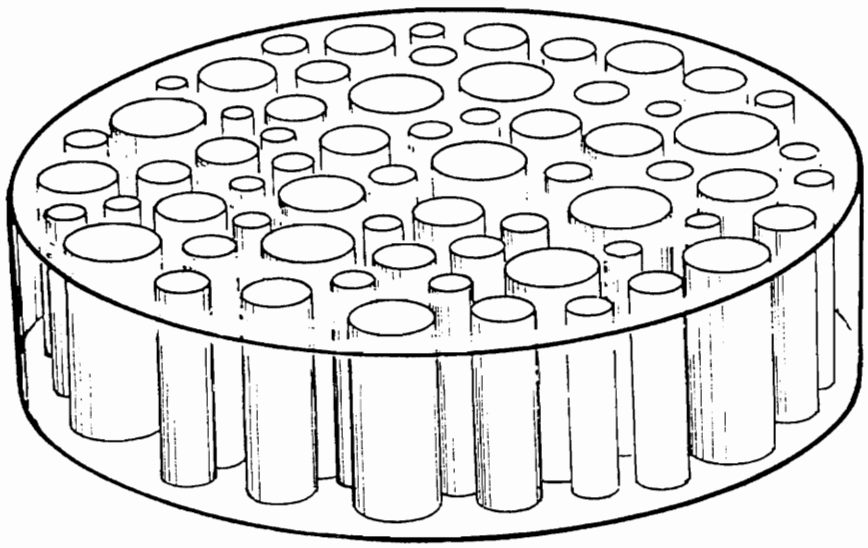

Figure 2 A pulse echo transducer.

In a sensor application the purpose of the structure built around the sensor material (e.g., the arched metal disks) is to make the mechanical forces so bear on the sensor material that the electromechanical coupling of the sensor material is maximized. The rules in the case of actuator-structure interaction are no different. The actuator should be so connected to the structure that the full potential of the actuator is utilized. Although this research was not motivated by the above sensor applications, the idea is similar - to find an efficient way of utilizing the available actuator energy for structural control. The proposed configuration of discretely attached actuators aims at enhancing the authority of applied forces and moments without requiring additional energy input to the system.

To increase the domain of intelligent structures, better actuator materials and architectural issues, such as those addressed in this research, will have to move hand in hand. The analysis and experimental results presented in this dissertation are a first step towards addressing issues of optimally architecting actuators into structures for increased authority.

7.1 Conclusions

1. Discretely attached actuators, when used for inducing flexure, can enhance structural control in two ways:

i) by taking advantage of the geometrically nonlinear structural response;

ii) by optimizing the offset distance with respect to actuator force/stroke saturation.

2. The degree of control enhancement depends on both the force and stroke capability of the actuator. While the increase in the displacement due to nonlinear effects requires a certain minimum force and stroke, the increase due to optimally offset actuators occurs regardless of the force and stroke capability of the actuator.

3. The theoretical formulation necessary to predict the structural response of an induced strain actuator discretely attached to a beam has been developed and verified experimentally. Both shape memory alloy-type actuators (possessing negligible flexural stiffness) and PZT-type actuators (possessing flexural stiffness) are considered. The key actuator and structural parameters which influence response are identified and their effects considered.

4. The formulation is generic and has been developed without reference to a specific actuation strain mechanism and therefore can be used for any type of induced strain actuator.

5. An alternate derivation for a bonded beam actuator structure which treats the actuator and the beam as separate bodies is also developed. The equations necessary to predict the response of a beam with a symmetric actuator patch and an actuator patch on one side only, are developed and presented. This derivation illustrates the similarities and differences between the bonded and discretely attached actuator configurations, and also provides better insight into actuator-structure interaction. The formulation specifically lays out the method for accounting for the flexural stiffness of an active structural member (actuator) when using mechanical moment-curvature equations.

7.2 Recommendations

In order to ensure the acceptance of the idea of discretely attached actuators, several issues relating to the implementation of the concept in real structures must be addressed:

a) To stabilize the discretely attached brittle piezoelectric-type actuators, a honeycomb or a foam-type filler has been suggested. This idea must be physically tested to ensure feasibility and also to identify any problems.

b) Since most of the currently available actuators are ceramic-based, they are very weak in tension. Implementation of this concept where the actuator

is pre-loaded in compression must be investigated. In the simple beam-actuator configuration, this could be done by bending the beam, at the time of attaching the actuator, in such a manner that when released it preloads the actuator in compression. Another possibility is to apply a bias field, which causes the actuator to contract, prior to bonding. After bonding, when the bias field is removed, the substrate structure would induce residual compression into the actuator.

c) Several long-term utility issues must be addressed. These include strength, fatigue, and fracture of actuator materials. Stress concentration points must be identified and the design modified to alleviate them.

d) To better model the problem of a discretely attached actuator, the effects of the adhesive shear layer and shear deformation should be included in the formulation. Also, because the constitutive law for most actuator materials are stress and field dependent, a fully coupled analysis incorporating the actuator constitutive law will be more useful from a practical implementation standpoint.

7.3 References

Bailey, T., and Hubbard, J. E., 1985, "Distributed Piezoelectric-Polymer Active Vibration Control of a Cantilever Beam", Journal of Guidance, Control, and Dynamics, Vol. 8, No. 5, pp. 605-611.

Crawley, E. F. and de Luis, J., 1987, "Use of Piezoelectric Actuators as Elements of Intelligent Structures," AIAA Journal, Vol. 25, No. 10, pp. 1373-1385.

Lee, C. K., Chiang, W. W. and O'Sullivan, T. C., 1991, "Piezoelectric Modal Sensor/ Actuator Pairs for Critical Active Damping Vibration Control," Journal of the Acoustical Society of America, 90(1), pp. 374-383.

Dimitriadis, E. K., Fuller, C. R., and Rogers, C. A., 1991, "Piezoelectric Actuators for Distributed Vibration Excitation of Thin Plates," J. of Vibration and Acoustics, Vol. 113, January, pp. 100-107.

Baz, A., and Poh, S., 1988, "Performance of an Active Control System with Piezoelectric Actuators," J. Sound and Vibration, 126(2), pp. 327-343.

Fuller, C. R., Hansen, C. H., and Snyder, S. D., 1991, "Experiments on Active Control of Sound Radiation from a Panel using a Piezoceramic Actuator," Journal of Sound and Vibration, 150(2), pp. 179-190.

Oh, K, Nayfeh, A. H. and Pai, P. F., 1992, "Control of the Resonant Response of a Cantilever Plate using PVDF Films as the Sensor/Actuator System: An Experimental Study," Proceedings, Conference on Recent Advances in Adaptive and Sensory Materials and Their Applications, Virginia Polytechnic Institute and State University, Blacksburg, Virginia, April 27-29, 1992, Technomic Publishing Co., Inc., Lancaster, PA.

Rogers, C. A., 1990, "Active Vibration and Structural Acoustic Control of Shape Memory Alloy Hybrid Composites: Experimental Results," Proceedings International Congress on Recent Developments in Air-and Structure-Borne Sound and Vibration, Auburn University, 6-8 March, 1990, pp. 695-708.

Smith, A. S., 1992, "The Key Principle for Piezoelectric Ceramic/Polymer Composites," Proceedings, Conference on Recent Advances in Adaptive and Sensory Materials and Their Applications, Virginia Polytechnic Institute and State University, Blacksburg, Virginia, April 27-29, 1992, Technomic Publishing Co., Inc., Lancaster, PA.

Vita

Zaffir Ahmed Chaudhry was born in Karachi, Pakistan on April 16, 1955. His father being in the army he lived and studied all over Pakistan. He got his higher secondary school certificate from Forman Christian College in Lahore in 1972. He joined the Pakistan Air Force College of Aeronautical Engineering in 1973, and graduated from the same college with a B.S. degree in aerospace engineering in 1977. He served as a maintenance engineering officer in the Pakistan Air Force from 1977 to 1983, at which time he was selected to attend AFIT. He graduated from AFIT with an M.S. degree in aeronautical engineering in March 1985. From 1985 to 1989 he served as an instructor in the Aerospace Department of the College of Aeronautical Engineering, Risalpur, Pakistan. He came to Virginia Tech in the fall of 1989 and started working in the area of intelligent structures in the summer of 1990. He graduated with a Ph.D. in mechanical engineering in July, 1992.

Zaffir A. Chaudhry